SPATIO-TEMPORAL VARIABILITY IN GROUNDWATER DISCHARGE AND CONTAMINANT FLUXES ALONG A CHANNELIZED STREAM IN WESTERN KENTUCKY

DISSERTATION

A dissertation submitted in partial fulfillment of the
requirements for the degree of Doctor of Philosophy in the
College of Arts and Sciences
at the University of Kentucky

By
Ganesh Nath Tripathi
Lexington, Kentucky
Director: Dr. Alan E. Fryar, Associate Professor of Earth and Environmental Sciences
Lexington, Kentucky
2013

ABSTRACT OF DISSERTATION

SPATIO-TEMPORAL VARIABILITY IN GROUNDWATER DISCHARGE AND CONTAMINANT FLUXES ALONG A CHANNELIZED STREAM IN WESTERN KENTUCKY

Surface and groundwater discharges and contaminant fluxes can vary with time and space depending upon the hydrogeological processes and geological setting of the area of interest. This study examined a ~300-m-long, channelized reach of a first-order perennial stream, Little Bayou Creek, in the Coastal Plain of far western Kentucky during the period October 2010–February 2012. Along the study reach, springs discharge groundwater contaminated by the chlorinated organic compound trichloroethene (TCE) and radionuclide technetium-99 (^{99}Tc) released as a result of past activities at the U.S. Department of Energy's Paducah Gaseous Diffusion Plant. The study addressed variability in groundwater discharge patterns and contaminant concentrations at various timescales (seasonal, annual, and decadal) and the extent to which the discharge sites are spatially persistent. Understanding patterns of groundwater discharge along a stream can be important for assessing the fate and transport of aqueous contaminants.

Groundwater discharge was estimated during baseflow conditions using different mass-balance approaches, including velocity-area and dye-dilution gauging. Discharge fluctuated seasonally but typically increased downstream, indicating the entire study reach to be gaining throughout the year. Discharge rates of individual springs also fluctuated seasonally. Tracer test data were utilized to model flow and transient storage along the reach using the USGS software OTIS-P. Cross-sectional area determined from OTIS-P was similar to that measured by velocity-area gauging. Reach area-normalized discharge fluxes were comparable to values determined by Darcy's law calculations from a pair of monitoring wells at the downstream end of the study reach. Temperature data acquired from probing along grids in winter and summer, from fiber-optic sensing along the reach in autumn, and from data-loggers and manual measurements in springs were used to delineate focused discharge locations. Comparison of temperature-probing results with prior studies indicated that locations of some springs persisted over a decade, whereas other springs emerged and disappeared. Because the stream is located in unlithified sediments, discharge rates of springs appear to fluctuate with soil piping and collapse along joints in fractured clay. Contaminant concentrations in springs decreased

downstream along the reach and were lower than observed during September 1999 – May 2001. The continued occurrence of dissolved oxygen and the absence of TCE daughter products in springs suggest that the decrease in TCE concentrations resulted from the installation of upgradient extraction wells, rather than from intrinsic reductive degradation.

KEYWORDS: Contaminant fluxes, trichloroethene, technetium-99, baseflow, temperature probing.

Ganesh N. Tripathi

April, 2013

SPATIO-TEMPORAL VARIABILITY IN GROUNDWATER DISCHARGE AND CONTAMINANT FLUXES ALONG A CHANNELIZED STREAM IN WESTERN KENTUCKY

By

Ganesh N. Tripathi

Dr. Alan E. Fryar

Director of Dissertation

Dr. Alan E. Fryar

Director of Graduate Studies

April, 2013

Date

ACKNOWLEDGEMENTS

First of all, I would like to express my sincere gratitude to my advisor, Dr. Alan E. Fryar, for being so supportive and encouraging from the very beginning until the end of my project. I cannot imagine I could have accomplished it without his generous guidance and continuous support. I am thankful to Dr. James Dinger, Dr. Steve Workman and Dr. Edward Woolery for kindly serving on my committee and providing fruitful comments and suggestions.

I am equally thankful to the U. S. Department of Energy for funding my research through the Kentucky Research Consortium for Energy and Environment (KRCEE). My special thanks go to Mr. Steve Hampson, KRCEE, for providing additional help and support through the entire project period. I would like to acknowledge the Tennessee Valley Authority and Kentucky Department of Fish and Wildlife Resources for allowing conducting my research within their property. I would also like to thank Mr. James C. Currens from the Kentucky Geological Survey and Dr. Gail Brion, and John May from the Environmental Research Training Laboratories, University of Kentucky, for their help in sample analysis. I was lucky enough to get help from a group of wonderful people: Kelley Lynn, Brandon Daley, Jeremy Paessler and Steve Meiners from Tricord Inc.; Dr. Ahmed Fekri, Faculté des Sciences Ben M'sik, Morocco; Francisco Suarez, Christine E. Hatch and Dr. Scott Tyler, Center for Transformative Environmental Monitoring Programs (CTEMPs).

Last but not least, I would like to thank my family for always being there as a continuous source of support and inspiration. Needless to say, I am indebted to my wife, Kalpana Bhandari, for taking complete responsibility of our two kids and letting me work on my research without any interruption.

TABLE OF CONTENTS

LIST OF TABLES

LIST OF FIGURES

Chapter 1. Introduction

1.1 Background

In the past, groundwater and surface water bodies were considered as separate entities and the links between the two systems were not fully understood. Because of their hydraulic inter-connection, changes in one system could affect the other. If either of the systems is contaminated, the other could also be affected. Groundwater and stream water interact mainly in three different ways: gain water, lose water or both (Winter et al., 1998). Along a stream reach all three processes mentioned above could occur or any of the three may be prevalent. Groundwater discharges to the stream where the water table in the adjacent area is higher than the stream water level; the reverse is true when the water table is lower than the stream stage. Stream reaches with groundwater inflow and surface water outflow are termed as gaining and losing reaches, respectively. Both groundwater inflow and loss of stream water through the stream bed (outflow) take place in the hyporheic zone (Fig. 1.1). In this zone, mixing of groundwater and stream water plays an important role in maintaining a unique aquatic ecosystem (Winter et al., 1998). During flood stage, temporary flow reversals can occur due to the change in hydraulic gradient (Fig. 1.1) (Winter et al., 1998). The transition zone between terrestrial and aquatic environments, the riparian zone, plays an important role in controlling the stream chemistry during baseflow and storm events (Hill, 2000).

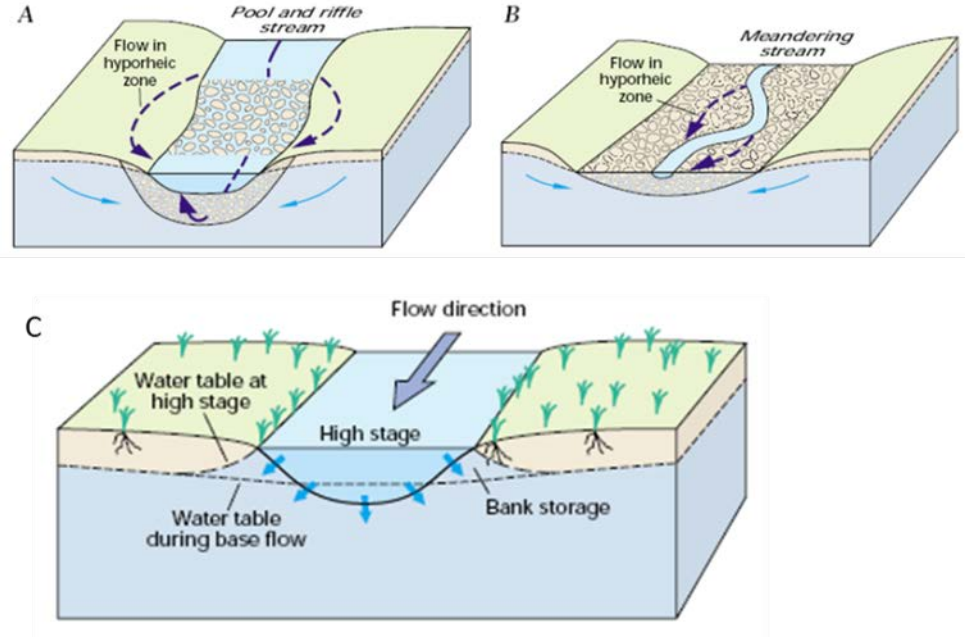

Figure 1.1. Hyporheic zone associated with abrupt change in streambed slope (A) and meandering stream (B), and drainage reversal due to bank storage (C) (Winter et al., 1998).

Understanding patterns of groundwater discharge along a stream can be important for assessing the fate and transport of aqueous contaminants. Depending upon the chemistry of contaminants and the geologic setting, contaminants in groundwater may or may not be attenuated (e.g., by processes such as adsorption and biodegradation) in the discharge zone (LaSage et al., 2008b). The proposed study reach of the stream has been contaminated by plumes of groundwater containing the chlorinated organic compound, trichloroethene (TCE), and the radionuclide technetium-99 (^{99}Tc), which were released as a result of past activities at the U. S. Department of Energy's (DOE's) Paducah Gaseous Diffusion Plant (PGDP) (Fryar et al., 2000; Mukherjee et al., 2005; LaSage et al., 2008b) (Fig. 1.2, 1.3). If, as inferred by LaSage et al. (2008b), contaminant fluxes from groundwater to Little Bayou Creek are spatially focused, then targeted remediation approaches (such as installing passive reactive barriers in the discharge zone) may be feasible.

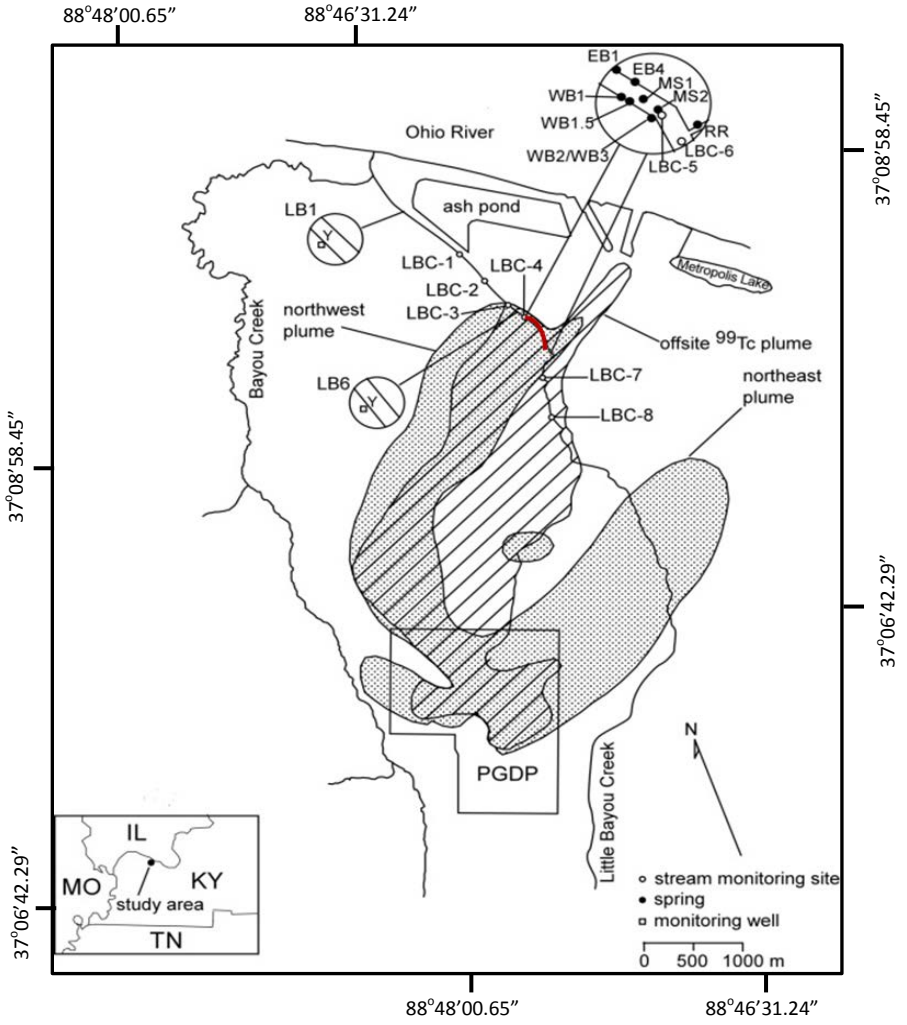

Figure 1.2. Location map showing Paducah Gaseous Diffusion Plant and northeast and northwest contaminant plumes along with previous and current (highlighted in red) study sites (modified from LaSage et al. [2008b]).

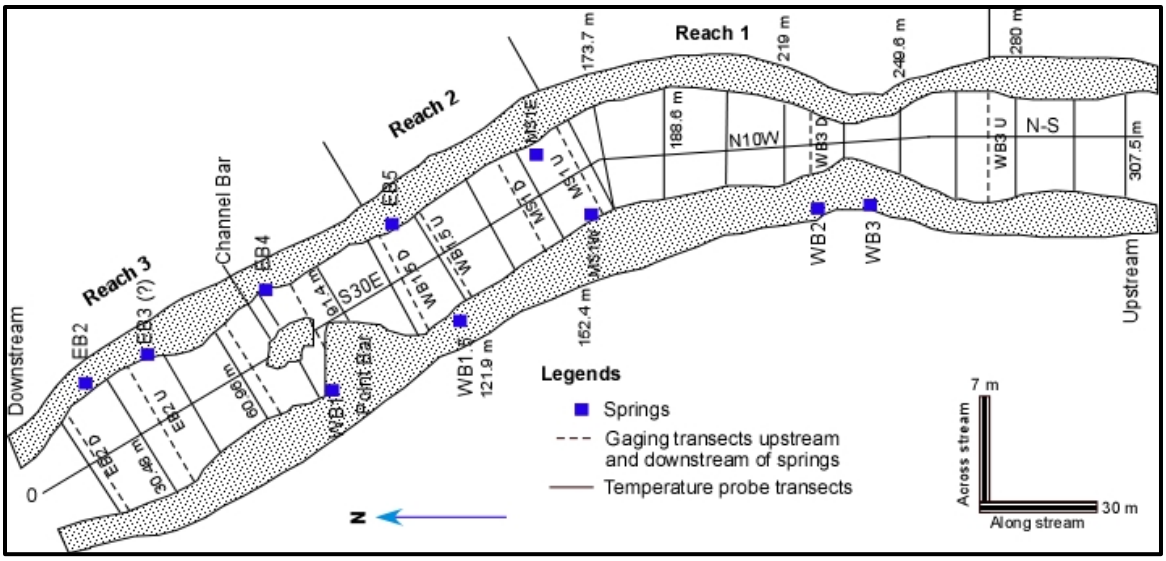

Figure 1.3. Close-up views of the study reach sketched based on the measurements taken during stream gauging and temperature probing.

Multiple studies have delineated and quantified groundwater discharge locations along streams (e.g., Conant, 2004; Conant et al., 2004; LaSage et al., 2008a, Schuetz and Weiler, 2011). Groundwater may discharge diffusely or at focused points (i.e., springs [LaSage et al., 2008a]). Conant (2004) developed a conceptual model on the basis of field investigations carried out along a 60-m long section of the Pine River, Ontario, Canada. He characterized groundwater discharge regimes as short-circuit, high, low to moderate, no discharge, and recharge, depending upon the hydrogeological characteristics of the streambed sediments, rates of discharge, and subsurface geological architecture.

1.2 Study area

1.2.1 Paducah Gaseous Diffusion Plant (PGDP)

Paducah Gaseous Diffusion Plant started producing enriched uranium in 1952. The plant produced more than 600 kg of technetium-99 (^{99}Tc), a by-product of a multi-step process of enriching uranium oxide into uranium hexafluoride, from 1953 to 1976 (LaSage, 2008; Smith, 1984). Similarly, the plant also used TCE as a solvent to decontaminate equipment and as a degreasing agent for about 40 years beginning in 1953 (Clausen, 1997; Clausen, 1992). In 1988, four residential drinking water wells north of PGDP were found to be contaminated with TCE concentrations ranging from 1.5 to 960 µg/L and ^{99}Tc concentrations ranging from 25 to 400 pCi/L (ATSDR [Agency for Toxic Substances and Disease Registry], 2009). Due to the elevated TCE and ^{99}Tc concentrations in groundwater, this site was added to the U. S. Environmental Protection Agency's (USEPA's) National Priorities List (NPL) on May 31, 1994 (http://www.epa.gov/region4/

superfund/sites/fedfacs/pgasdifky.html). Contaminated groundwater occurs in two main plumes (northeast and northwest), which were informally named according to the parts of PGDP from which they originate (Fig. 1.2). Highest detected concentrations of TCE and ^{99}Tc in the northwest plume were 16,000 µg/L and 4800 pCi/L, respectively (Clausen, 1993). TCE concentrations increasing with depth and approaching the solubility limit (1100 mg/L) indicated a dense, non-aqueous-phase liquid source in the area (Clausen, 1993).

Prolonged consumption of water with TCE concentration more than 5 µg/L (the USEPA-defined maximum contaminant level [MCL]) could cause cancer and may damage the liver, kidneys, immune and endocrine systems (USEPA, 2000). Similarly, consumption of water with ^{99}Tc concentrations more than 900 pCi/L (the site-derived MCL) may increase the risk of cancer and other radiation-related health effects (USEPA, 2007). The residential area of potential threat has been identified and an alternative supply of potable water has been provided. Other areas with contaminated surface water are restricted for public access to avoid possible exposure to contaminants.

Several remediation methods have been proposed for the cleanup of the contaminated aquifer and overlying sediments. The proposed methods include dynamic underground stripping, a permeable treatment zone, Lasagna technology, and pump-and-treat (http://www.ananuclear.org). Six-phase soil heating technology was successfully tested at PGDP and the method was approved by DOE (Smart, 2005). Lasagna technology for in-situ soil remediation was also tested in a 6.4 × 9.2 m area at depths up to 13.7 m. The method utilizes electro-osmosis to mobilize the contaminant through the treatment cells between two large electrodes. The test result ended with mixed results of being efficient in some sites and less effective in others (Ho, 1999). The distribution of contaminants vertically at greater depths (up to nearly 30 m) in the source area may be the reason for ineffectiveness of this method at this site (Clausen, 1993). Pump-and-treat has been implemented at several sites in the contaminant plumes and the effectiveness of this method is still being monitored and evaluated (www.ananuclear.org). Placement of a permeable reactive barrier may not be feasible in the up-gradient area because of the depth of contamination. However, it may be applicable in the discharge zone along Little Bayou Creek.

1.2.2 Site hydrogeology

The study area lies in McCracken County in the Gulf Coastal Plain of western Kentucky. The area is underlain by Mississippian carbonate bedrock at depths of about 91–122 m below land surface. The bedrock is overlain by the Upper Cretaceous McNairy Formation, which is characterized by sands, silts and clays of fluvial-deltaic origin (Clausen et al., 1992). The McNairy Formation is successively overlain by the Paleocene

Porters Creek Clay, Miocene to Pleistocene continental deposits (mainly cobbles and gravel), Pleistocene loess and Holocene alluvium (Olive, 1980; Clausen et al., 1992) (Fig. 1.4). The lower and upper continental deposits are equivalent to the Mounds Gravel and the Metropolis Formation, respectively, of southern Illinois (LaSage et al., 2008a). In the study area the Mounds Gravel is termed as the regional gravel aquifer (RGA). The overall trend of groundwater flow in the RGA tends to be north-northeastward towards the Ohio River. However, flow may be redirected by an east-west trending paleochannel beneath PGDP and by northeast-southwest trending faults (Clausen et al., 1992; Langston et al., 1998; LaSage et al., 2008a). Groundwater flow is predominantly vertical in the overlying semi-confining unit (Metropolis Formation). The aquifer is mainly recharged by leakage from the lagoons at PGDP and infiltration after precipitation (LaSage et al., 2008a). Diffuse groundwater discharge appears to occur along tributaries of the Ohio River in the flood plain, such as Bayou and Little Bayou creeks (Fryar et al., 2000). In addition, groundwater discharge is focused through springs in the banks and bed along a ~300-m reach of Little Bayou Creek. These springs appear to coincide with heterogeneities in the Metropolis Formation, and channelization of the creek (i.e., incision into the confining unit) may have promoted groundwater discharge (LaSage et al., 2008a).

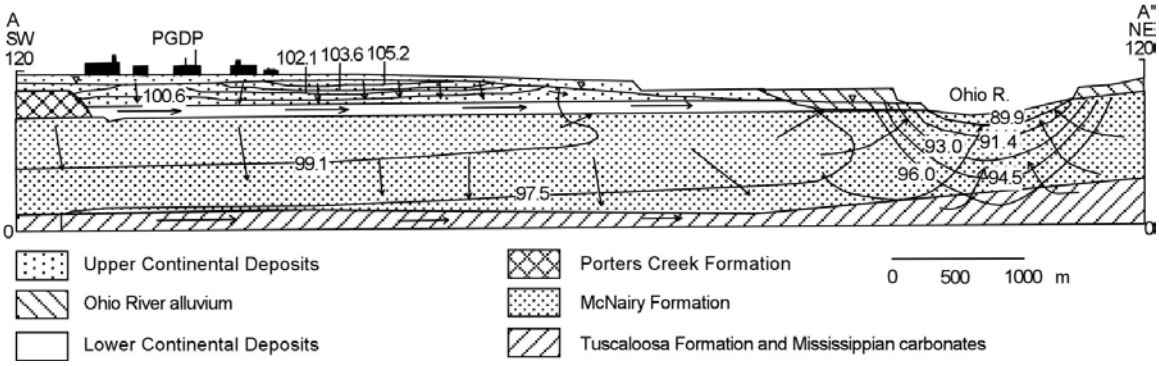

Figure 1.4. Hydrostratigraphic cross-section along PGDP, about a kilometer upstream of the study reach and across Ohio River (Fryar et al., 2000).

Springs along Little Bayou Creek intercept the northwest plume, thus partly "short-circuiting" the flow of contaminated groundwater toward the Ohio River. Samples were collected by LaSage et al. (2008b) from springs (June 1999 through May 2001) and the stream (June 1999–October 2002) for analysis of VOCs and ^{99}Tc (Fig. 1.2). TCE and ^{99}Tc were detectable in surface water downstream of the springs and did not appear to be attenuated within the discharge zone (LaSage et al., 2008b). In the stream samples, the concentrations of contaminants were highest in June (1999 and 2002) and lowest in January (2000, 2001 and 2002), respectively, reflecting seasonal effects. However, LaSage et al. (2008b) did not notice consistent seasonality in TCE and ^{99}Tc concentrations for spring samples. Contaminant concentrations progressively decreased

from upstream springs to downstream springs. There was minimal evidence of reductive biodegradation and TCE sorption to stream bed sediments (LaSage et al., 2008b). Attenuation of TCE was primarily due to volatilization from the stream surface (Mukherjee et al., 2005).

1.3 Previous studies of groundwater-stream interactions

Groundwater discharge to a stream, depending on the geology of the interface, may exhibit focused flow along preferential flowpaths such as fractures, joints or other structural discontinuities, or more diffuse flow along localized inhomogeneities (Fryar et al., 2000; Conant, 2004; LaSage et al., 2008a). The terms groundwater sapping and piping are commonly and interchangeably used to explain mass wasting related to groundwater discharge. However, Howard (1988) noted that "Groundwater sapping, as distinct from piping, is a generic term for weathering and erosion of soils and rocks by emerging groundwater, at least partially involving inter-granular flow (as opposed to the channelized throughflow involved in piping)". Hagerty (1991) described these two terms as a coupled mechanism in the development and modification of landscapes during the process of groundwater exfiltration. Groundwater sapping can produce valleys with steep sidewalls and flat bases, such as Box Canyon, Idaho (Kochel and Piper, 1986; Lamb, 2008). Laity and Malin (1985) identified groundwater sapping as a primary contributor to the development of theater-headed canyons in the Navajo Sandstone in the Colorado Plateau. Groundwater sapping was also found to be one of the principal contributors in shaping the Western Desert of Egypt (Luo, 1997).

Various studies have evaluated the reliability and accuracy of different measurement methods to characterize groundwater-surface water interactions (Kalbus, 2006). Groundwater discharge to streams is not constant throughout the year; it can vary seasonally, if not daily (LaSage et al., 2008a). A gaining segment of a stream at one time of the year may become losing or neutral at another time of the year (Winter et al., 1998). Frequently-used techniques to quantify exchange between groundwater and surface water include differential velocity gaging (seepage runs) and tracer dilution gaging at up- and downstream ends of the stream segment of interest (Kalbus, 2006). Stream discharge can be measured directly by wading along a stream cross-section using a current meter with top-setting rods (velocity-area method). Carter (1968), Kilpatrick (1985) and Rantz (1982) have provided greater details on measuring stream discharge using current meters and tracers. Effects of downstream advection within the hyporheic zone (i.e., downwelling and upwelling) can be minimized by conducting in-stream tracer tests using a chemically conservative solute (e.g., an anion or fluorescent dye) that can be readily detected at concentrations above background (Kilpatrick and Cobb, 1985; Kilpatrick and Wilson, 1989; Mukherjee et al., 2005). Measurement of breakthrough curves allows calculation of inflows corresponding to dilution of the tracer. The difference in discharge

between down- and upstream ends of the reach or stream segment is considered as the net exchange between surface water and groundwater, provided that all other components of lateral inflow and outflow have been taken into account. However, this approach can underestimate or overestimate inflows if advection within the hyporheic zone is significant. Zellweger et al. (1989) and Harvey et al. (2000) have recommended conjunctive use of velocity and dilution gaging techniques to isolate the net exchange into inflow and outflow. Because of the limitations and uncertainty inherent in each quantification method, integrated use of techniques has become popular. For example, McCallum et al. (2012) used differential flow gauging and water chemistry data to quantify net and gross groundwater inflows at three different sites at eastern Australia. If concentrations of an ambient, conservative solute differ significantly among groundwater, upstream water and downstream water, unmixing calculations can be used to estimate the fraction of groundwater inflow.

Groundwater discharge can be identified at different spatial scales by different means. At the sub-meter to meter scale, discharge sites can be located by temperature probing during summer and winter, when temperature contrasts between groundwater and stream water are pronounced (Conant, 2004; LaSage et al., 2008a). In addition, distributed fiber-optic temperature sensing (DTS) enables identification of thermal anomalies associated with groundwater discharge (Selker et al., 2006). Discharge (Q) can be measured using conventional manual techniques (i.e., a stopwatch and container [bucket and/or graduated cylinder] or cutthroat flume) where spring orifices occur along the bank or by using seepage meters in the stream bed (LaSage et al., 2008a; Kennedy et al., 2010). Seepage meters have been widely used since the 1970s to measure point-scale groundwater inflow into surface-water bodies (Lee, 1977). However, the accuracy of these meters has been questioned (Fryar et al., 2000; Libelo, 1994; Murdoch, 2003; Shaw and Prepas, 1989). Vertical groundwater fluxes (q) can be calculated using streambed piezometers or potentiomanometers to measure hydraulic gradient and hydraulic conductivity for Darcy's law calculations (Kennedy et al., 2007, 2010). Alternatively, q can be calculated by recording time series of T fluctuations at different depths below the bed and fitting the results to a 1-D solution of the coupled advection-conduction heat equation (Hatch et al., 2006; Shanafield et al., 2011).

1.4 Purpose of the study and hypotheses

Natural streams are dynamic systems and fluvial morphology is likely to change over time and space. This study examines variability in groundwater and contaminant discharge patterns along a channelized stream at various timescales (seasonal, annual, and decadal) and the extent to which the discharge sites are spatially persistent. Spatial scales of study include individual springs (meter scale), groups of springs at the sub-reach scale (tens of meters), and the reach scale (hundreds of meters). Because the stream is located in unlithified sediments, discharge rates of springs could fluctuate with soil

piping and collapse along joints in fractured clay. This study addresses the following questions:

(1) Where do groundwater and contaminants discharge along Little Bayou Creek?

(2) How have locations, timing, and amounts of groundwater discharge changed since previous studies (1999-2002)?

(3) How have contaminant concentrations and fluxes changed?

In particular, this study aims to address data gaps from previous studies at the site, including monitoring of groundwater and contaminant fluxes at finer spatial resolution and continuous monitoring of groundwater flux and temperature at selected points. Based on previous studies, I hypothesize that:

- In comparison with stream temperature, groundwater temperature is likely to be relatively constant, which will enable delineation of focused discharge.
- Groundwater discharge along the study reach is the result of lateral inhomogeneity and structural discontinuity in the semi-confining unit (Metropolis Formation). Groundwater discharge locations associated with joints and fractures along the confining unit may persist longer than the groundwater discharge locations associated with lateral inhomogeneity. So, some sites of focused discharge will persist over a decade, whereas others will not.
- Contaminants are introduced into the creek mainly through focused discharge.

Chapter 2. Methods

2.1. Differential stream gauging

Reach to sub-reach scale groundwater discharge can be determined using the differential gauging (seepage runs) technique (Cey et al., 1998; Ruehl et al., 2006; McCallum et al., 2012; Kikuchi et al., 2012). Ten locations were gauged along a ~300-m reach of Little Bayou Creek using a current meter and top-setting rods (Appendix I) (Marsh-McBirney, Frederick, Maryland). The field measurements were conducted on October 22, 2010; January 23, 2011; June 23, 2011; October 22, 2011; and February 19, 2012 to study the seasonality in groundwater discharge. Gauging occurred when runoff was assumed to be negligible. Five pairs of transects were chosen upstream and downstream of visible springs. Velocity and the stream depth were measured at 6-inch (15-cm) intervals where the channel was relatively wide (≳ 20 feet [6 m]) and at 3-inch (7.5-cm) intervals where the channel was narrow except for October 2010, when 1-foot (30-cm) and 6-inch intervals were used. Net discharge was calculated between each pair of gauging transects.

Figure 2.1. Stream gauging in October 2010 along transect EB2U, upstream of farthest downstream spring EB2, which is located behind exposed roots on far bank.

2.2. Spring discharge measurements

Spring discharge was measured manually whenever and wherever practically feasible during different seasons. In most cases, spring water was collected in a bucket for a certain time, depending upon the inflow amount, and the volume of the collected water was measured using a graduated cylinder. This process was repeated at least three times for each spring and the average discharge rate was calculated. In February 2012, we used a cut-throat flume (Baski Inc., Denver, Colorado) for comparison with bucket-and-stopwatch measurements. However, only two springs met the required criteria for using the flume. Discharge could not be estimated with the flume for springs with upstream gauge height less than 0.11 feet (3.4 cm). It was also impractical to maintain a ratio of downstream to upstream gauge height less than 0.5 for most of the springs.

2.3 Dye dilution tracer test

Rhodamine WT dye solution (RWT) was used to measure streamflow dilution along the study reach. Advantages of RWT as a solute tracer include its strong fluorescence, negligible adverse environmental impact, and detectability at very low concentrations (1µg/L) (Wilson et al., 1986). Dye dilution tracer tests were conducted on January 22, 2011; June 24, 2011; October 24, 2011; and February 20, 2012. In each case, 150 mL of RWT solution was added to each of two carboys containing 20 L of stream water separately and manually mixed. The carboys were poured across the width of the stream at the upstream end of the study reach, which took ~ 1 minute. Samples were collected subsequently at four downstream locations (WB3U, MS1U, WB1.5, and EB2D). At each site, the first grab sample was collected midstream, using a 40-mL amber glass vial with a screw-on plastic cap, prior to arrival of the visible dye cloud. Samples were collected at approximately the same location when the cloud arrived and at intervals of 2 minutes to 10 minutes thereafter, depending on the distance from the injection point and the time since injection. At the end of each tracer test, samples were refrigerated until approximately 24 hours prior to analysis, when they were allowed to warm to room temperature along with the standard prepared for analysis. October 2011 and February 2012 samples were analyzed within a week of collection. June and January 2011 samples were analyzed within 3 and 2 weeks, respectively, of collection. Because samples had been refrigerated in amber glass vials in the dark, degradation was considered to be negligible (Smart, 1977).

Figure 2.2. Rhodamine WT dye cloud moving downstream. Photograph taken in January 2011 during dye dilution tracer test.

Standards were prepared following U.S. Geological Survey guidelines (Wilson et al., 1986), except that a 400 µg/L working solution (instead of the 100 µg/L solution mentioned in the guidelines) was used to accommodate expected higher concentrations in our samples (Table 2.1). The final working solution was obtained by three-step serial dilution as follows:

$$Cf = CsSG\left(\left[\frac{V_d}{V_w + V_d}\right] \times \left[\frac{V_d}{V_w + V_d}\right] \times \left[\frac{V_d}{V_w + V_d}\right]\right)$$

where Cf = final concentration of standard after third step of serial dilution; Cs = concentration of the dye solution indicated by the manufacturer; V_d and V_w = volume of dye and of water, respectively; and SG = specific gravity of the initial dye solution. The stock solution used in our field test was 5 % RWT with specific gravity 1.03 ± 0.05. From the working solution, 12 standards (300, 200, 100, 60, 40, 24, 16, 8, 4, 2, 1, and 0.4 µg/L) were prepared by stepwise dilution as follows:

$$Cn = Ci\left[\frac{Wd}{Vw + Vd}\right] = CiSG\left[\frac{Vd}{Vw + Vd}\right]$$

where Ci and Cn = initial and new concentrations, respectively, and Wd = weight of the initial solution. These standards were used to develop a calibration curve and samples were analyzed on a Varian Cary Eclipse fluorescence spectrophotometer (Agilent Technologies, www.agilent.com) at the Kentucky Geological Survey.

Table 2.1. Three-step serial dilutions for preparation of working solution (modified from Wilson et al., 1986).

Dye used in test	Serial dilutions							Working Solution, in µg/L
	First			Second		Third		
		V_d (mL)	V_w (mL)	V_d (mL)	V_w (mL)	V_d (mL)	V_w (mL)	
Rhodamine WT (5 percent; SG 1.03 ± 0.05)	(a)	50	3,792	20	3,500	20	3,500	400
	(b)	25	2,585	20	3,000	20	3,000	400
	(c)	20	2,068	20	3,000	20	3,000	400
	(d)	20	1,158	10	2,000	10	2,000	400

2.4 One-dimensional mathematical model

The mathematical simulation model OTIS (One-dimensional transport with inflow and storage [Runkel, 1998]), was used to simulate dye concentrations at different downstream locations from injection points. This program solves the modified governing advection-dispersion equation for solute (mass) transport using a Crank-Nicolson finite-difference solution. OTIS-P, an upgraded version of OTIS, with the added capability of automated parameter estimation using non-linear regression was used for the simulation.

The model primarily assumes that changes in concentration occur only along the stream and that concentrations are uniform with depth and width. Additional assumptions were made separately for main channel and storage zone areas. The model also assumes that the change in solute concentrations along the main channel is a result of physical processes (such as advection, dispersion, lateral inflow, lateral outflow, and transient storage) and chemical processes (such as sorption and first-order decay). Model parameters related to physical and chemical processes may be spatially variable and the model parameters associated with advection and lateral inflow may be temporally variable. The model further assumes that the change in concentration in storage zone is the result of sorption and first-order decay.

Dye concentrations determined by spectrophotometer were used to simulate the concentrations at successive downstream sampling locations and then to estimate parameters (i.e. main channel cross-sectional area, storage zone cross-sectional area, dispersion coefficient and storage zone exchange coefficient) using OTIS-P [Runkel, 1998]).

2.5 Sampling and field parameter measurement

Groundwater and surface-water samples were collected during each round of field work (January 2011, June 2011, October 2011 and February 2012). The samples were collected simultaneously with stream gaging except for January 2011, when surface water

sampling was done before dye tracing on January 22, followed by stream gaging on January 23. Groundwater (spring) sampling was done on January 24 along with field parameter measurements and spring discharge measurements. Samples for TCE and other volatile organic compounds (VOCs) were collected in 40-mL amber glass vials with Teflon-lined screw caps (Fig. 2.3). The samples were collected by submerging and facing the vials downstream to minimize suspended particles in the samples. A positive meniscus was maintained after addition of 4-5 drops of 6N HCl as a preservative and the vial was carefully capped to avoid any gas bubbles in the samples. Finally, the sample bottle was inverted to confirm the absence of bubbles. Each sample was collected in duplicate and two field blanks were also collected during each sampling round. Technetium-99 samples were collected in 1-L high-density polyethylene (HDPE) bottles following the same procedure as for VOC samples (Fig. 2.3), but without preservatives. VOC samples were refrigerated and submitted within 1 week for analysis by USEPA method 8260B (gas chromatography-mass spectrometry) at McCoy and McCoy Laboratories (Madisonville, Kentucky). Technetium-99 samples were analyzed by liquid scintillation counting in September 2012 at Eberline Services (Oak Ridge, Tennessee).

Figure 2.3. Sample collected for VOCs and ^{99}Tc analyses in January 2011. Samples resting over the ice sheet on top of the stream surface.

Temperature of groundwater and surface water was measured using a YSI multifunction meter (YSI, Yellow Springs, Ohio) at selected locations during October 2010, January 2011, June 2011, October 2011, and February 2012. Dissolved oxygen (DO) was measured using the YSI meter in October 2010 for springs and stream water, and by

Winkler titration (Wood, 1981) using a Hach kit (Hach Company, Loveland, Colorado) for springs in June 2011, October 2011, and February 2012.

2.6 Deployment of logging thermistors and transducers

At three springs along the study reach (EB2, MS1W, and WB3), temperatures were continuously monitored at 5-minute intervals from September 22, 2011, to February 19, 2012, using HOBO U22 Water Temp Pro v2 dataloggers (Onset Computer Corporation, Bourne, Massachusetts). Each HOBO was cabled to a piece of ⅜-inch (1-cm) iron rebar pounded into the bank adjacent to the spring (see Section 2.9) and was anchored by a brick. Prior to deployment, the HOBOs were programmed using proprietary software (HOBOware®). The recorded data were downloaded using an optical USB communications interface.

Hydraulic heads and groundwater temperatures were also continuously recorded in two monitoring wells (LB6Y and LB6Z) along the west bank of the creek at the downstream end of the study reach using Levelogger Edge sensors (Solinst Canada Ltd., Georgetown, Ontario). These wells are cased by 2 inch (5.08 cm) PVC pipe (external diameter 2.375 inch [6.03 cm], thickness 0.154 inch [0.39 cm]) with perforated extension. Barometric pressure was continuously recorded above the water table in another monitoring well (BB3Y), located ~ 3.6 km to the west, using a Solinst Barologger. Readings were taken at 5-minute intervals from September 23, 2011 to February 8, 2012. Data were downloaded via an optic shuttle using proprietary software, which enabled hydraulic heads to be compensated for barometric pressure fluctuations.

2.7 Slug tests

Slug tests were performed on July 5-6, 2012, in monitoring wells LB6Y and LB6Z. Iron rebar 2 feet (0.61 m) long and 1 inch (2.5 cm) diameter was inserted into each well and hydraulic head was monitored at 1-second intervals using Levelogger Edge sensors. As before, hydraulic heads were corrected for barometric pressure fluctuations. The drawdown versus time record from the point of maximum displacement in water level after the slug insertion was used to calculate the hydraulic conductivity (K) following the Hvorslev method (Hvorslev, 1951; Schwartz and Zhang, 2003 [Table 12.1]). According to this method, each drawdown value is divided by the maximum value. The drawdown ratio is plotted on a log scale versus time on a linear scale and a best-fit line is generated. Corresponding head ratios (H_1 and H_2) for times t_1 and t_2 are picked from the best-fit line and used to calculate K according to the following equation:

$$K = \frac{R^2}{2L(t_2 - t_1)} \ln\left[\frac{L}{R}\right] \ln\left[\frac{H_1}{H_2}\right]$$

$$for\ \frac{L}{R} > 8$$

where L is the length of the well screen and R is the radius of the well.

2.8 Temperature probing

Streambed temperature was measured on a grid using a 4-foot (1.2-m) long stainless steel probe connected to a YSI digital thermometer with 0.01°C temperature resolution (Fig. 2.4). Temperature probing was conducted along transects at intervals of 10 feet (3 m) along the stream and 3 feet (0.9 m) across the stream. At each point, temperatures were measured at the sediment-water interface and at the maximum depth (refusal depth) to which the probe could be inserted manually (LaSage et al., 2008a). This approach allows determination of streambed topography beneath mobile bed sediment.

Measurements were made along a 307-308 m-long reach during January 4-8, 2011 (1638 points), and August 5-9, 2011 (1396 points). Differences in numbers of points for each set of measurements reflect seasonal differences in stream width (probing did not extend beyond the wetted perimeter of the stream). Because of bends along the reach, it was subdivided into three segments (reaches 1, 2, and 3) for mapping using Surfer 9 (Golden Software, Golden, Colorado). Natural neighbor interpolation was used to create maps of temperature anomalies and streambed topography.

Figure 2.4. Temperature probing in January 2011 showing groundwater inflow location with anomalously higher temperature (12.10°C) when the average stream temperature was 4°C.

2.9 Distributed temperature sensing

Distributed temperature sensing (DTS) system is now being used in fields other than its intended primary application in fire and pipeline monitoring because of its ability to

measure temperature continuously in space and time (Tyler, 2009). DTS may be applied wherever regular monitoring of temperature is an issue. In hydrology, especially in surface-groundwater interactions, researchers are attracted to this technology because of its effectiveness in measuring temperature within 0.1^{o}C at sub-minute temporal resolution and sub-meter spatial resolution (Selker, 2006). Along stream segments (up to 30 km) the temperature data can be utilized to pin-point focused groundwater inflow locations very conveniently and efficiently (Lowry, 2007).

2.9.1 Basic principles

DTS is used to measure temperature along a fiber optic cable based on the time of travel and behavior of a reflected (backscattered) laser light pulse (Selker, 2006; Smolen and Spek, 2003). Three main techniques are commonly employed: fiber Bragg grating, Brillouin scattering, and Raman scattering (Selker, 2006). In the fiber Bragg grating technique, change in temperature is related to the expansion and contraction in original gratings in the cable, as adsorption of light of specific frequency depends on the spacing between gratings. Measurement precision for this method has reached 0.1^{o}C (Rao, 1997). Brillouin scattering is a non-elastic type that produces backscattered light of different wavelengths than the incident light pulse. Backscattered light with wavelength greater and less than the incident laser light is respectively termed as Stokes and anti-Stokes light (Fig. 2.5). A slight change in the density of the fiber optic cable results in a change of acoustic velocity, which affects the wavelength shift of Stokes and anti-Stokes scattering (Selker, 2006). Stokes and anti-Stokes scattering is then analyzed to determine the temperature along the cable. This method can yield temperature resolution of $\pm 0.1^{o}$C at 0.5 to 1.0 m spatial resolution and 1-minute scale temporal resolution depending upon the integration time (Selker, 2006). Raman scattering is probably the most frequently used DTS technique in hydrologic investigations. This method utilizes the change in optical properties when a laser light pulse travels along an optical fiber. Part of the light may be reflected, adsorbed, reemitted, or collectively backscattered. In this process, the backscattered light may have higher (anti-Stokes backscatter) or lower (Stokes backscatter) frequency than the incident light (Selker, 2006).

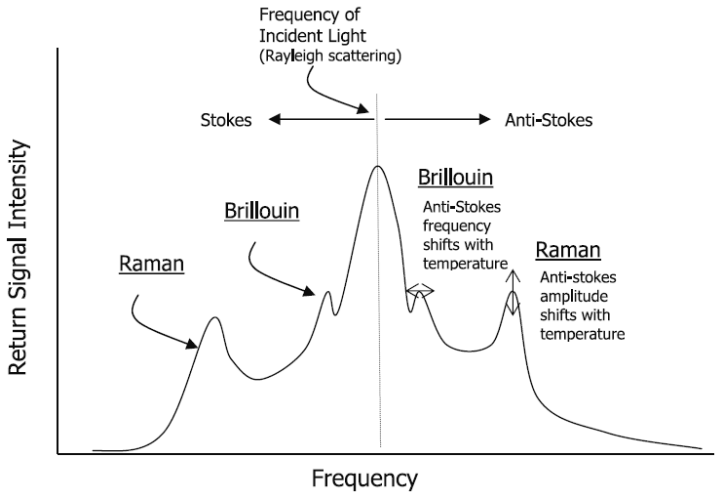

Figure 2.5. Rayleigh, Raman, and Brillouin return scattering intensity below (Stokes) and above (anti-Stokes) the frequency of the injected light (Selker et al., 2006).

While Stokes and anti-Stokes backscatters are a function of intensity of illumination, anti-Stokes backscatter responds exponentially to changes in optical-fiber temperature (Selker, 2006). The fraction of anti-Stokes scattering at higher temperature will increase compared to the Stokes scattering because of the greater number of electrons in high-energy states. Therefore, the ratio of anti-Stokes to Stokes signal will produce a quantity that is dependent solely on temperature changes along the fiber and the sampling location can be determined by the two-way travel time of the light pulse (Tyler, 2009). The precision of temperature measurement with this method largely depends on the integration time. Precision of 0.1^{o}C can be achieved for a 1000-m layout with 1-m spatial resolution and 1 minute integration time with the current technology, and precision may increase to the level of 0.02 ^{o}C for 1-hour integration time (Selker, 2006).

2.9.2 Instrumentation and field layout

An Oryx DTS unit (Sensornet, Elstree, U.K.) was rented from the Center for Transformative Environmental Monitoring Programs (http://ctemps.org/instruments). This is a robust unit which runs on solar power or 110/220 VAC and is designed to operate in adverse field conditions (Fig. 2.6). The system needs two additional 70 amp-hour deep discharge batteries besides the solar panels provided by CTEMPs. The DTS unit also contains 32 MB on-board memory, which can store about 600 separate measurements (Oryx, 2007). The system is equipped with a laptop loaded with the Oryx software where raw data are processed and finally stored. Stored data can be accessed and downloaded remotely via a 3G compatible cellphone link.

Figure 2.6. Distributed temperature sensing (DTS) equipment deployed in the field in Sept. – Oct. 2011.

Fiber-optic cable of 1000 m length was laid out along our study reach from September 22, 2011, through October 10, 2011. The DTS unit was installed at the flood plain close to the east bank of the creek. The fiber optic cable was laid out along the west bank (near the sediment-water interface) toward the upstream end of the study reach and looped around a tree, then continued along the east bank before connecting to the DTS unit. The cable was anchored to the streambed at various locations with loops cut from baling wire. The cable was also coiled at the springs where Hobos were deployed to perform independent temperature measurements. Calibration baths were set up at the two extremes of the cable in two coolers: one contained water (ambient bath) and the other contained a water-ice mixture (ice bath). Approximately 8-10 m of the DTS cable was coiled around a plastic bracket to avoid possible contact with the cooler wall and placed inside each calibration bath. Each cooler contained a bubbler to maintain uniform temperature throughout the measurement period. Sensornet Oryx software installed in the onboard laptop (Oryx, 2007) was used to configure the DTS system to take double-ended measurements along every meter of the cable at 5-minute intervals.

2.9.3 Data processing

Downloaded field data were transferred to an Excel spreadsheet using a MATLAB script written especially for DTS data. Besides the automated calibration performed by the DTS system, the recorded temperature data were calibrated using PT100 platinum temperature sensors in the calibration baths. Because the PT100 in the ice bath was not recording reference temperature correctly, we used the reference temperature record for the ambient

bath to calibrate the entire data set. The locations where the cable was out of water along the east and west banks were noted. After DTS recording was finished, the cable was found to be offset from its initial layout position by ~ 2 m. The temperatures recorded along the creek by DTS were segmented to match with our three sub-reaches defined for the temperature probing and dye tracing studies. Temperature data were processed on a daily basis and the difference between the maximum and minimum temperature (ΔT) was determined for each 24-hour period each meter along the cable. Finally, average values of ΔT for the 9-day monitoring period were calculated for each measurement location.

2.10 Stream channel morphology and stake survey

Iron rebar of ⅜-inch (0.95 cm) diameter was pounded into the bank at eight locations along the study reach to assess evolution in channel morphology between January 2011 and February 2012. Each of these stakes was installed adjacent to previously identified bank springs (LaSage et al., 2008a). The heights of the top of each stake above the stream and the bank were measured using a folding rule in January, June, and October 2011 and February 2012. We used Impulse 200 LR laser surveying equipment (Laser Technology, Centennial, Colorado) to measure the elevation of the top of the stake above mean sea level referenced to a nearby benchmark. We used these elevation data to recalculate the stage of the stream and bank elevation relative to the individual stakes.

Figure 2.7. Pounding the iron rebar close to the east bank spring EB4 to monitor changes in channel morphology (October 2010).

Chapter 3. Results

3.1 Effects of precipitation on surface and groundwater hydrology

Daily precipitation data for the study period (October 2010 – February 2012) were obtained from the National Weather Service station at Barkley Airport (Paducah) (http://wwwagwx.ca.uky.edu) (Fig. 3.1a). Daily discharge data for the Ohio River and Massac Creek were obtained from the USGS gauging stations 03611500 and 03611260, respectively (http://waterdata.usgs.gov) (Fig. 3.1b). The Ohio River station drains an area of ~ 526,000 km^2 while the Massac Creek station drains only about 37.5 km^2. The gauging stations on Massac Creek and the Ohio River are ~ 5.6 km and 9.7 km, respectively, from Barkley Airport. Massac Creek responded almost synchronously to all precipitation events. Maximum precipitation (10.29 cm) and the maximum discharge (44.17 m^3/s) along Massac Creek were both recorded April 24, 2011. Average annual (study period) precipitation was 0.43 cm while average discharge was 0.77 m^3/s. The response of Ohio River to precipitation was similar to that of Massac Creek, but with a time lag of about 10 days. Maximum discharge (35,679 m^3/s) during the study period was measured May 5–7, 2011, and minimum discharge was 753.23 m^3/s on October 26, 2010, with an average of 9878 $m^3/$ s. The catchment area for the Ohio River gauge is very large and it responds to regional precipitation as well as local precipitation.

The hydrograph separation program WHAT (https://engineering.purdue.edu/~what) was used to estimate baseflow for Massac Creek and the Ohio River. Average baseflow for Massac Creek during the entire study period was 0.2 m^3/s, with a maximum of 5.6 m^3/s on April 27, 2011, and a minimum of 0.0014 m^3/s on October 2, 2010 (Fig. 3.2a). The average baseflow for the Ohio River was 7065 m^3/s with a maximum of 24,590 m^3/s on May 13, 2011 and minimum of 127.7 m^3/s on October 2, 2010 (Fig. 3.2b).

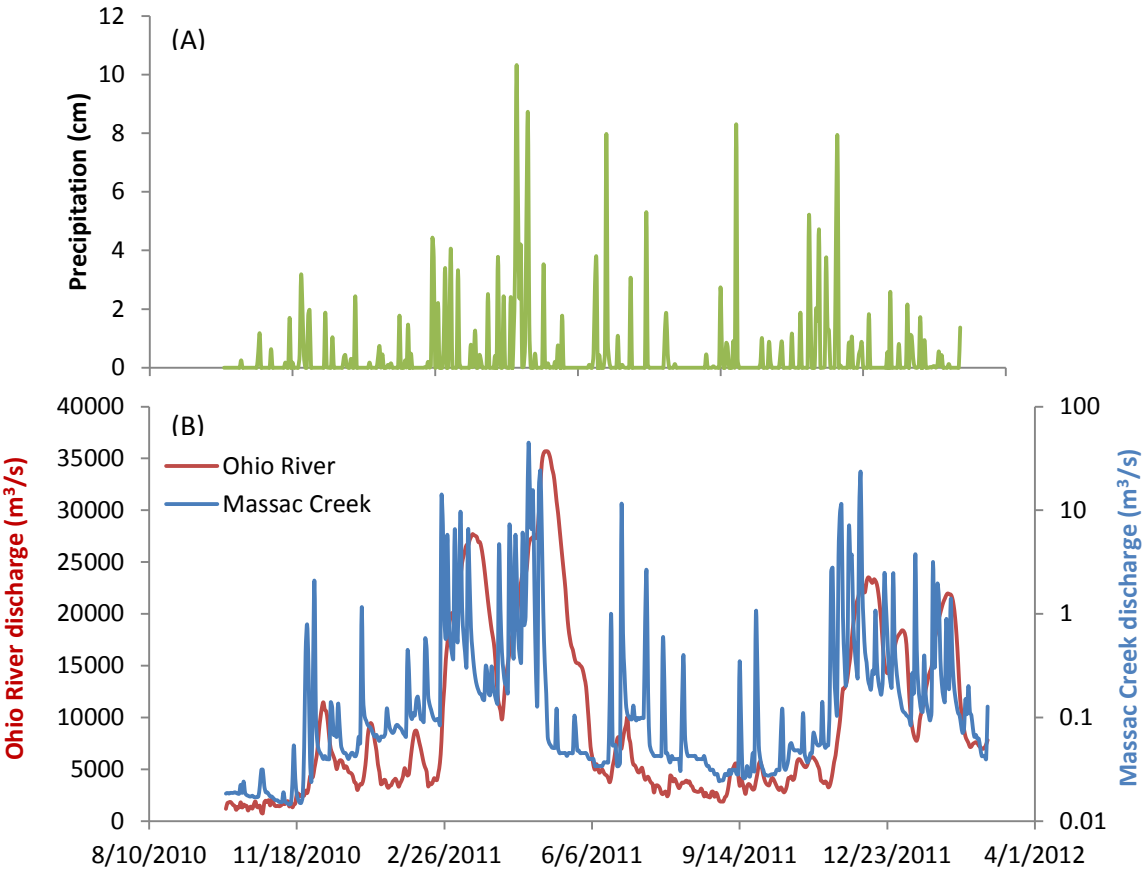

Figure 3.1. Ohio River and Massac Creek discharge (B) representing regional and local (nearby Little Bayou Creek) response to precipitation (A).

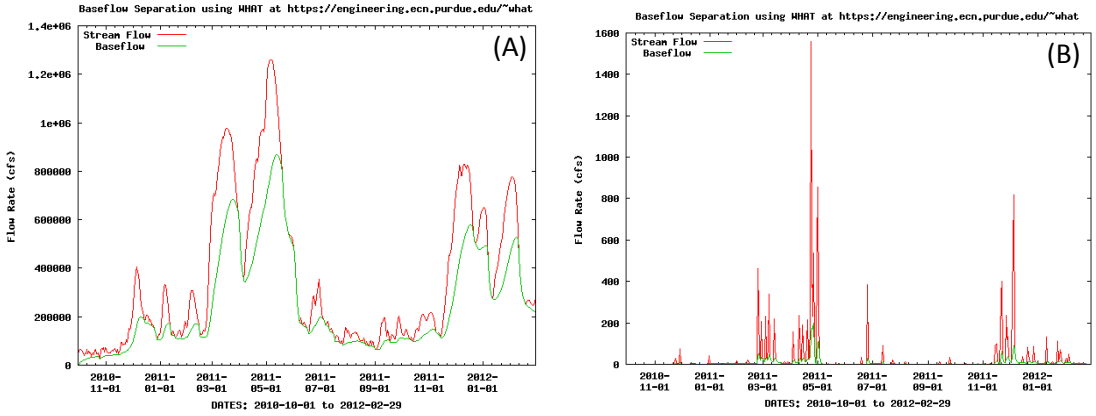

Figure 3.2. Baseflow of Ohio River (top) and Massac Creek (bottom) separated from stream flow for the study period. Values are shown in cfs (ft^3/s; 1.00 cfs = 0.0283 m^3/s).

Precipitation at Barkley Airport was broadly similar to that recorded at two nearby meteorological stations during the study period (Fig. 3.3). The TVA Shawnee Plant maintains a meteorological station ~ 400 m from our study reach (J. M. Boggs, TVA,

personal communication) and the National Weather Service operates a station at Brookport Dam on the Ohio River ~ 14 km to the east (Steve Hampson, KRCEE, personal communication). Most rainfall events were captured by all three stations, but the rainfall intensities varied. Precipitation totals recorded at the Shawnee station during the 30 days prior to each stream-gauging run were 1.0 cm (October 23, 2010), 3.4 cm (January 23, 2011), 8.4 cm (June 23, 2011), 6.5 cm (October 22, 2011), and 33.6 cm (February 19, 2012).

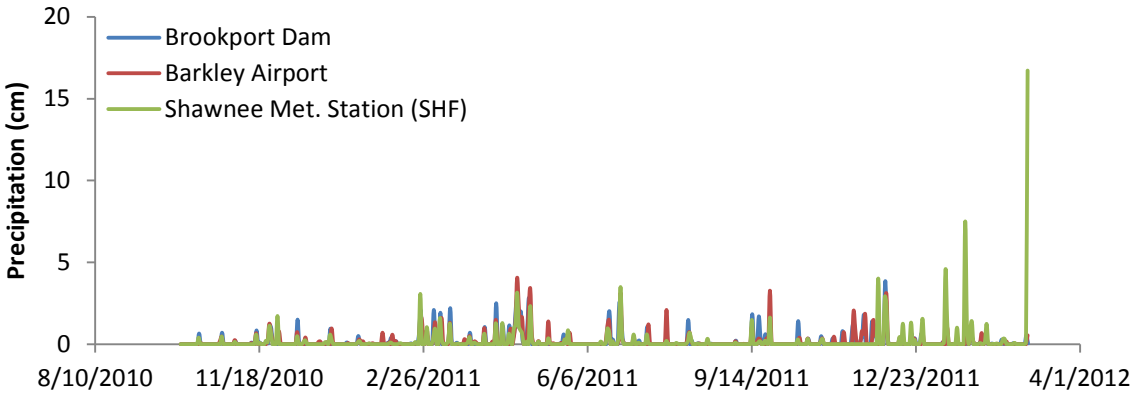

Figure 3.3. Precipitation recorded at three nearby meteorological stations.

Temporal trends of the Ohio River stage and the water levels in the monitoring wells were generally synchronous (i.e., there was no time lag), which suggests strong inter-connection between the two systems. However, during early October to early November 2011 the changes in hydraulic heads and stage did not correspond (Fig. 3.4). The higher Ohio River stage during most of the study period indicates either hydraulic-gradient reversal or the location of the USGS station upstream of the discharge area for these monitoring wells. In contrast, cross-correlation analyses indicate that water-level changes in the wells lag precipitation recorded at Shawnee plant by about 3 to 4 days (Fig. 3.5).

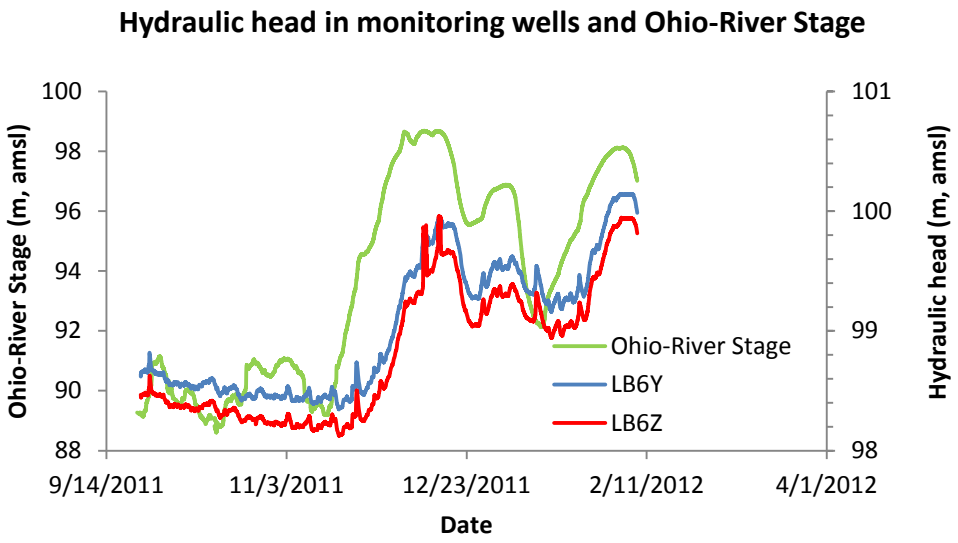

Figure 3.4. Ohio River stage and hydraulic heads in the monitoring wells at the downstream end of the study reach.

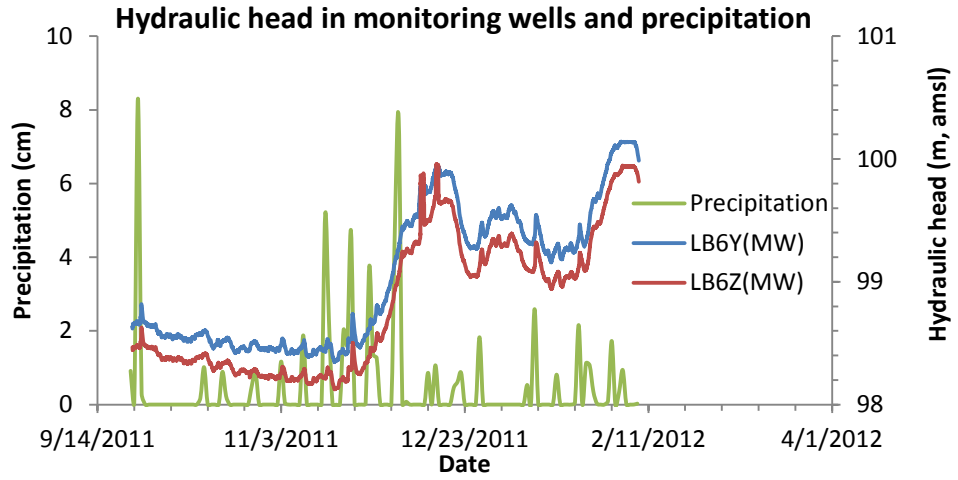

Figure 3.5. Precipitation records at Shawnee plant station and monitoring well response.

3.2 Stream discharge measurement by velocity-area method

Discharge measurements were made when no rainfall had been recorded for at least 24 hr at all three nearby weather stations (October 23, 2010: no rainfall for 10 days; January 23, 2011: no rainfall for 48 hr; June 23, 2011: no rainfall for at least 24 hr; October 22, 2011: no rainfall for at least 48 hr; February 19, 2012: no rainfall for at least 48 hr at Barkley and Shawnee and for at least 72 hr at Brookport). These results support the inference that gauging occurred when the stream was at baseflow. For all measurement

periods, discharge measured at the farthest downstream site (EB2D) was always greater than the discharge measured at the farthest upstream site (WB3U), even accounting for the calculated measurement error (Appendix II), indicating the whole reach was gaining (Fig. 3.6). For a few of the intermediate sections, downstream discharge was less than the upstream discharge, but all these differences were within measurement error. Increase in discharge between WB3U and EB2D was 0.51 m^3/min in October 2010, 0.55 m^3/min in January 2011, 2.09 m^3/min in June 2011, 0.73 m^3/min in October 2011, and 2.65 m^3/min in February 2012. The increases were greatest in June and February, which is consistent with greater precipitation within the 30 days preceding gauging than at other times when gauging occurred. A comparison of gauged discharge at EB2D with calculated baseflow of Massac Creek for the same dates and with total monthly precipitation indicates that baseflow along both creeks tracks precipitation (Fig. 3.7). Stream discharges measured during 1999–2003, which were also inferred to be baseflow (except for January 2003 [Mukherjee et al., 2005]), were compared to discharges measured during 2010–2012 (Figs. 3.8, 3.9). In general, streamflow gains were also observed along the study reach during 1999–2001 (LaSage et al., 2008a). No inference about gaining conditions during 2002–2003 can be drawn because gauging did not occur upstream of EB3D (Mukherjee et al., 2005). Seasonality is reflected in stream discharge during both measurement periods, with peak discharge in late winter to late spring and minimum discharge in fall to early winter.

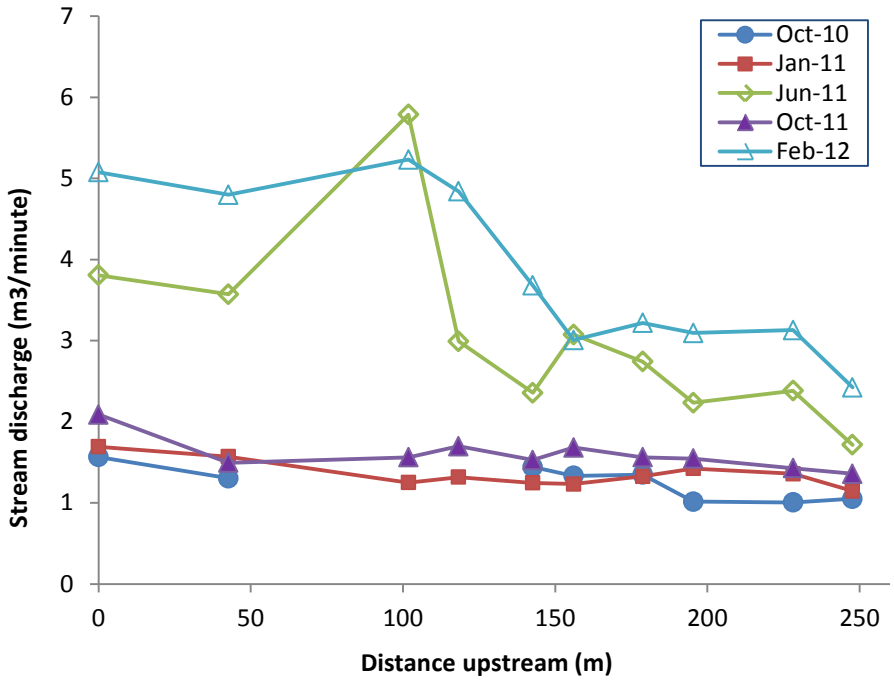

Figure 3.6. Stream discharge measured at ten different locations along the study reach. Discharge increased downstream in all measurement periods.

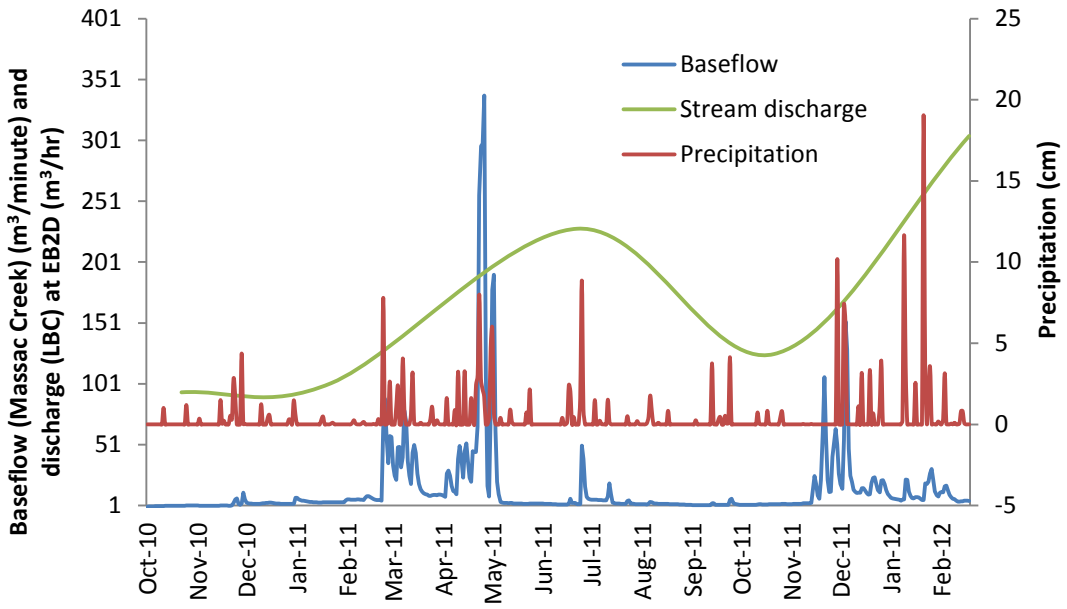

Figure 3.7. Discharge at EB2D broadly tracks baseflow of Massac Creek and precipitation during the study period.

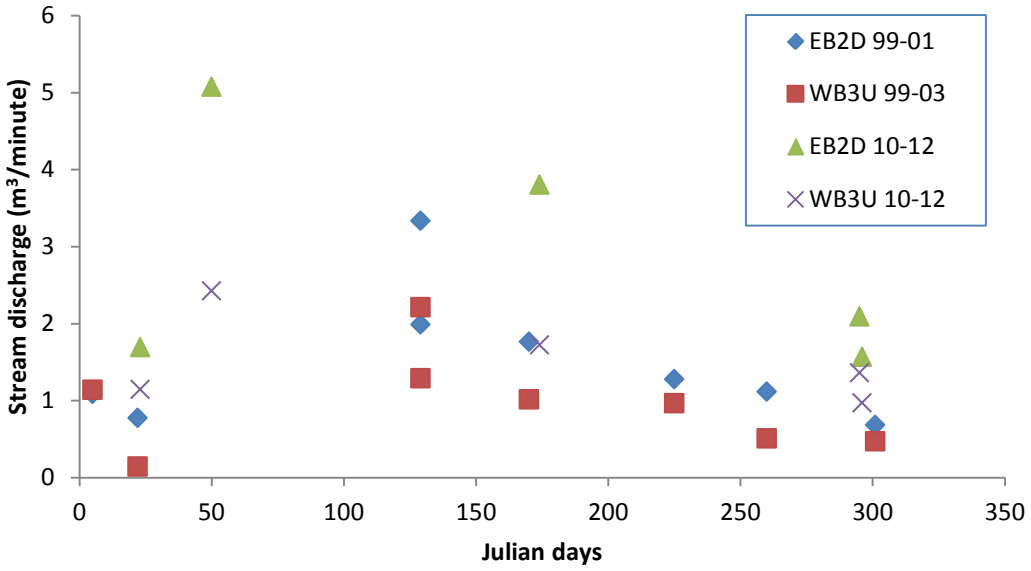

Figure 3.8. Stream discharge showing seasonality in both 1999–2001 and 2010–2012 stream gauging.

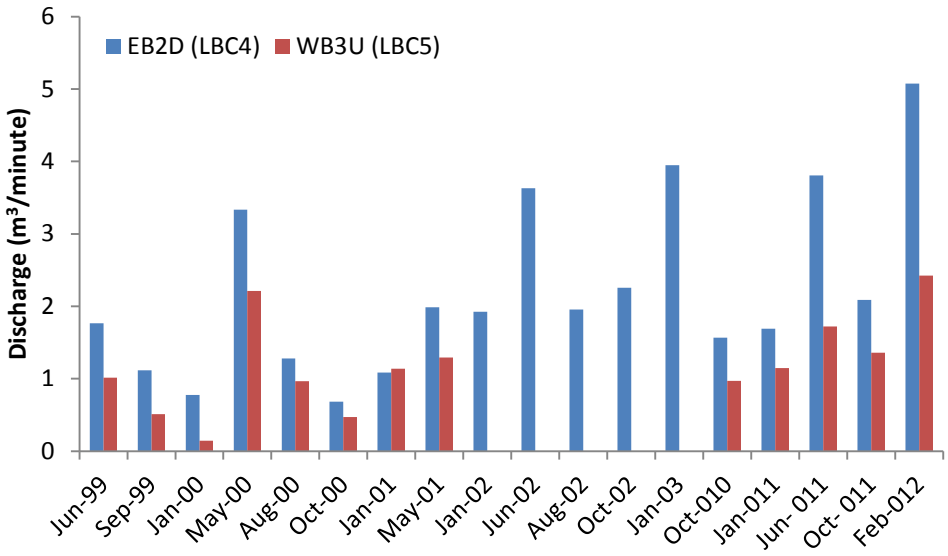

Figure 3.9. Temporal variation in stream discharge at farthest up- and downstream ends of the study reach.

3.3 Manual spring discharge measurements

Discharge could not be measured for every visible spring because some were located below the stream surface and some emergent springs had orifices that could not be captured by a bucket. Discharge was measured at the bank springs EB5, WB1, WB2, and WB3 in January, June, and October 2011 and in February 2012. Spring discharges were distinctly higher in early summer and late winter and distinctly lower in early winter and autumn (Fig. 3.10). The farthest upstream spring WB3 consistently had the highest measured discharge rate, ranging from 0.02 to 0.13 m^3/minute, with the highest value in June and lowest in January.

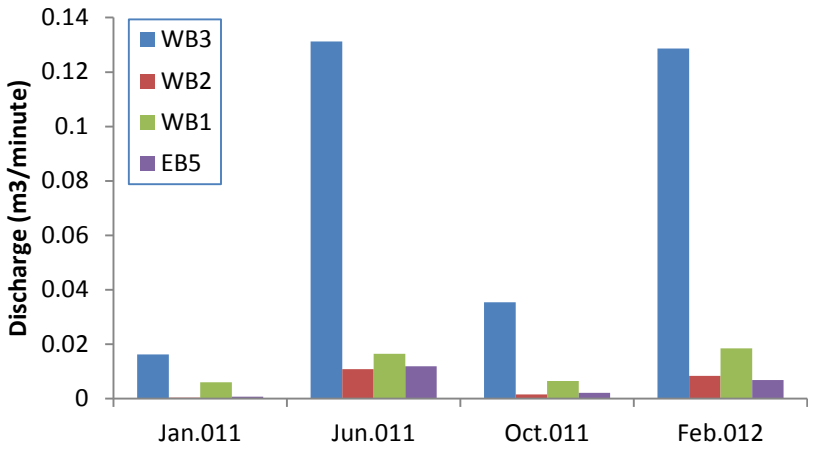

Figure 3.10. Temporal variation in spring discharge.

3.4 Dye-dilution tracer test

Mass recovery of dye for all sites were calculated for each measurement period. The following simple mass-balance relation was used for this calculation:

$$\text{Mass Recovery } (M_R) = [(\text{Mass Recovered} / \text{Mass Injected}) \times 100] \%$$

For each sampling location during all four rounds of tracer tests, dye mass flux at each time interval was calculated as a product of adjusted sample concentration (sample concentration – background concentration) times sampling interval. Total mass flux obtained after adding all the incremental mass fluxes was divided by the mass of dye injected to get the fraction of mass recovered.

Mass recovery calculations show greater than 100% recovery for 14 out of 16 sampling events with two close to 100% and one close to 70 % recovery (Table 3.1). In general, the mass recovery calculations suggest that the stream discharge was overestimated at almost all sampling locations, which could be the result of the discharge measurement error associated with the velocity-area method.

Table 3.1. Rhodamine WT mass recovery.

Sampling Locations	**Mass recovery**			
	Jan-11	**Jun-11**	**Oct-11**	**Feb-12**
EB2D	101.0	137.9	133.9	147.6
WB1.5D	68.3	119.0	108.9	107.6
MS1U	94.6	147.9	115.5	122.1
WB3U	127.1	174.5	134.8	135.9

Mixing length (L_m) was calculated separately for each round of dye injection following Kilpatrick and Cobb (1985):

$$L_m = K \frac{vB^2}{E_z}$$

$$\text{and } E_z = 1.13\ d^{3/2}s^{1/2}$$

where K is a coefficient dependent on the location and number of injection points as well as percentage of mixing; E_z is the transverse mixing coefficient; v, B, and d are mean stream velocity, width and depth, respectively; and s is the water-surface slope. Velocity, width, and depth data were taken from velocity gauging measurements and water surface slope (0.007) was computed using the laser survey data (Sect. 2.9). Width is not expected to vary much because of the artificially channelized reach, and the water-surface slope is expected to remain unchanged being close to the local base level (Ohio River).

Calculated mixing lengths were 9 m (29 ft) for January 2011, 29 m (97 ft) for June 2011, 23 m (76 ft) for October 2011 and 40 m (132 ft) for February 2012. The closest sampling location was ~ 40 m (131 ft) from the dye injection locations. With the result of higher mass recovery we can estimate at least 98% mixing comfortably for our dilution test. The K value for injected dye at two points is 0.035 (Kilpatrick and Cobb 1985).

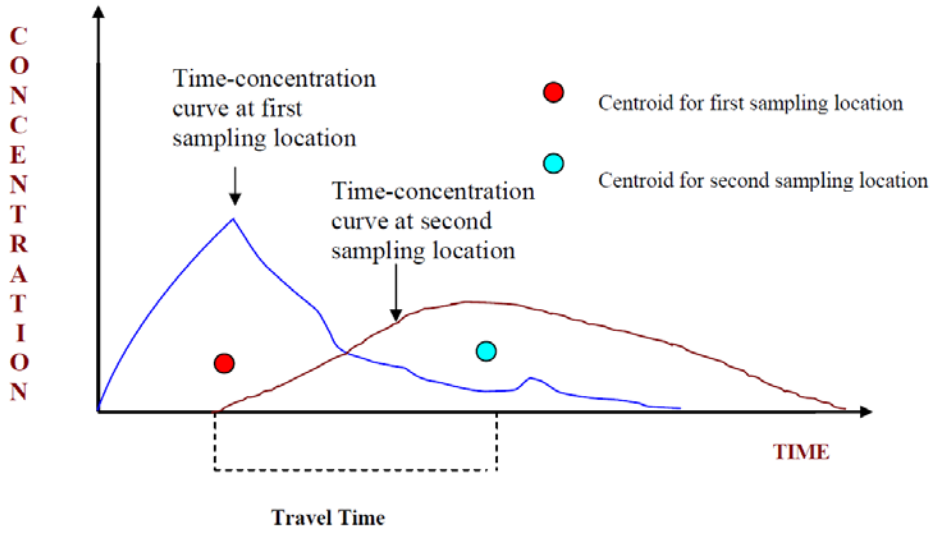

Figure 3.11. Schematic representation of travel time calculation (Mukherjee, 2003)

Dye dilution discharge was calculated for each sampling location using the following formula (Kilpatrick and Cobb, 1985):

$$Q = 5.89 \times 10^{-7}[\frac{S_G V_S C_S}{A_C}]$$

where Q = stream discharge, S_G = specific gravity of the dye solution, V_s = volume of concentrated dye solution, C_s = concentration of injected dye, and A_c = area under the response (breakthrough) curve. Area under each breakthrough curve (BTC, Fig. 3.11) was determined using the trapezoidal rule (i.e., dividing the area under the curve after subtracting the background concentration into the smallest practical trapezoids and summing them to get the total area). Although Clow and Fleming (2008) reported errors of 7 to 11% in estimated discharge using RWT dilution gauging, accuracy of dye-dilution discharge could not be independently calculated along our study reach because it is continuously gaining.

For all four dye injection tests, the BTC closest to the dye dilution point had the highest peak concentration with sharp peak and short tail, while BTCs for downstream locations exhibited broader peaks and longer tails (Figs. 3.12-3.15). Dye travel times from injection to sampling locations were calculated using MATLAB function “centroid.m” (Appendix III, B). This routine determines the center of mass of each breakthrough curve (Fig. 3.11)

and calculates the travel time from the dye injection point to each centroid. Travel times were 30.8 min to WB3U, 60.1 min to MS1U, 104.6 min to WB1.5D and 149.6 min to EB2D in January 2011; 16.7 min to WB3U, 48.21 min to MS1U, 81.7 min to WB1.5D, and 118.69 to EB2D in June 2011; 19.37 min to WB3U, 62.57 min to MS1U, 110.57 min to WB1.5D and 165.47 min to EB2D in October 2011; and 10.07 min to WB3U, 31.04 min to MS1U, 41.9 min to WB1.5D and 66.67 min to EB2D in February 2012 (Fig. 3.16). Dye traveled fastest in February 2012 and slowest in October 2011 (except for the first sampling location, WB3U, where it traveled faster in January 2011) (Fig. 3.16).

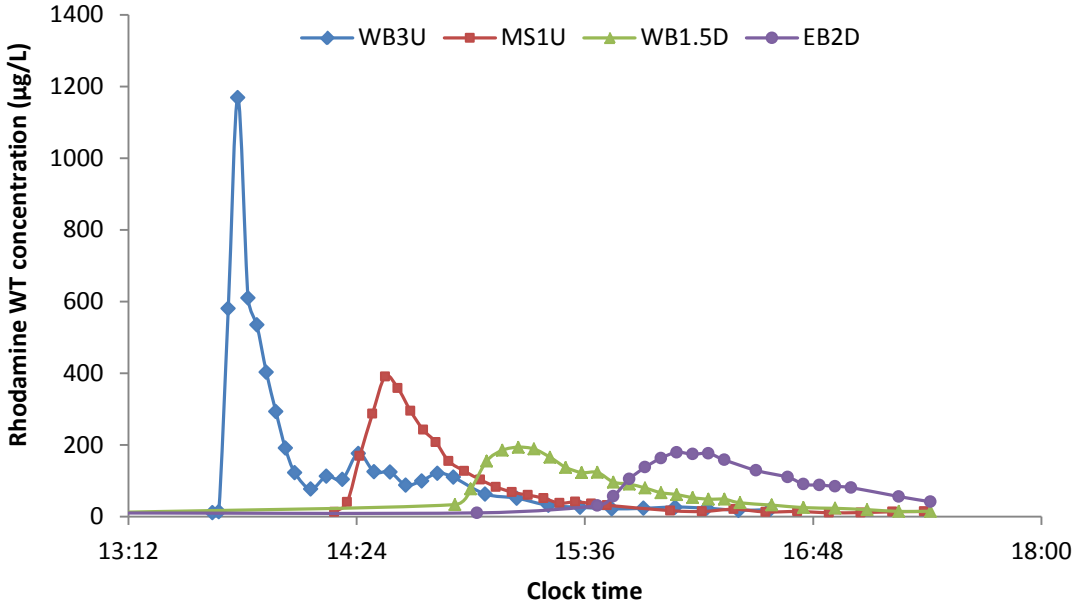

Figure 3.12. Breakthrough curves for January 2011 tracer test.

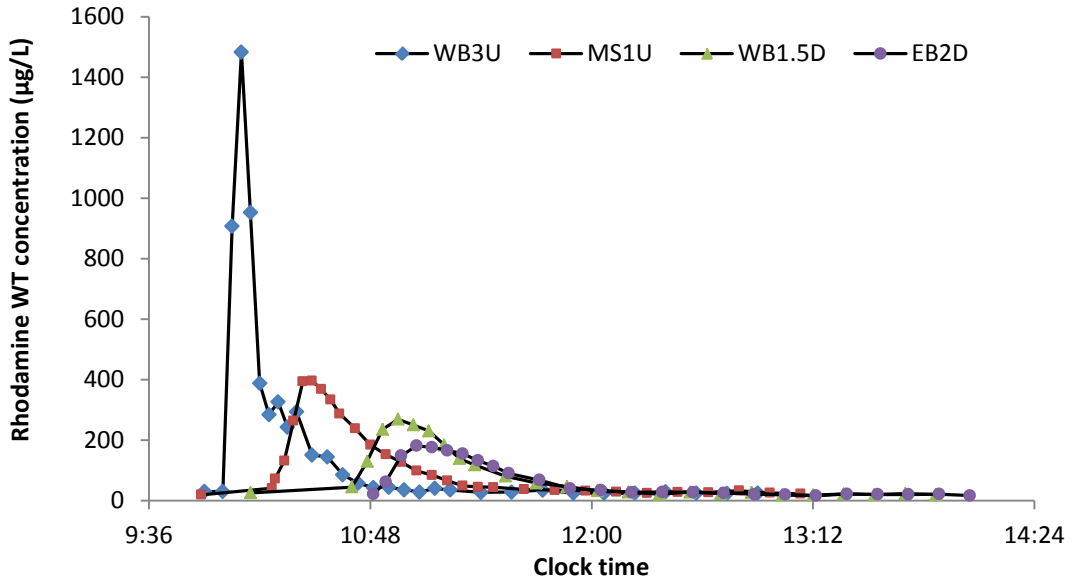

Figure 3.13. Breakthrough curves for June 2011 tracer test.

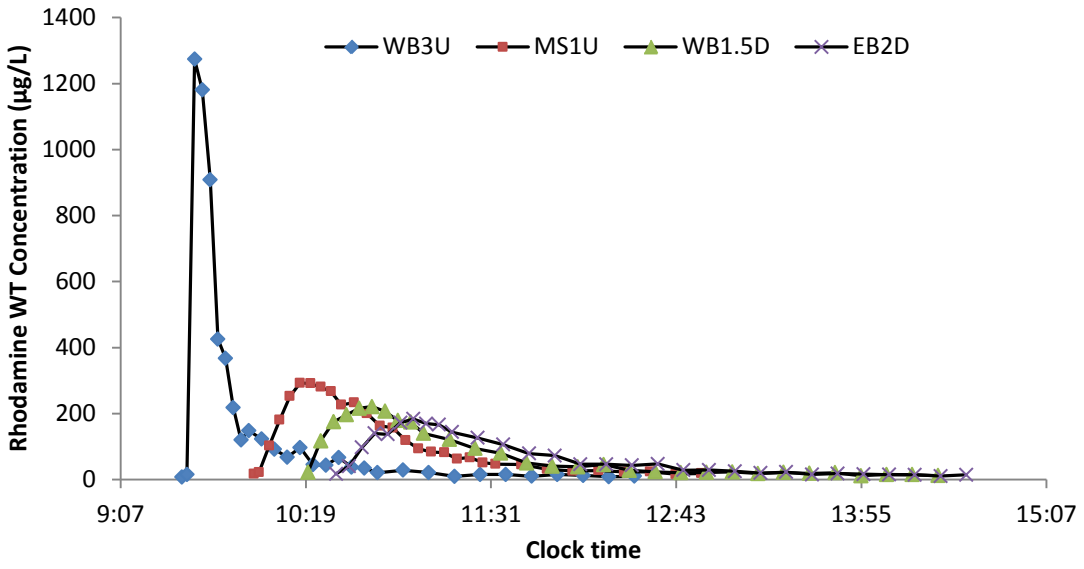

Figure 3.14. Breakthrough curves for October 2011 tracer test.

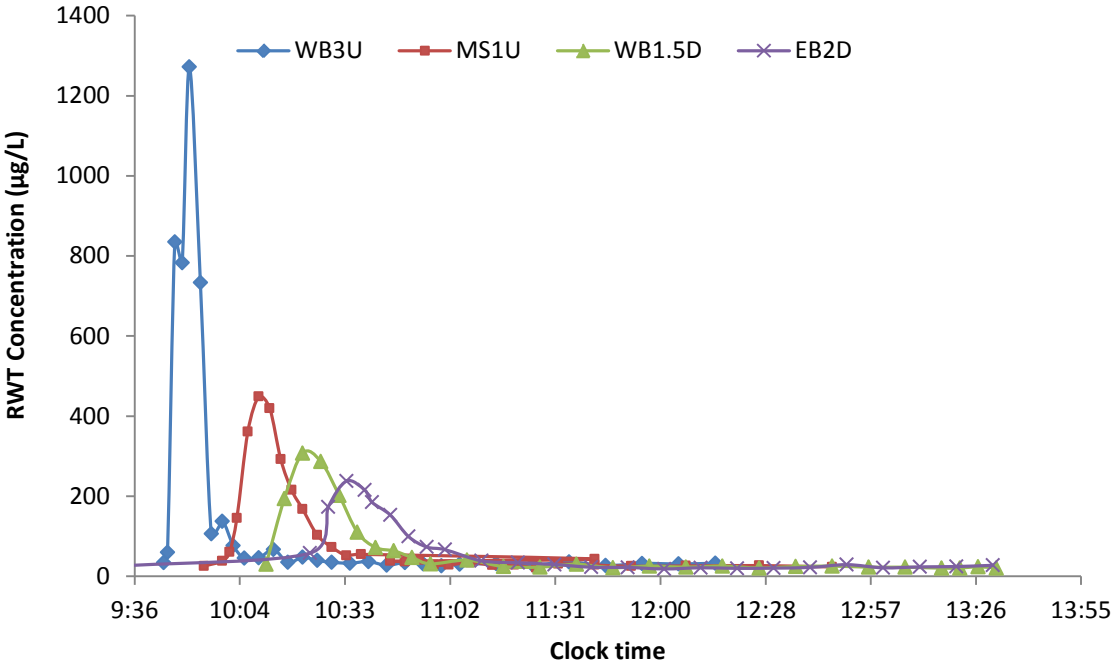

Figure 3.15. Breakthrough curves for February 2012 tracer test.

Shapes of the BTCs for all sampling locations are close to ideal (i.e. steep rising limb with sharp peak, relatively gentle falling limb with long tail and without any secondary peaks), which suggests sufficient mixing of dye before sampling. Except for WB1.5D and EB2D in January 2011, discharge computed from dye dilution continuously increased downstream, consistent with gaining conditions. For January 22, 2011, stream

discharge calculated for the farthest upstream sampling location (WB3U, 0.94 m^3/min) was lower than for downstream sampling locations (1.63 m^3/min for MS1U, 1.8 m^3/min for WB1.5D, and 1.7 m^3/min for EB2D). For June 24, 2011, calculated discharge was 1.7 m^3/m at WB3U, 1.9 m^3/min at MS1U, 2.2 m^3/m at WB1.5D, and 3.8 m^3/min at EB2D. For October 24, 2011, calculated discharge was 1.05 m^3/m at WB3U, 1.3 m^3/min at MS1U, 1.66 m^3/min at WB1.5D, and 1.73 m^3/min at EB2D. For February 20, 2012, calculated discharge was 1.9 m^3/min at WB3U, 2.6 m^3/min at MS1U, 3.2 m^3/min at WB1.5D, and 3.7 m^3/min at EB2D. Dye recoveries calculated for all four sampling sites were greater than 100%. RWT concentrations were measured above 95% confidence level against 13 lab standards with correlation coefficients of 0.99 (Appendix III, C), which suggests that the gauged stream discharge used to calculate dye recovery may have been overestimated.

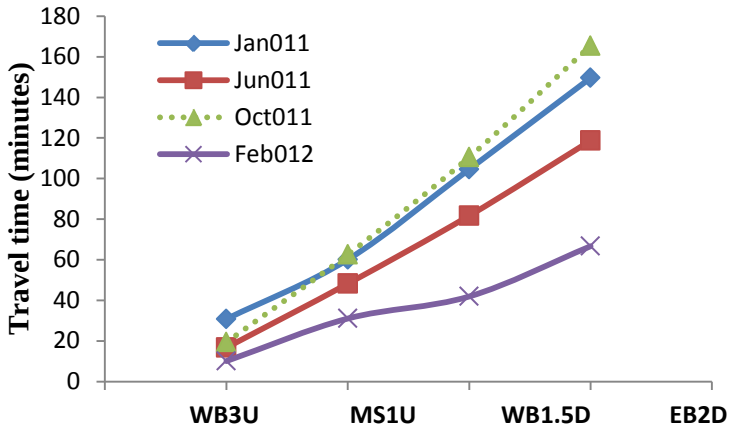

Figure 3.16. Travel time determined for four rounds of tracer tests.

3.5 Sub-reach to reach-scale water fluxes

Sub-reach to reach-scale maximum and minimum water fluxes were calculated after correcting for measurement error (Table 3.2). Measurement error was computed for each gauging location during each round of field study (Appendix II) and was uniformly assumed to be 9% for dye dilution discharge, as found in previous studies (Clow and Fleming, 2008). Because stream gauging was performed at ten locations along the reach, whereas dye dilution was determined only at four locations, the sub-reaches were defined as follows: WB3U-MS1U (reach 1), MS1U-WB1.5D (reach 2), and WB1.5D-EB2D (reach 3). For both gauging and dye dilution, inflow was greater in June and February than in January and October. For all four rounds of gauging, inflow was greatest along reach 3. In contrast, dye dilution results along reach 3 indicated losing conditions in January. Along reach 2 in January and October, ΔQ values were positive for dye dilution but negative for gauging, which may represent the potential area of hyporheic exchange.

Table 3.2. Maximum and minimum net groundwater exchange computed from velocity-area and dye dilution gauging.

Maximum and minimum net exchange (ΔQ), stream gauging (m^3/minute)								
Reach	**Jan-11**		**Jun-11**		**Oct-11**		**Feb-12**	
	ΔQ_{max}	ΔQ_{min}	ΔQ_{max}	ΔQ_{min}	ΔQ_{max}	ΔQ_{min}	ΔQ_{max}	ΔQ_{min}
Reach 1	0.36	0.21	0.59	0.45	0.23	0.15	0.81	0.52
Reach 2	-0.24	-0.14	0.14	0.11	-0.02	-0.01	0.71	0.45
Reach 3	0.58	0.34	1.64	1.26	0.68	0.46	1.69	1.08
Whole reach	0.71	0.41	2.37	1.82	0.88	0.59	3.20	2.06
Maximum and minimum net exchange (ΔQ), dye dilution (m^3/minute)								
Reach 1	0.75	0.63	0.19	0.16	0.28	0.23	0.80	0.66
Reach 2	0.21	0.18	0.29	0.24	0.39	0.32	0.63	0.53
Reach 3	-0.14	-0.11	1.77	1.48	0.07	0.06	0.57	0.48
Whole reach	0.83	0.69	2.25	1.88	0.74	0.62	2.00	1.67

3.6 Mathematical simulation model

Concentration data from the first sampling location (WB3U) were used to define the upstream continuous concentration boundary for all simulations as recommended by Runkel (1988). Therefore, the first simulated location (1 m downstream) did not exactly coincide with the sampling location, but the downstream simulation and sampling locations did coincide. Input text files were created following the instruction in the software manual and results were obtained as an output text files after execution (Fig. 3.17). Example of input text files are presented in Appendix III (D).

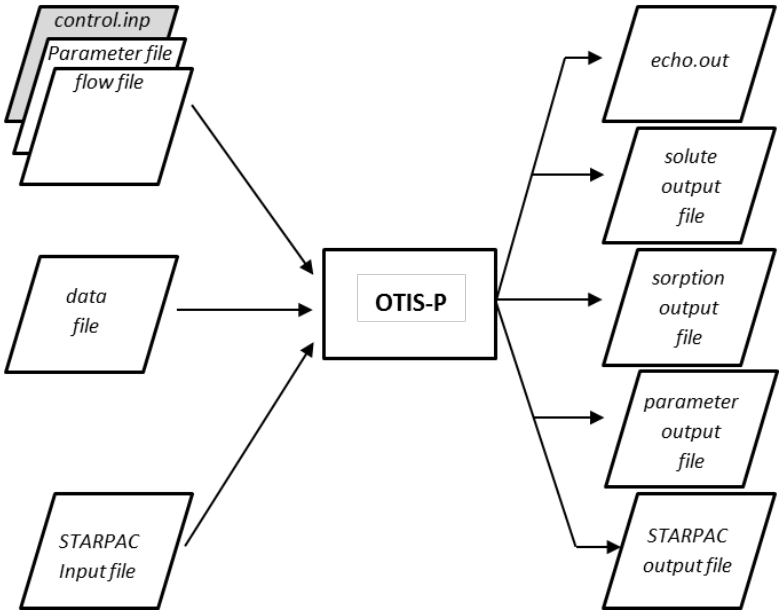

Figure 3.17. OTIS input/output files (Runkel, 1998).

3.6.1 January 2011

Simulation results for January 2011 show good agreement with the observed data. The peak time of the modeled BTC for the nearest sampling location was 1 minute later than the observed peak time. The difference between observed and simulated peak times increased downstream, with simulated peak times 8 minutes, 40 minutes and 70 minutes earlier than the observed peak times (Fig. 3.18). Observed and simulated peak times correlate closely, with a regression coefficient of 0.94 and standard error of 0.13 at 95 % confidence level. Observed and simulated peak concentrations have a regression coefficient of 0.99 and a standard error of 0.02 at 95% confidence level (Fig. 3.19).

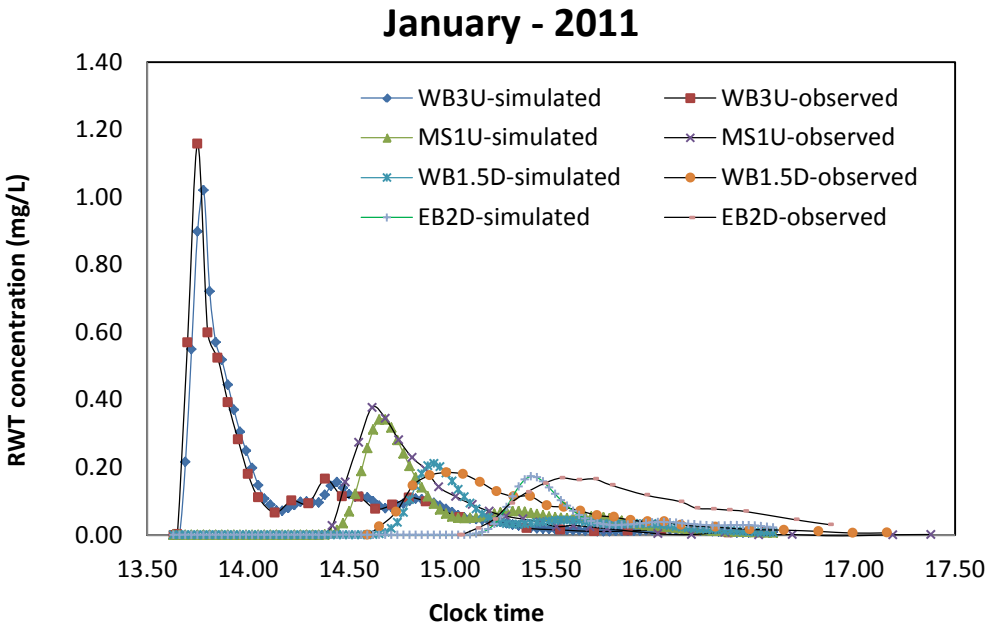

Figure 3.18. Observed vs. simulated BTCs for January 2011.

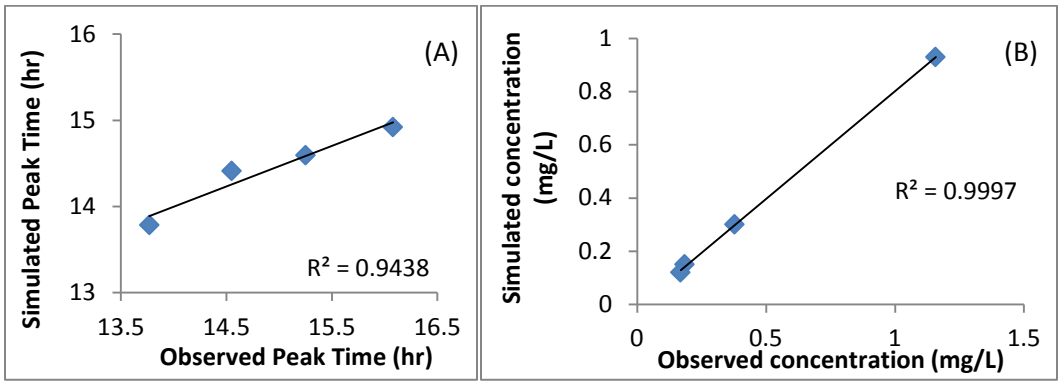

Figure 3.19. Correlations between observed and simulated values of (A) peak time and (B) peak concentration for January 2011.

3.6.2 June 2011

For June 2011, the simulated peak time matched the observed peak time for WB3U but, as in January, the simulated peak times became progressively earlier than the observed peak time (by 21, 46, and 48 minutes) with increasing distance downstream (Fig. 3.20).

Compared to the January 2011 results, the match between simulated and observed peak times for June 2011 was slightly weaker (Fig. 3.21), but the regression coefficient of 0.90 with standard error of about 0.02 was statistically significant at a 95% confidence level. There was closer agreement between simulated and observed peak concentrations, with a 0.99 regression coefficient and 0.03 standard error at 95 % confidence level.

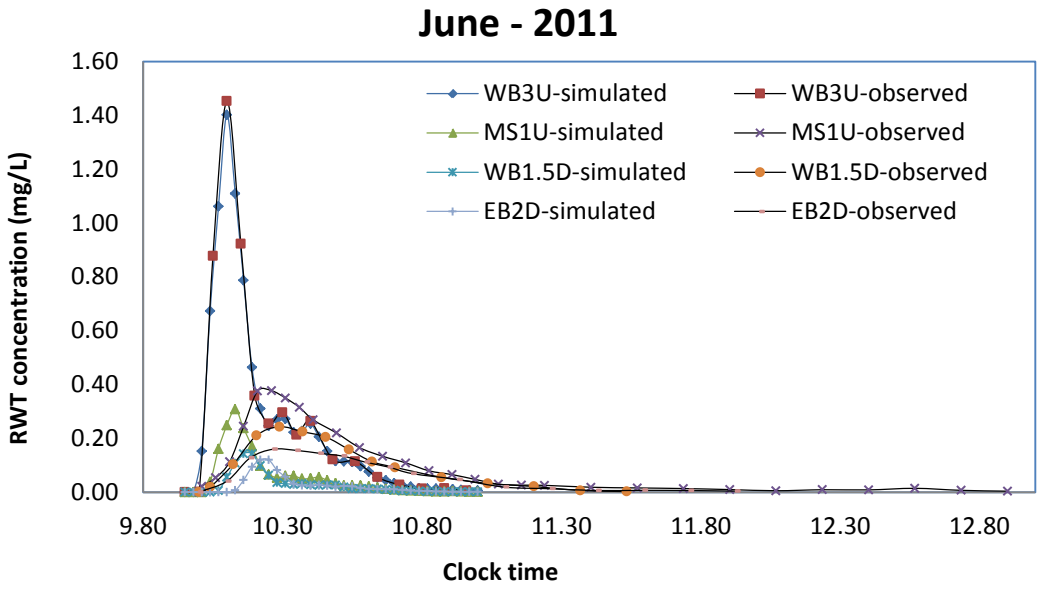

Figure 3.20. Observed vs. simulated BTCs for June 2011.

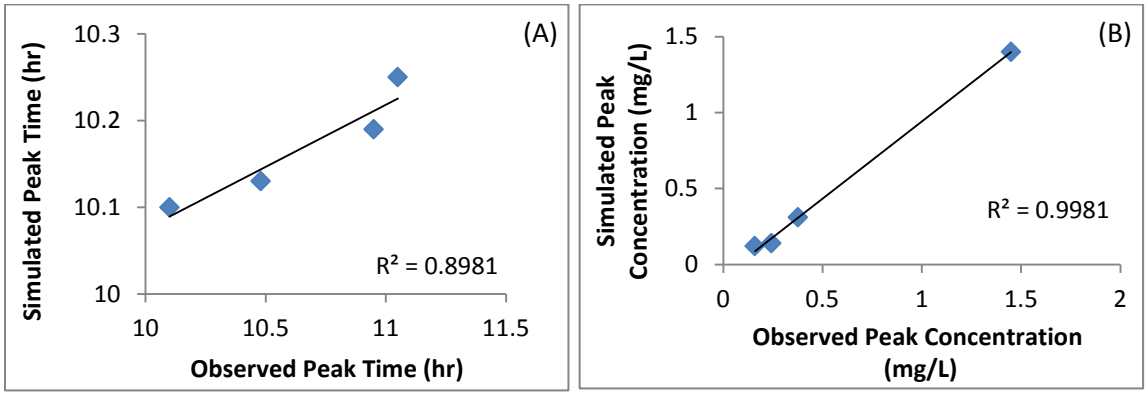

Figure 3.21. Correlations between observed and simulated values of (A) peak time and (B) peak concentration for June 2011.

3.6.3 October 2011

October 2011 simulations closely replicated the observed data. Peak time for the simulated BTC at WB3U was only about a minute earlier than the observed peak time (Fig. 3.22). The simulated peak time was 21 minutes later than the observed peak time for MS1U, coincided with the observed peak time for WB1.5D, and lagged the observed peak time by 2 minutes for EB2D. Regression analysis of simulated and observed peak times resulted in a statistically significant correlation with a regression coefficient of 0.92 and standard error of 0.2 at 95% confidence level. There was a near-perfect match between simulated and observed peak concentrations, with a regression coefficient of 0.99 and standard error 0.02 at 95% confidence level (Fig. 3.23).

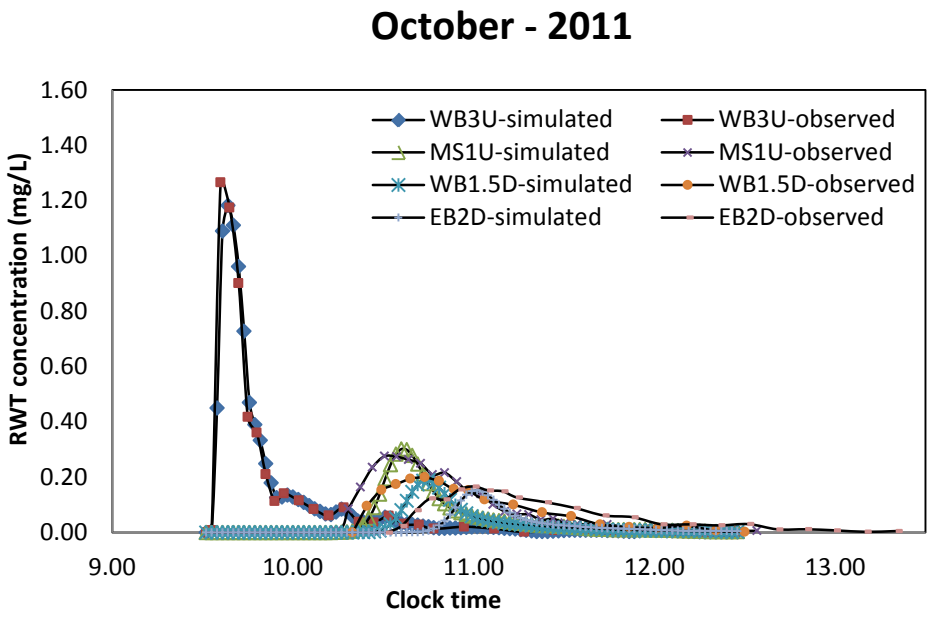

Figure 3.22. Observed vs. simulated BTCs for October 2011.

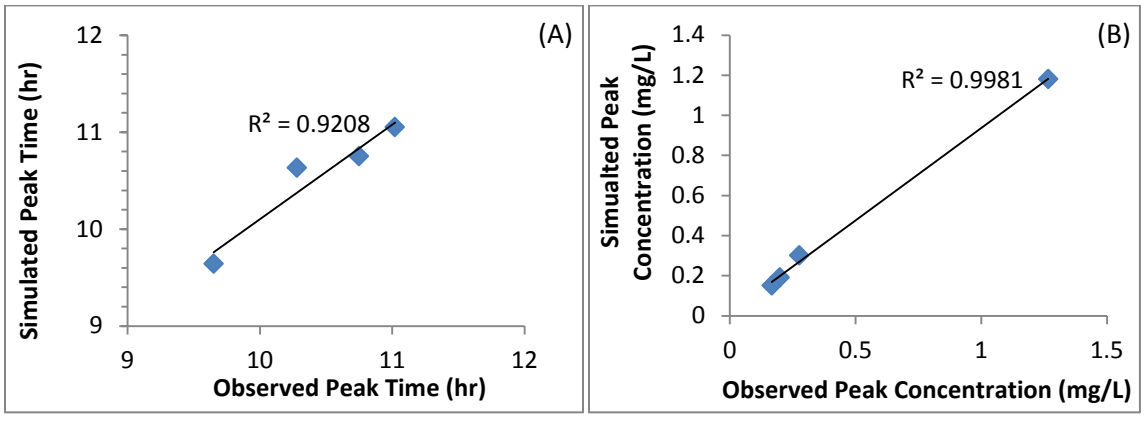

Figure 3.23. Correlations between observed and simulated values of (A) peak time and (B) peak concentration for October 2011.

3.6.4 February 2012

As in the previous simulation results, the sampling location close to the continuous concentration boundary (farthest upstream sampling location) had the best fit, which decreased slightly with increasing distance downstream (Fig. 3.24). The difference between observed and simulated peak times increased downstream, with simulated peak times 3 minutes later, 10 minutes earlier and 19 minutes earlier than the observed peak times (Fig. 3.25). The match between simulated and observed peak times was the weakest among all four rounds of simulations, but was still statistically significant at a 95% confidence level, with a regression coefficient of 0.82 and standard error of 0.09. As for other simulations, modeled and observed peak concentrations correlated more closely, with a regression coefficient of 0.99 and standard error of 0.03 at a 95% confidence level

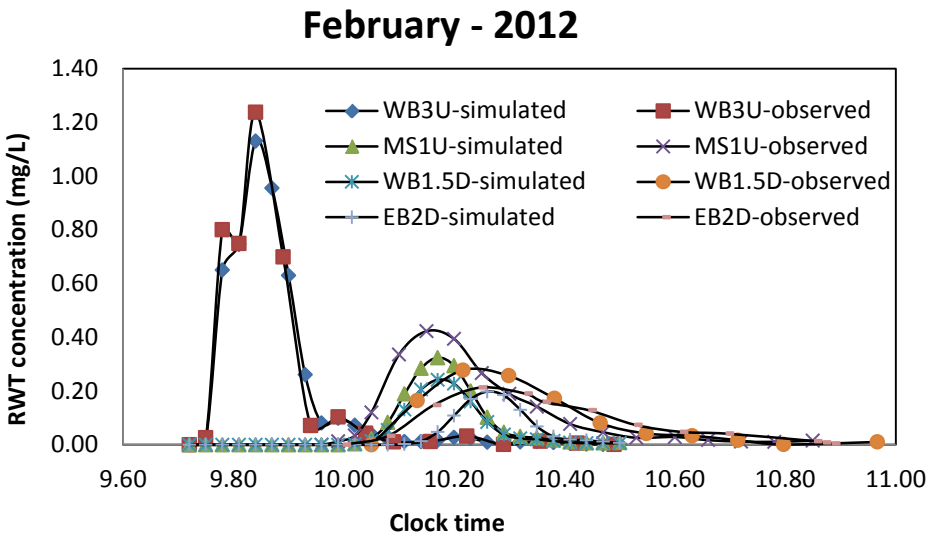

(Fig. 3.25).

Figure 3.24. Observed vs. simulated BTCs for February 2012.

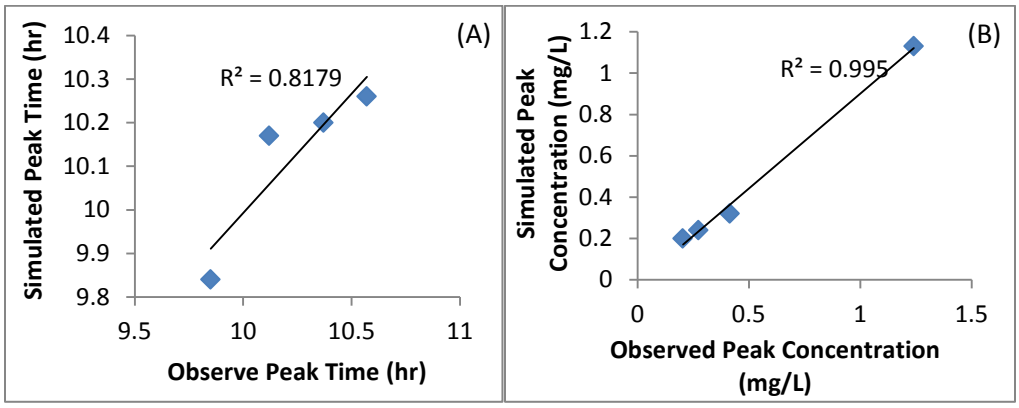

Figure 3.25. Correlations between observed and simulated values of (A) peak time and (B) peak concentration for February 2012.

3.6.5 Parameter estimation and model sensitivity

Four hydrologic parameters (dispersion coefficient, main channel cross-sectional area, storage zone cross-sectional area, and storage zone exchange coefficient) were estimated at the sub-reach scale for all four sampling periods using OTIS-P (Table 3.3). The dispersion coefficient varied from 0.01 to 0.4 m^2/s for reach 1, 0.01 to 0.052 m^2/s for reach 2, and 0.01 to 0.05 m^2/s for reach 3. In general, the values of dispersion coefficients were slightly lower than those calculated by Mukherjee et al. (2005) (0.09 to 0.39 m^2/s) along a 241-m reach beginning ~ 60 m downstream of EB2D. The calculated main-channel cross-sectional area varied from 0.29 to 1.30 m^2 for reach 1, 0.6 to 1.07 m^2 for reach 2, and 0.75 to 1.6 m^2 for reach 3. The average main-channel cross-sectional area (average of sub-reach-scale values) calculated by OTIS-P for the whole study reach was 0.95 m^2, which is close to the cross-sectional area (0.99 m^2) calculated from our stream gauging data for the same time period. The relatively wide range in simulated main channel cross-sectional area (from 0.29 to 0.86 m^2) in June may be a result of lower velocities at upstream ends (EB2D 0.064 m/s, WB1.5D 0.06 m/s, MS1U 0.03 m/s, and WB3U 0.027 m/s). The calculated storage-zone cross-sectional area varied from 0.009 to 0.06 m^2 for reach 1 and 0.01 to 0.05 m^2 for both reach 2 and reach 3. The ratio of calculated storage zone to main channel cross-sectional area (A_s/A) ranged from 0.03 to 0.05 for reach 1, 0.02 to 0.05 for reach 2, and 0.01 to 0.03 for reach 3. These values compare with the upper range value (0.04) calculated for the downstream reach by Mukherjee et al. (2005). Values of the storage zone exchange coefficient varied over relatively narrow ranges (1.3×10^{-5} to 5.0×10^{-5} m/s for reach 1, 1.1×10^{-5} to 1.7×10^{-5} m/s for reach 2, and 1.1×10^{-5} to 1.8×10^{-5} m/s for reach 3).

The accuracy of gauged stream discharge as an input (QSTART) to OTIS-P was found to have a significant effect on simulated peak concentration. Changing the dispersion coefficient had no apparent effect on the width of the breakthrough curve but affected the peak concentration slightly. Changing storage zone exchange coefficient did not change the simulated results, but excluding lateral inflow resulted in a very high simulated concentration compared to the observed concentration. The best match between simulated and observed breakthrough curves seems to occur with dispersion coefficient of 0.0005 m^2/s, QSTART ~ 30% more than the gaged Q, and lateral inflow about 50% more than the measured spring discharge. The most critical input parameter during the simulation was found to be QSTART (discharge at the upstream boundary).

Table 3.3. Estimated parameters using OTIS-P simulation

Calculated parameters from OTIS-P	**Stream Reach**												Average
	Reach 1 (upstream)				**Reach 2 (intermediate)**				**Reach 3 (downstream)**				
	Jan-11	Jun-11	Oct-11	Feb-12	Jan-11	Jun-11	Oct-11	Feb-12	Jan-11	Jun-11	Oct-11	Feb-12	
Dispn. coeff. (m^2/s)	0.0100	0.4247	0.0107	0.0268	0.0100	0.0100	0.0500	0.0524	0.0101	0.0100	0.0500	0.0500	0.0596
Main channel X-sectional area (m^2)	1.1273	0.2920	1.2996	1.0587	1.0700	0.7100	0.6301	0.9548	1.6010	0.8600	1.0704	0.7551	0.9524
Storage zone X-sectional area (m^2)	0.0271	0.0091	0.0639	0.0476	0.0500	0.0500	0.0130	0.0134	0.0236	0.0500	0.0145	0.0368	0.0333
Storage zone exchange coeff. (ALPHA)(m/s)	0.00001	0.00004	0.00005	0.00004	0.00001	0.00001	0.00001	0.00002	0.00002	0.00001	0.00001	0.00001	0.00002

3.7 Slug test to determine hydraulic conductivity

Drawdown ratios from the point of maximum displacement after slug insertion were plotted against time for each monitoring well (Fig. 3.26). Water levels were displaced 1.35 ft (0.411 m) higher in the shallower monitoring well LB6Y and 1.09 ft (0.332 m) higher in the deeper well LB6Z. The corresponding pairs of head ratios were picked from the best-fit line to calculate K values (section 2.6), which were 3.0 ft/day (0.91 m/day) for LB6Y and 5.8 ft/day (1.8 m/day) for LB6Z.

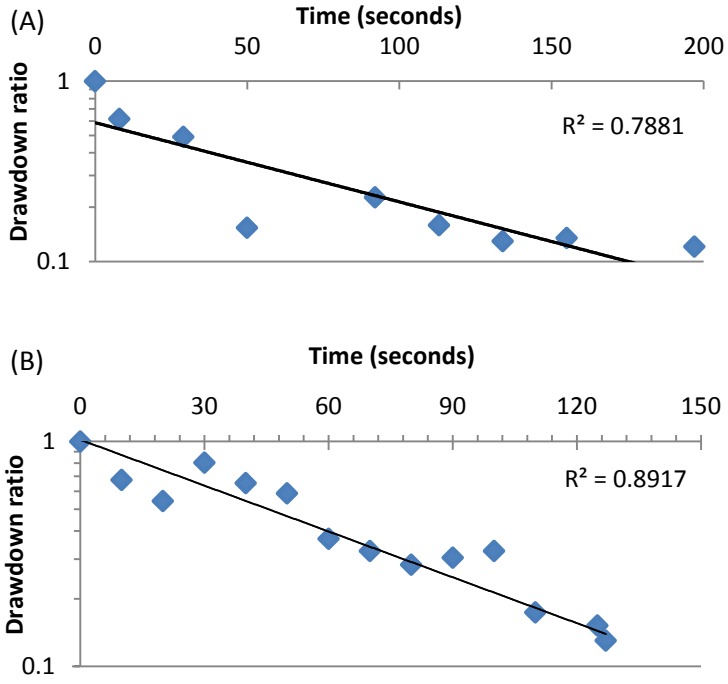

Figure 3.26. Drawdown ratio vs. time from slug test (July 5-6, 2012) in monitoring wells LB6Y (A) and LB6Z (B).

3.8 Temperature measurements

3.8.1 Manual measurements of spring and stream temperatures

Average temperatures for monitored bed and bank springs were 15.3 ^{o}C on October 22, 2010; 11.7 ^{o}C January 22, 2011; 14.0 ^{o}C on June 22, 2011; 15.0 ^{o}C on October 23, 2011; and 13.9 ^{o}C on February 18, 2012. Spring temperatures fluctuated in the range of ±0.1 to ±1.7 ^{o}C from the mean temperature, with the maximum fluctuation in January and the minimum in October (Fig. 3.27).

Stream temperatures at pairs of sites up- and downstream locations of five springs were measured on the same dates. Average surface water temperatures ranged from 1.33 to 23.9 ^{o}C, with the minimum 0.66 ^{o}C in January 2011 and the maximum 25.8 ^{o}C in June

2011. Surface water temperatures fluctuated in the range of ±0.2 to ±1.2 ^{o}C from the mean.

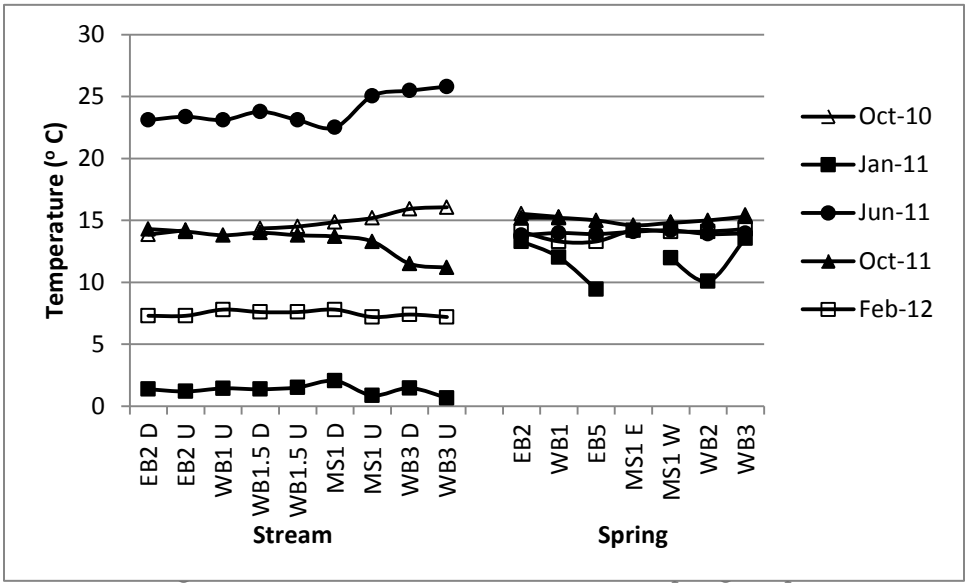

Figure 3.27. Temporal variability in stream and spring temperature.

3.8.2 Continuous monitoring of temperature in springs and monitoring wells

Temperatures were continuously monitored at springs EB2, WB3, and MS1W from September 22, 2011 to February 19, 2012 (Fig. 3.28a). However, temperatures were more variable after the sensors had been downloaded and redeployed on October 22, 2011. This variability suggests that the sensors had been inadequately anchored and were thus measuring stream rather than spring temperatures. Therefore, results for the first month of monitoring are emphasized here (Fig. 3.28b). At the farthest downstream spring, EB2, temperatures ranged from 14.9 to 16.5 ^{o}C, with an average of 15.1 ^{o}C and a standard deviation of 0.1 ^{o}C. At MS1W, near the midpoint of the study reach, temperatures ranged from 12.6 to 17.2 ^{o}C, with an average of 14.8 ^{o}C and 0.5 ^{o}C standard deviation. For WB3, the farthest upstream spring, temperatures ranged from 13.0 ^{o}C to 18.6 ^{o}C, with an average of 15.5 ^{o}C and a standard deviation of 0.7 ^{o}C. The similarity in average temperature for all three locations (14.8 to 15.5 ^{o}C) and relatively low standard deviation indicates that the sensors were primarily measuring groundwater temperature during the first month. Values for spring MS1W were used as a reference for groundwater discharge in the interpretation of temperature probe data.

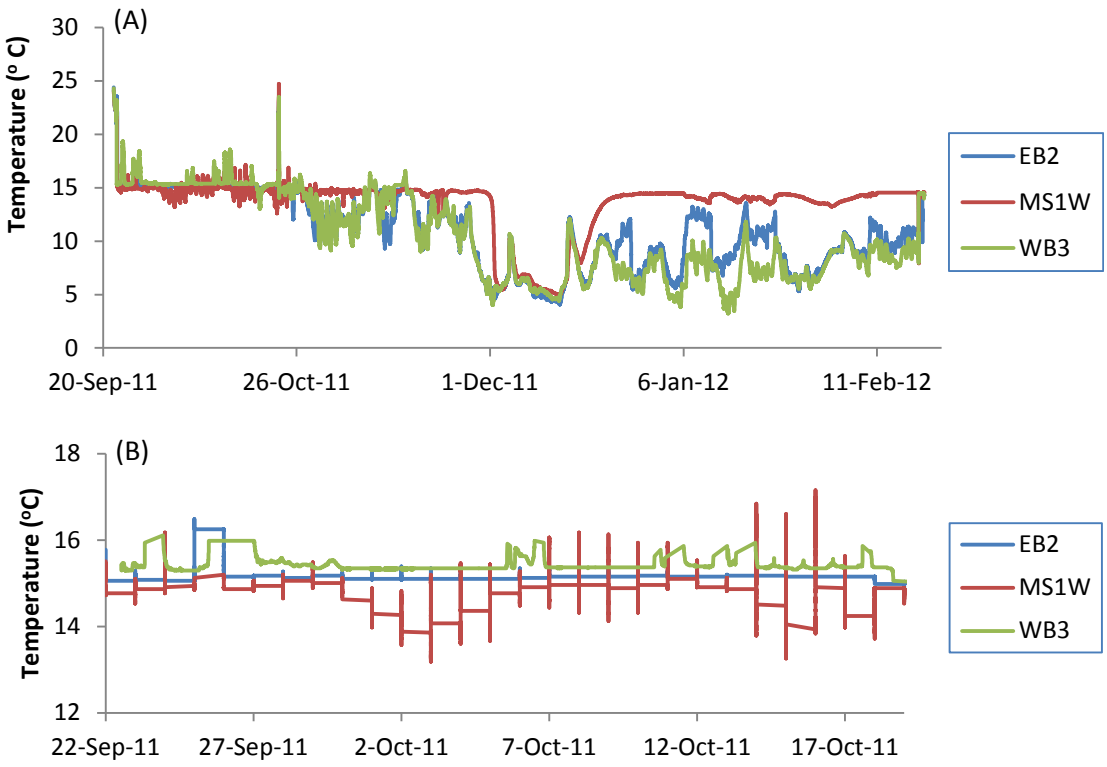

Figure 3.28. Spring temperatures monitored at 5-minute intervals for complete monitoring period (A) and for first month (B).

3.8.3 Temperature probing

3.8.3.1 Streambed temperature and probe-depth

Probe-penetration-depth was controlled by the streambed lithology because probe was driven manually. The depth of penetration could be the result of lateral inhomogeneity in the semi-confining unit (Metropolis Formation) and bedload above it. Because we probed to the refusal depth, the depth at which the temperature was measured varied from about an inch to the entire probe length (4 ft [1.2 m]). Temperature increased with depth in January and decreased with depth in August (Fig. 3.29).

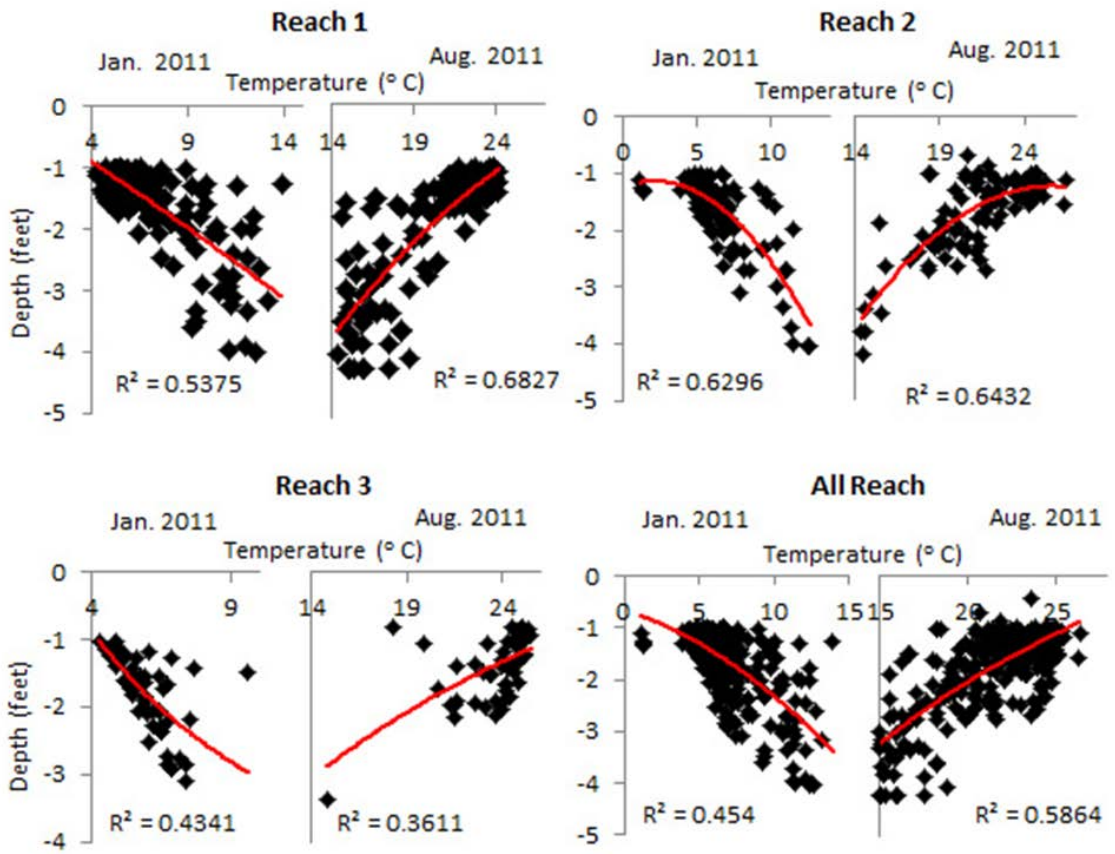

Figure 3.29. Sub-reach to reach scale temperature variation with depth.

Overall, there was a discernable correlation between temperature and depth with r^2 values ranging from 0.36 to 0.68 (Fig. 3.29). However, depth may not be the only parameter controlling temperature. Best fits were obtained using polynomial second order regression for reach 1, reach 2, and all reaches together, whereas logarithmic regression best fitted the data for reach 3. At focused discharge points, measured temperature was significantly higher or lower than the background even at shallow depth in both measurement periods. The sub-reach to reach scale streambed-temperature profiles are broadly similar to empirical profiles for a hypothetical gaining reach (Constantz et al., 2008) (Fig. 3.30).

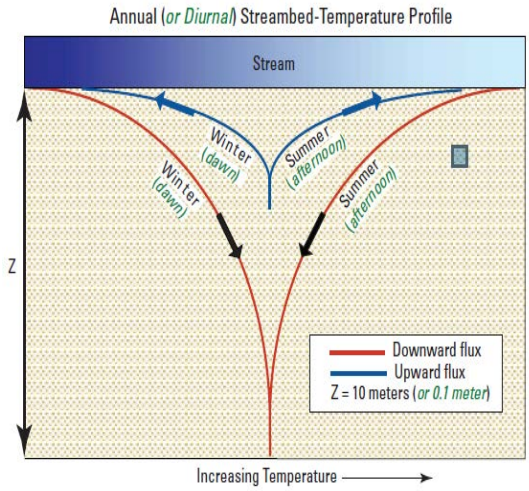

Figure 3.30. Annual (or diurnal) streambed-temperature profile for a hypothetical gaining reach (Constantz et al., 2008).

3.8.3.2 January 2011

During the winter survey period (January 4 to 8, 2011), hourly air temperature recorded at the Paducah airport from 8:00 AM to 6:00 PM varied from -7.2 to 7.8 ^{o}C, with an average of 2.1 ^{o}C and a standard deviation of 4.5 ^{o}C. Temperatures measured by probing varied from 0 to 13.4 ^{o}C at the sediment-water interface and 1.3 to 13.9 ^{o}C at refusal depth.

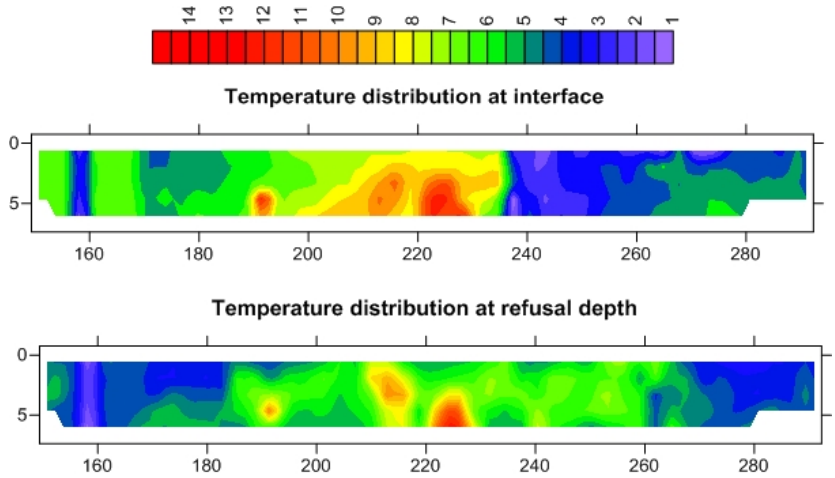

Figure 3.31. Temperature surface maps at interface and at depth for reach 1, January 2011; x-axis denotes distance from farthest downstream point and y-axis denotes stream width (in meters).

The interpolated surface maps represent temperature anomalies, in this case higher temperatures, at the interface and at depth along the streambed. Along reach 1, anomalies associated with the west bank springs WB2 and WB3 are clearly evident at ~ 215 and 225 m, respectively (Fig. 3.31). Another anomaly at ~ 190 m does not coincide with a

visible spring. Along reach 2, the anomaly at ~ 140 m along the east bank represents the spring MS1E and the anomaly at ~ 145 m along the west bank represents the spring MS1W (Fig. 3.32). The midstream anomaly on the refusal depth map between ~ 110–115 m is not evident on the interface map. This anomaly appears to coincide with a swampy area observed along the east bank close to 110 m. Two of three anomalies on the refusal depth map between ~ 95–100 m coincide with the west bank spring WB1.5 and east bank spring EB5. The anomaly in the middle of the stream bed was not visible in the field. Along reach 3, only the segment between ~ 5–30 m, which coincides with east bank springs EB2, EB3, and EB4, appears to be dominated by groundwater discharge (Fig. 3.33). The anomalies appear on both maps but are more distinct on the refusal depth map.

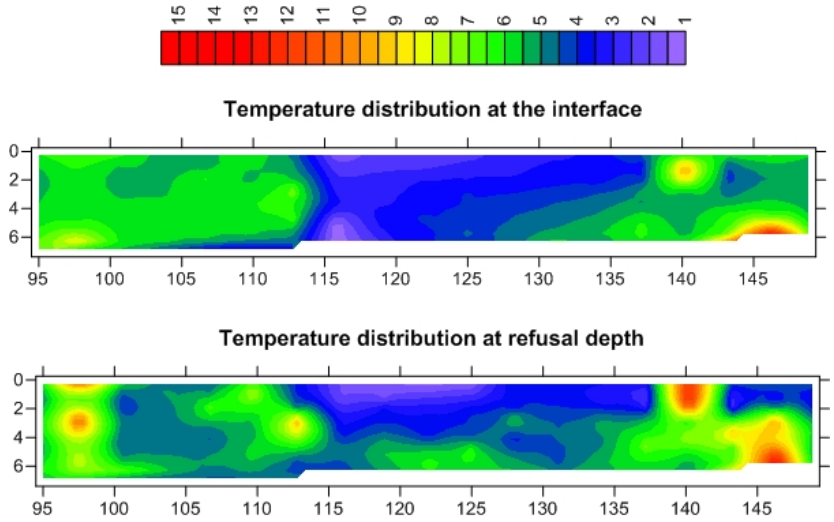

Figure 3.32. Temperature surface maps at interface and at depth for reach 2, January 2011; x-axis denotes distance from farthest downstream point and y-axis denotes stream width (in meters).

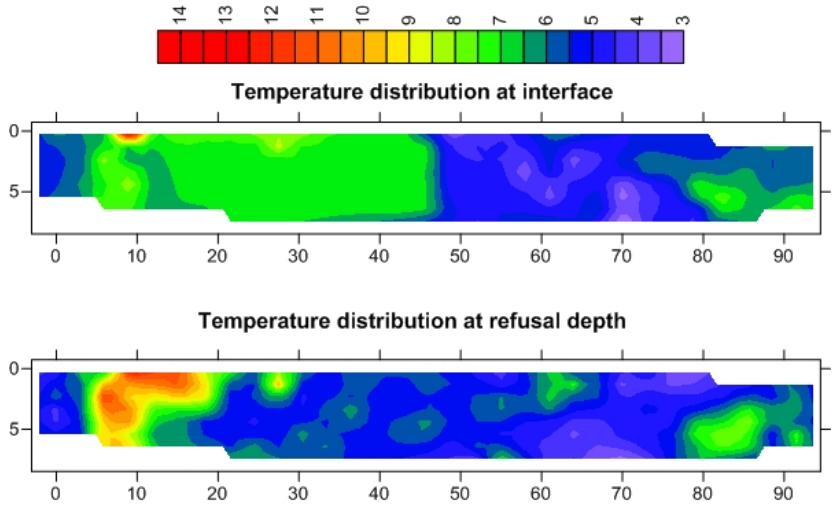

Figure 3.33. Temperature surface maps at interface and at depth for reach 3, January 2011; x-axis denotes distance from farthest downstream point and y-axis denotes stream width (in meters).

3.8.3.3 August 2011

During the summer survey period (August 5 to 9, 2011) hourly air temperature measured at the Paducah airport from 8:00 AM to 6:00 PM varied from 22.2 to 32.2 ^{o}C, with an average of 27.3 ^{o}C and a standard deviation of 2.9 ^{o}C. Temperature probe data varied from 14.6 to 29.1 ^{o}C at the sediment-water interface and 14.3 to 28.9 ^{o}C at refusal depth.

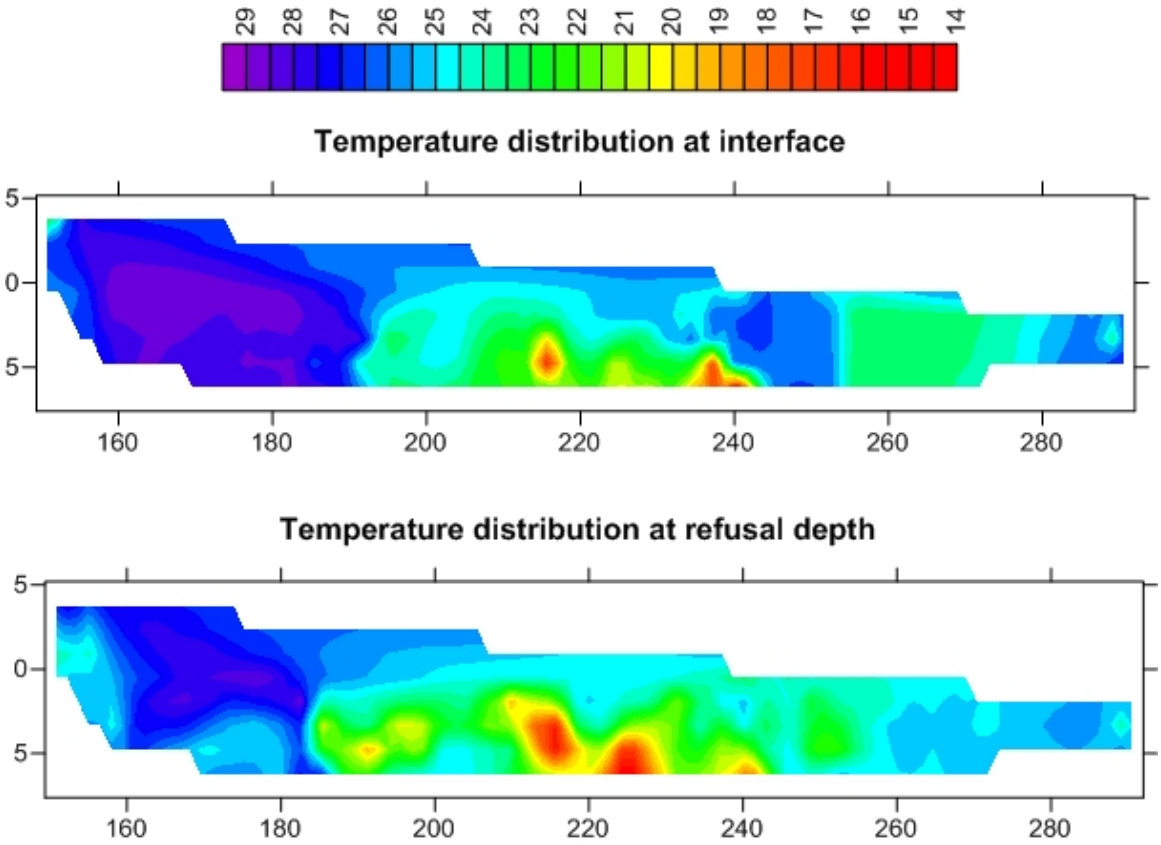

Figure 3.34. Temperature surface maps at interface and at depth for reach 1, August 2011; x-axis denotes distance from farthest downstream point and y-axis denotes stream width (in meters).

Cool anomalies observed in August tend to coincide with warm anomalies observed in January. Along reach 1, anomalies persisted close to springs WB2 and WB3 at ~ 215–225 m and emerged ~ 15 m upstream of WB3 on both the interface and refusal depth maps (Fig. 3.34). The anomaly at ~ 190 m near the west bank appears on the refusal depth map but not on the interface map. Along reach 2, anomalies are again associated with springs EB5 (~ 97 m), MS1E (~ 140 m), and MS1W (~ 145 m) (Fig. 3.35). Along reach 3, anomalies at ~ 5, 25, 60–65, and 75 m appear on both maps (Fig. 3.36). These coincide with springs EB2 (~ 5 m), EB3 and WB0.5 (~ 25 m), EB4 (~ 60–65 m), and WB1 (~ 75 m).

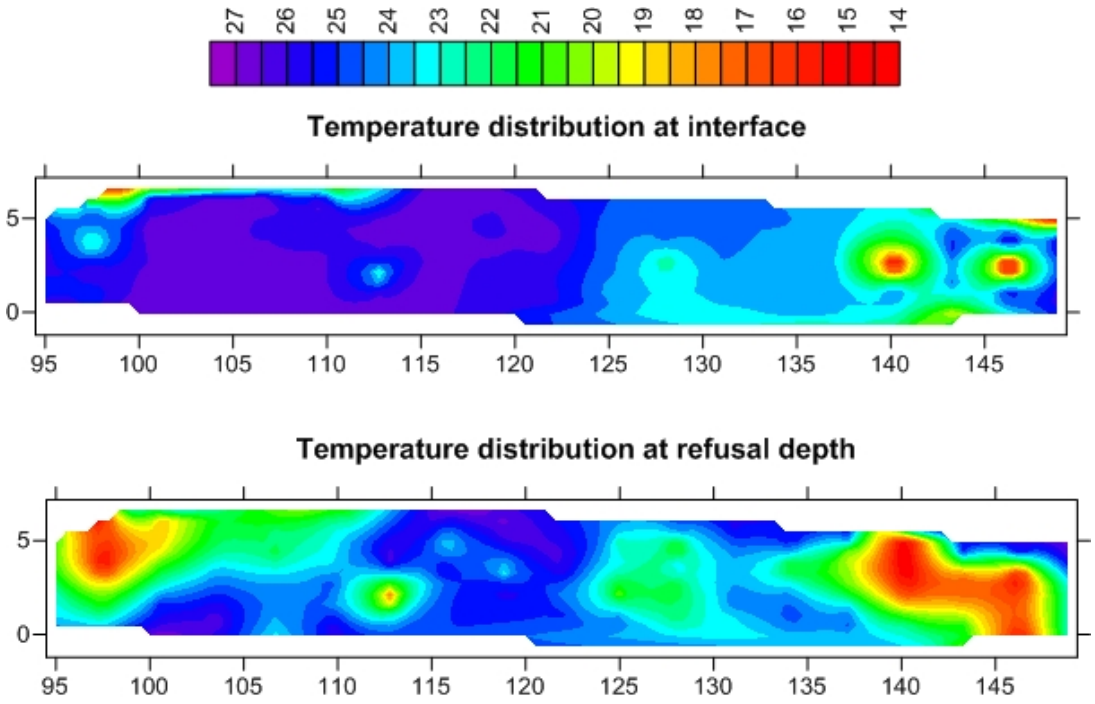

Figure 3.35. Temperature surface maps at interface and at depth for reach 2, August 2011; x-axis denotes distance from farthest downstream point and y-axis denotes stream width (in meters).

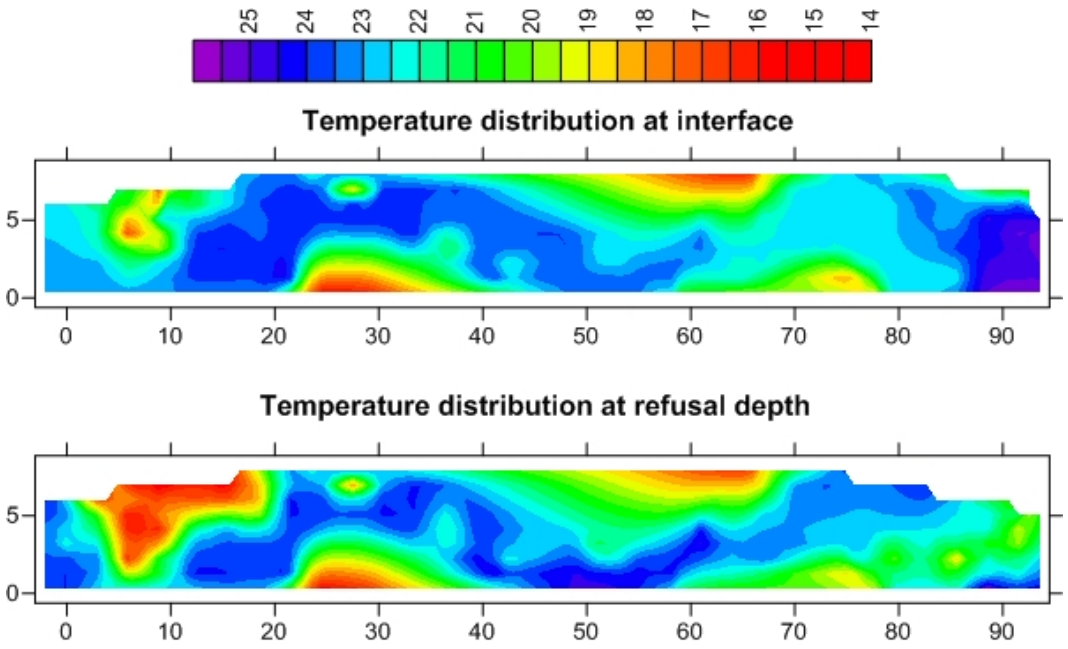

Figure 3.36. Temperature surface maps at interface and at depth for reach 3, August 2011; x-axis denotes distance from farthest downstream point and y-axis denotes stream width (in meters).

3.8.4 Distributed temperature sensing

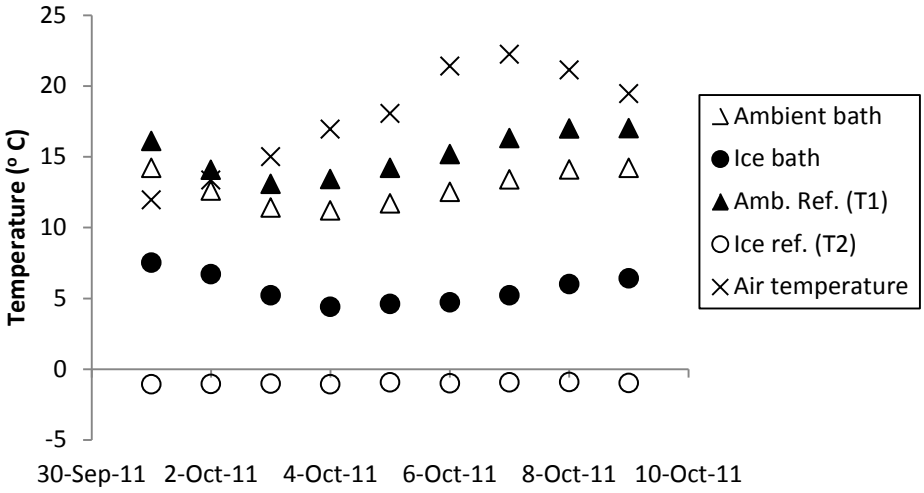

Figure 3.37. Ambient and ice bath temperatures (measured along fiber optic cable and with PT100 sensors) compared with daily average air temperature measured at Paducah airport.

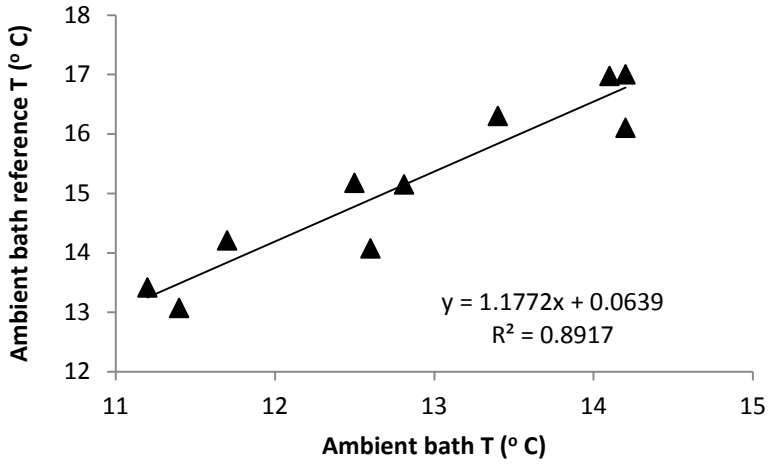

Figure 3.38. Correlation between the temperature measured by fiber optic cable and PT100 sensor in ambient temperature calibration bath.

Because the PT100 platinum temperature sensor placed in the ice calibration bath did not appear to function properly (Fig. 3.37), DTS measurements were corrected against the reference temperature (T1) recorded by the PT100 sensor in the ambient temperature calibration bath (Fig. 3.38). Apart from day-to-day fluctuations in temperature, spatial trends in DTS data were similar for each day of the monitoring period (October 1–9, 2011). DTS data from October 1 were chosen to delineate groundwater discharge locations along the study reach. Along reach 1, temperature fluctuations appear to be dampened in particular along the west bank at ~ 185, 220, and 240 m (Fig. 3.39). Along reach 2, temperature fluctuations are dampened along both banks at ~ 95, 130, and 145 m

(Fig. 3.40). Along reach 3, temperature fluctuations are dampened from ~ 10–40 m and ~ 85–95 m along the east bank. For the west bank, the low-temperature window was narrow around 10 m and 80 m and relatively wide from ~ 30–50 m along the profile (Fig. 3.41). In general, zones of dampened temperature fluctuations identified using DTS tend to coincide with anomalies delineated using temperature probing.

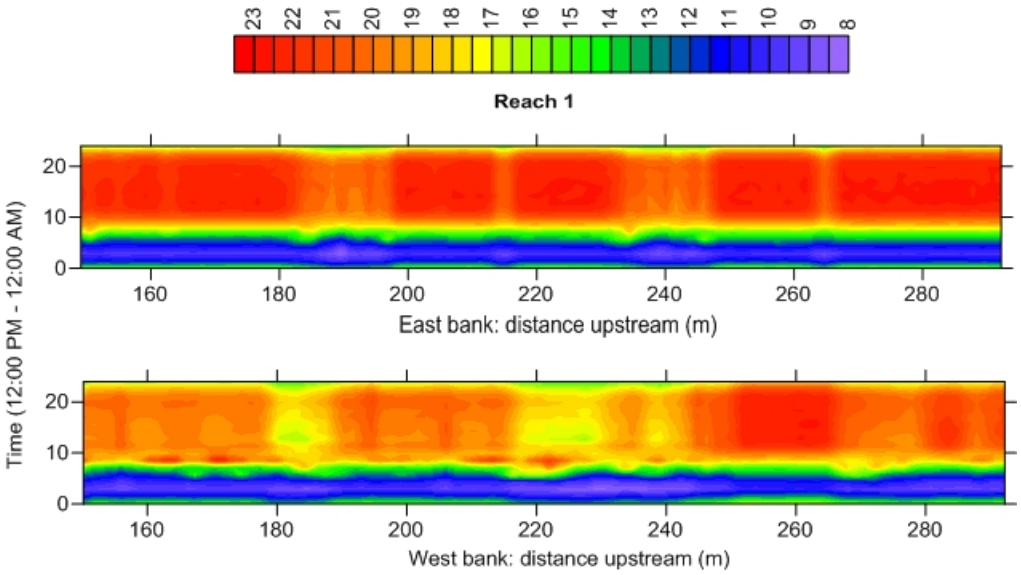

Figure 3.39. 24–hour continuous temperature record along the east and west banks, reach 1.

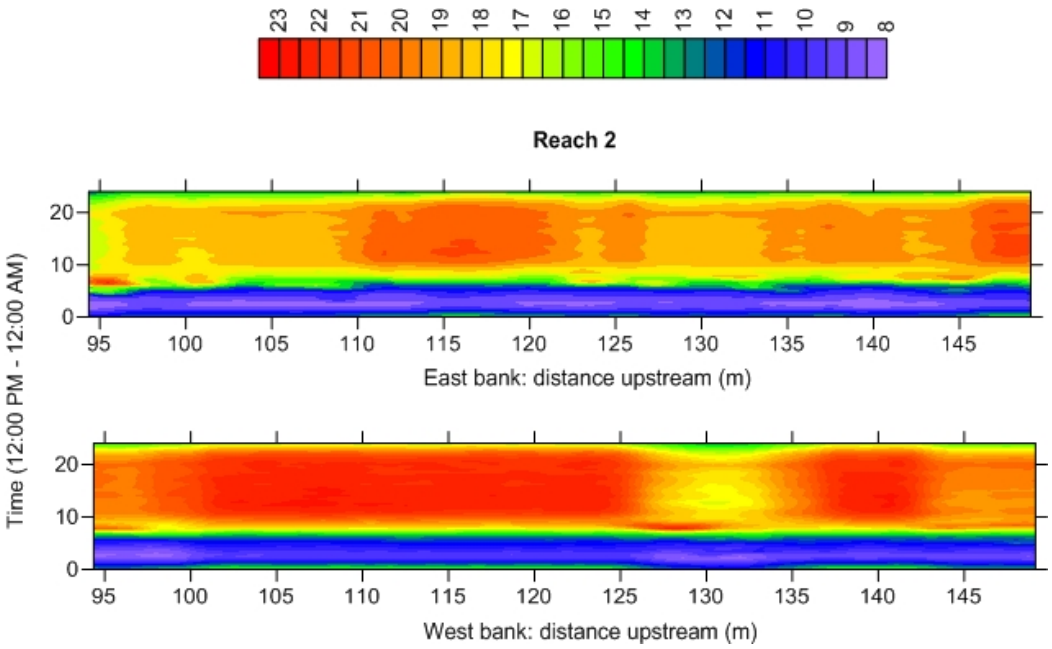

Figure 3.40. 24–hour continuous temperature record along the east and west banks, reach 2.

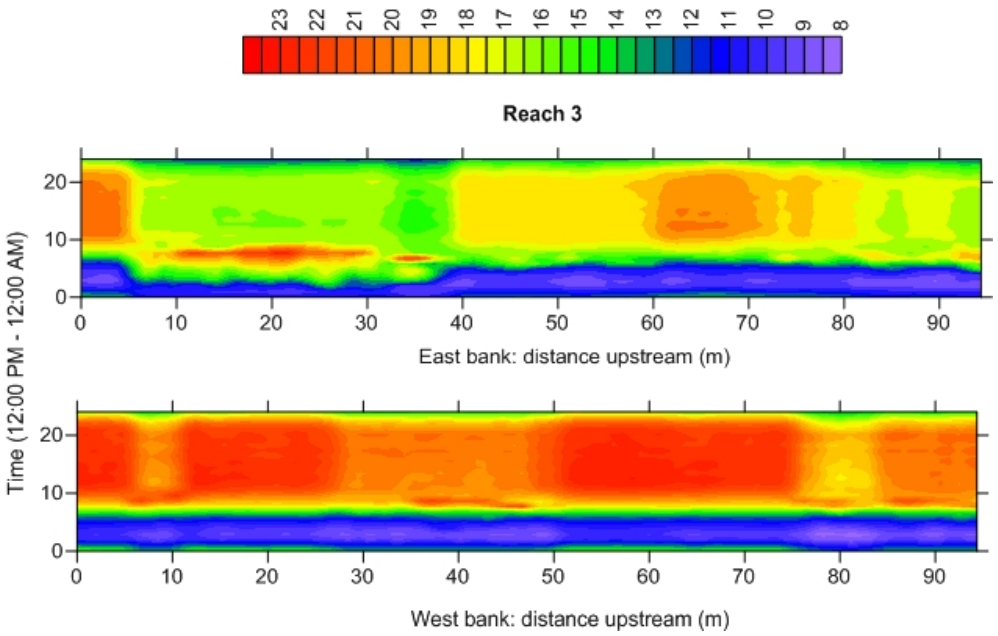

Figure 3.41. 24–hour continuous temperature record along the east and west banks, reach 3.

3.9 Dissolved oxygen

For all four rounds of measurement, DO in springs varied from 2.60 mg/L to 4.77 mg/L with an overall average of 3.60 mg/L (Table 3.4). Concentrations were > 3.0 mg/L except during June and October 2011 for MS1W and WB3. In general, DO concentrations for individual springs varied by < 1 mg/L; the maximum variation for a single spring was 1.43 mg/L for EB4.

Table 3.4. Dissolved oxygen in spring water samples.

Springs	Dissolved oxygen in spring water (mg/L)			
	10/22/2010	6/22/2011	10/23/2011	2/18/2012
EB2	3.95	3.90	3.62	3.78
WB0.5		3.90		
EB3		3.84		4.50
EB4	4.77		3.34	
WB1	3.66	3.28	3.36	3.92
EB5		4.18	2.84	3.62
MS1E		3.60	3.62	4.18
MS1EU			3.74	3.90
MS1W	3.49	2.96	2.6	3.10
WB2		3.76	3.74	3.64
WB3	3.47	2.96	2.98	3.32

The amount of DO in springs suggests aerobic conditions which do not favor the intrinsic reductive dechlorination of TCE at the discharge locations.

3.10 Contaminant concentrations

3.10.1 Contaminant concentration in stream

TCE and ^{99}Tc tended to track each other when baseflow was elevated in June 2011 and February 2012, but they were poorly correlated during low baseflow in January and October 2011. Maximum contaminant concentrations occurred in June, with TCE ranging from 20 to 28 µg/L (average 24.7 µg/L) and ^{99}Tc ranging from 11.81 to 18.67 pCi/L (average 15.9 pCi/L) (Table 3.5). Minimum contaminant concentrations were found in January, with TCE ranging from < 5 to 8.4 µg/L (average 6.12 µg/L) and ^{99}Tc ranging from 1.65 to 4.98 pCi/L (average 3.5 pCi/L). The contaminant pair correlated poorly for individual sampling rounds (seasonally), with highest r^2 value of 0.38 in June 2011, but the correlation for the entire data set was much stronger (r^2 = 0.89; Fig. 3.43).

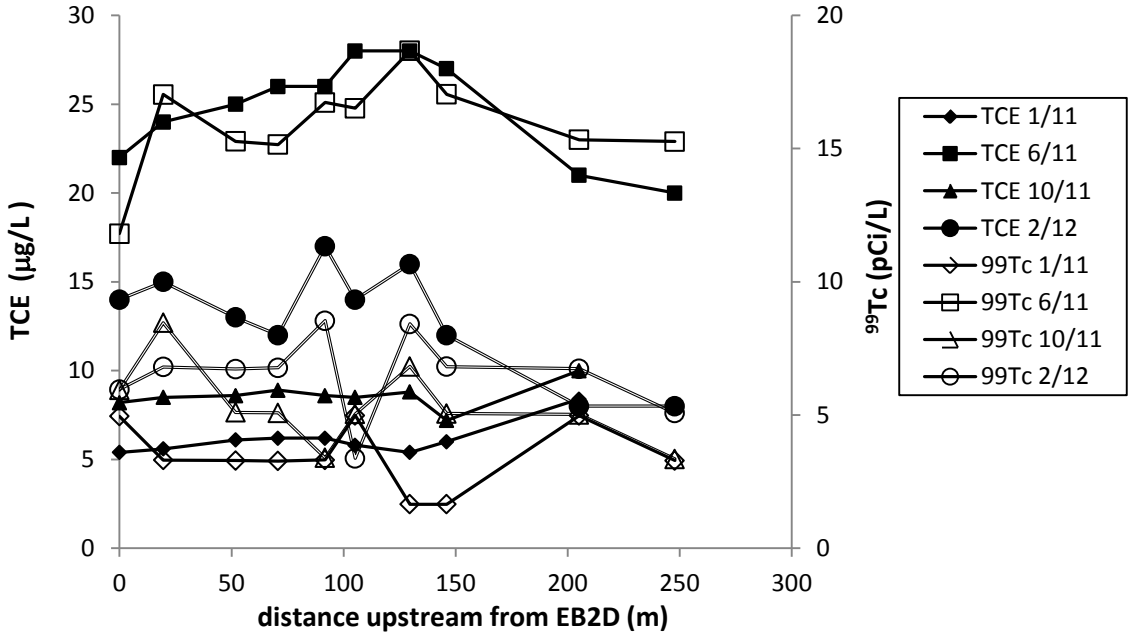

Figure 3.42. Surface water TCE and ^{99}Tc concentrations from January 2011 to February 2012. Below-detection limit results are not shown.

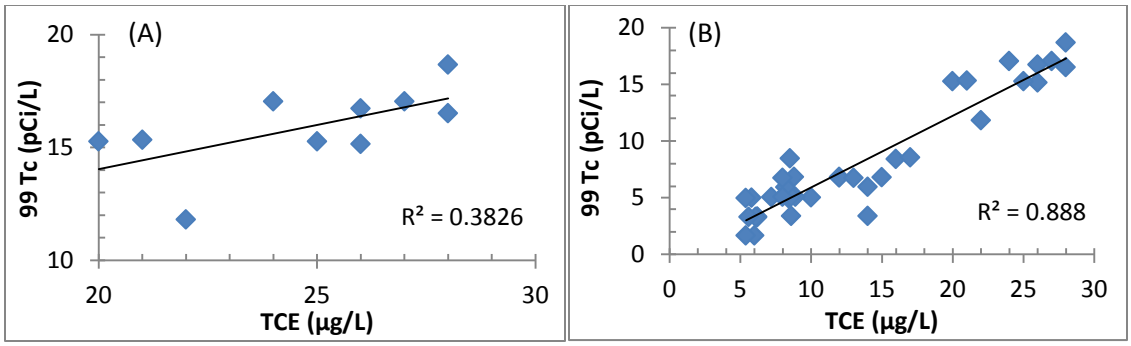

Figure 3.43. TCE–^{99}Tc correlations: seasonal (A), annual (B).

Table 3.5. Surface–water TCE and ^{99}Tc. Blank cells mean no sample was collected; values of 0 represents below detection limit.

Sampling locations	TCE (µg/L)				^{99}Tc (pCi/L)			
	1/11	6/11	10/11	2/12	1/11	6/11	10/11	2/12
LBC6			0	7			0±2.7	5.1±3.0
RRS			120				72.7±8.2	8.5±3.1
WB3U	0	20	0	8	3.3±2.8	15.3±3.4	3.4±2.8	5.1±2.9
WB3D	8.4	21	10	8	5.0±2.9	15.3±3.4	5.0±2.9	6.7±3.0
MS1U	6	27	7.2	12	1.6±2.8	17.0±3.5	5.0±2.9	6.8±3.0
MS1D	5.4	28	8.8	16	1.6±2.8	18.7±3.6	6.8±3.0	8.4±3.0
WB1.5U	5.8	28	8.5	14	4.9±2.9	16.5±3.4	5.0±2.9	3.4±2.9
WB1.5D	6.2	26	8.6	17	3.3±2.8	16.7±3.5	3.4±2.9	8.5±3.1
WB1U	6.2	26	8.9	12	3.3±2.3	15.2±3.4	5.1±2.9	6.8±3.0
WB1D	6.1	25	8.6	13	3.3±2.8	15.2±3.4	5.1±2.9	6.7±3.0
EB2U	5.6	24	8.5	15	3.3±2.8	17.0±3.5	8.5±3.1	6.8±3.0
EB2D	5.4	22	8.2	14	5.0±2.8	11.8±3.2	5.9±2.9	6.0±3.0

3.10.2 Contaminant concentrations in springs

In general, TCE and ^{99}Tc concentrations decreased asymptotically from upstream to downstream springs for all sampling rounds, and east bank springs had lower contaminant concentrations than west bank springs (Fig. 3.44 and Table 3.6). Concentrations were highest (TCE 160 µg/L and ^{99}Tc 51.68 pCi/L) for WB3 in January 2011 and were lowest (undetectable) in EB2. However, TCE and ^{99}Tc concentrations for the east bank spring MS1EU were higher than at the upstream spring WB2 in October 2011 and were higher than at WB2 and WB3 in February 2012. Unlike surface water, the contaminant pair correlated strongly for individual sampling rounds (seasonal) with r^2 = 0.98 for January 2011, r^2 = 0.99 for June 2011, r^2 = 0.98 for October 2011, and r^2 = 0.91 for February 2012 (Fig. 3.45). Correlation of all data (annual) also shows a strong linear relationship between the contaminants with r^2 = 0.94 (Fig. 3.45).

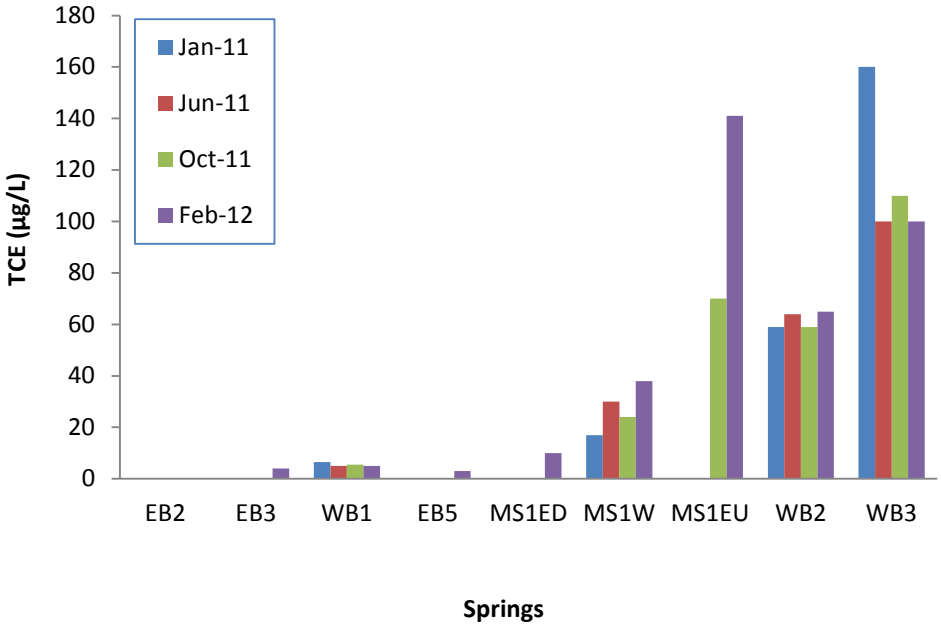

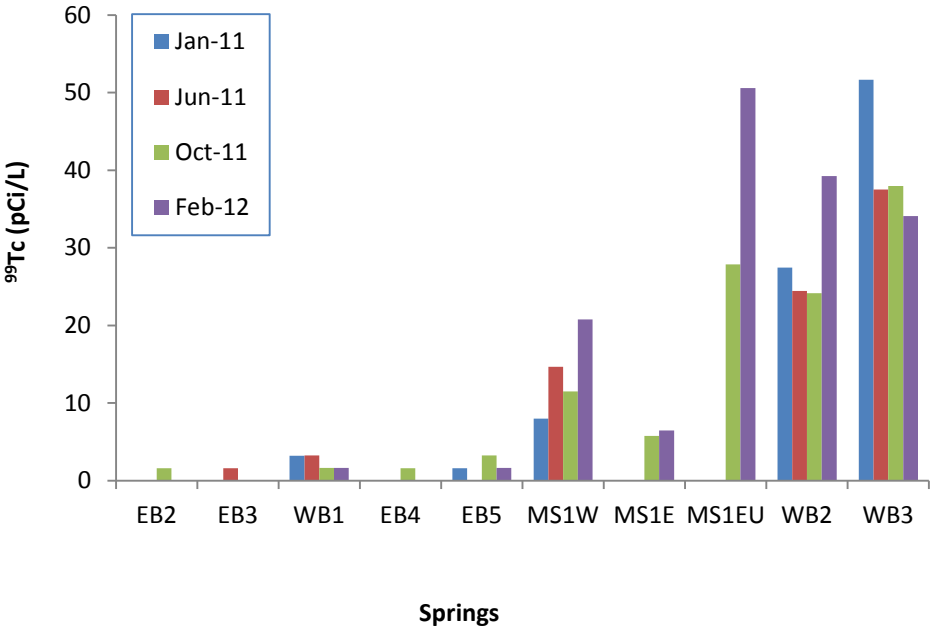

Figure 3.44. Spatial and temporal variation in TCE and ^{99}Tc concentration in springs.

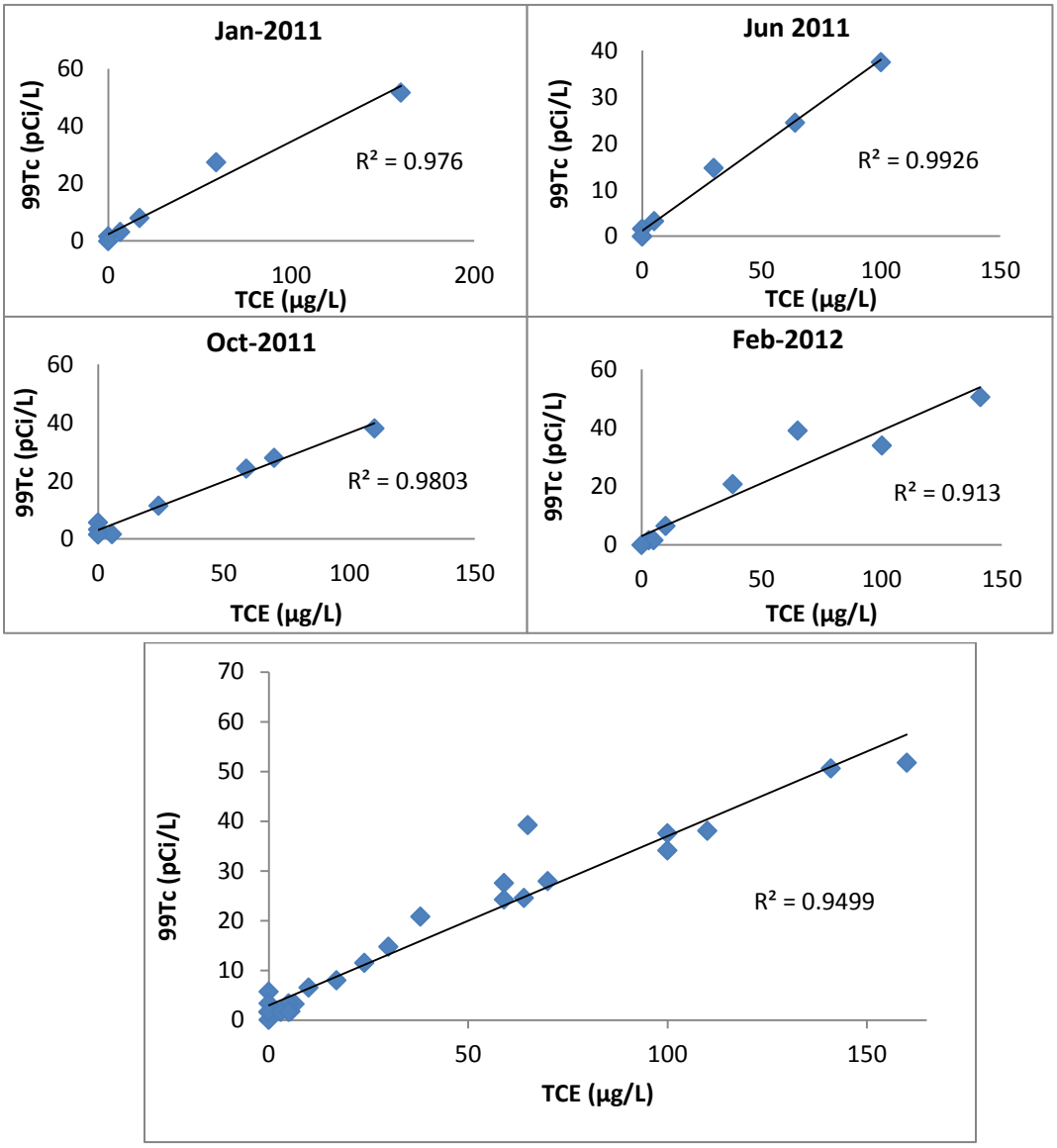

Figure 3.45. TCE–^{99}Tc correlations: seasonal (top), annual (bottom).

Table 3.6. TCE and ^{99}Tc concentrations in springs. Blank cells mean no sample was collected; values of 0 represents concentrations below detection limit.

Springs	Distance downstream (m)	TCE (µg/L)				^{99}Tc (pCi/L)			
		1/11	6/11	10/11	2/12	1/11	6/11	10/11	2/12
WB3U	0								
WB3	15	160	100	110	100	51.7±6.2	37.5±4.9	38.0±5.0	34.1±4.6
WB2	30	59	64	59	65	27.5±4.2	24.5±4.0	24.2±3.8	39.2±5.1
MS1EU	107.7			70	141			27.9±4.2	50.6±6.1
MS1W	109.2	17	30	24	38	8.0±2.9	14.7±3.3	11.5±3.1	20.8±3.6
MS1E	117.2		0	0	10			5.7±2.7	6.5±2.7
EB5	154.2	0	0	0	3	1.6±2.7	0±2.7	3.3±2.8	1.6±2.7
WB1	191.3	6.5	5	5.5	5	3.2±2.7	3.3±2.8	1.7±2.7	1.6±2.7
EB4	191.8							1.6±2.7	
EB3	228.8		0		4		1.6±2.7		
EB2	244.8	0	0	0	0	0±2.5	0±2.6	1.6±2.7	0±2.7

3.11 Streambed and bank dynamics

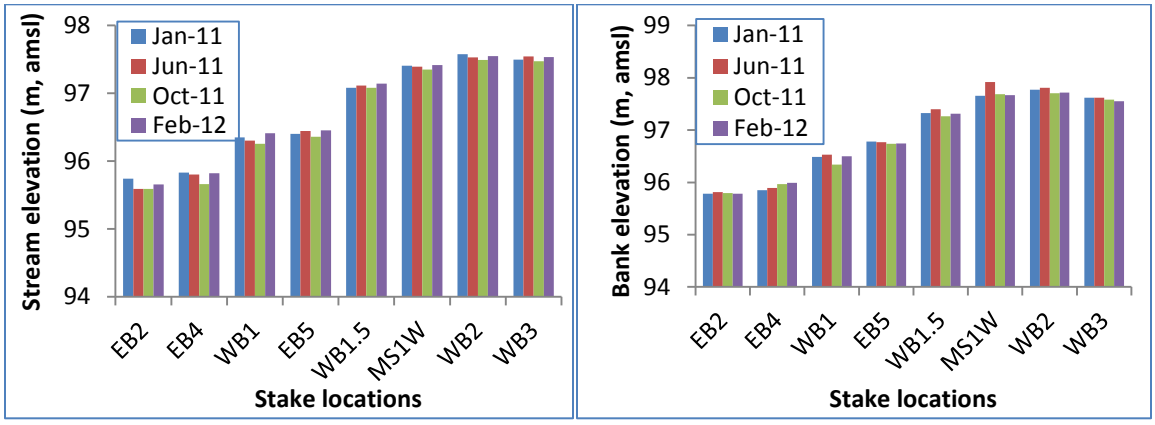

Figure 3.46. Survey data showing stream stage (A) and bank elevation (B) near springs.

Both stream stage and bank elevation data (Fig. 3.46, Appendix IV) show significant change in the stream gradient upstream and downstream of the stake location at MS1W, which is at the major bend along the reach. The calculated gradient was 0.001 between WB3 and MS1W (295 ft [90 m]) and 0.01 between MS1W and EB2 (436 ft [133 m]). Temporal variability in elevation was smallest for the stake at the east bank spring EB2, the farthest downstream spring along the study reach. Average bank elevation at this location was 95.793 m above mean sea level (amsl) with a standard deviation of 1.5 cm from January 2011 to February 2012. The stake at MS1W experienced the maximum change in bank elevation with a standard deviation of about 12 cm for the same study period. Average elevation at the stake close to the west bank spring WB1 was 96.466 m

amsl with a standard deviation of 8.5 cm. At the other survey locations, average channel elevation varied from 95.926 to 97.752 m amsl with standard deviation ranging from 3.0 to 6.0 cm. No seasonal signature was evident in the survey data.

Table 3.7. Standard deviation, range and average of bank elevation along the stream at stake locations.

Stake locations	Stdev (m)	Range (m)	Average (m, amsl)
EB2	0.015	0.034	95.793
EB4	0.064	0.137	95.926
WB1	0.085	0.192	96.466
EB5	0.021	0.043	96.757
WB1.5	0.055	0.134	97.326
MS1W	0.124	0.259	97.732
WB2	0.049	0.107	97.752
WB3	0.035	0.073	97.593

Chapter 4. Discussion

4.1 Spatial variability in groundwater discharge

Continuous records of hydraulic head in the monitoring wells, Ohio River stage, and precipitation showed a good inter-connection among the surface water and groundwater systems in the area (Figs. 3.1–3.5, 3.7). Precipitation was reflected in the form of increased baseflow in the stream as a result of aquifer recharge. Sub-reach and reach-scale discharge estimated using velocity and dye dilution gauging were comparable to each other for all four rounds of field work (Fig. 4.1). Overall, the sub-reach to reach-scale dye and gauged discharge values varied from 0.5 to 36 %.

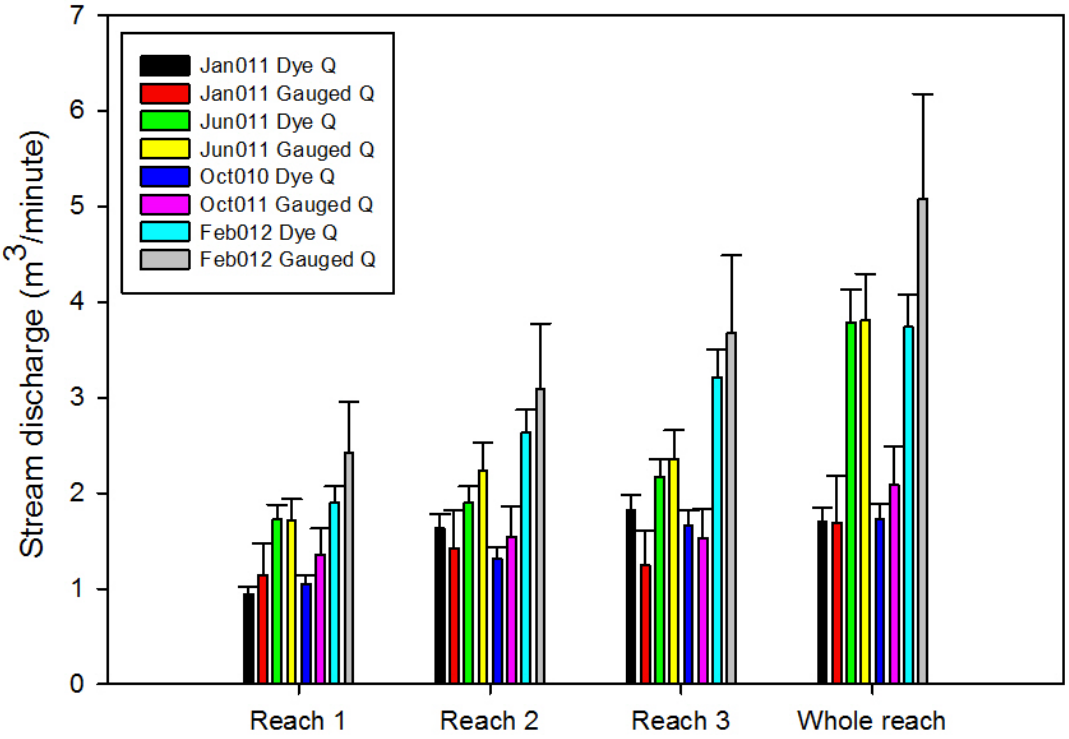

Figure 4.1. Sub-reach to reach-scale velocity-area and dye-dilution discharge.

Spatial variability in groundwater discharge was assessed in terms of point and sub-reach to reach scales. Point scale discharge from individual springs tended to be higher at upstream springs (WB3: 112 m^3/day) and lower at downstream springs (EB5: 8 m^3/day), but comparisons were hampered by the difficulty of measuring discharge from some orifices (e.g., MS1W and EB2). Sub-reach to reach-scale groundwater flux was estimated following three different techniques: velocity-area (seepage run, or current meter), dye dilution, and combined velocity/dye dilution (Harvey and Wagner, 2000). In combination, the velocity-area and dye-dilution methods can isolate the inflow and

outflow components of net exchange. Net groundwater exchange is computed by dividing the difference between gauged discharge at the downstream end and dye-dilution discharge at the upstream end by reach length. Groundwater inflow rate is obtained by dividing the difference between dye dilution discharge at downstream and upstream ends by reach length. The groundwater outflow rate is computed by subtracting net exchange from groundwater inflow. These components were computed by dividing by reach area instead of length in order to be consistent with the results obtained from other techniques as mentioned.

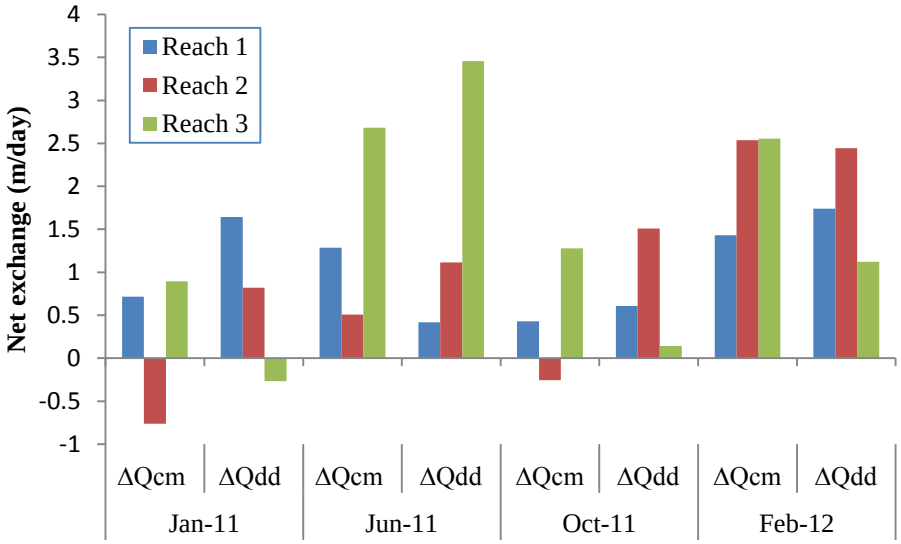

Figure 4.2. Sub-reach scale net exchange computed from velocity-area and dye dilution gauging. Subscripts 'cm' and 'dd' represent current meter and dye dilution, respectively.

Net exchanges (ΔQ) obtained from current meter and dye dilution gauging were estimated for each sub-reach for all four measurement periods by subtracting upstream discharge from downstream discharge (Fig. 4.2). Sub-reach scale values of ΔQ were positive except for current meter values along reach 2 in January and October 2011 and the dye dilution value along reach 3 in January 2011. The negative net exchange could be the result of the uncertainty associated with the measurement error, incomplete mixing of dye and/or stream-parallel flow or underflow. Reach-scale ΔQ values correlated more closely than the sub-reach scale values (Fig. 4.3).

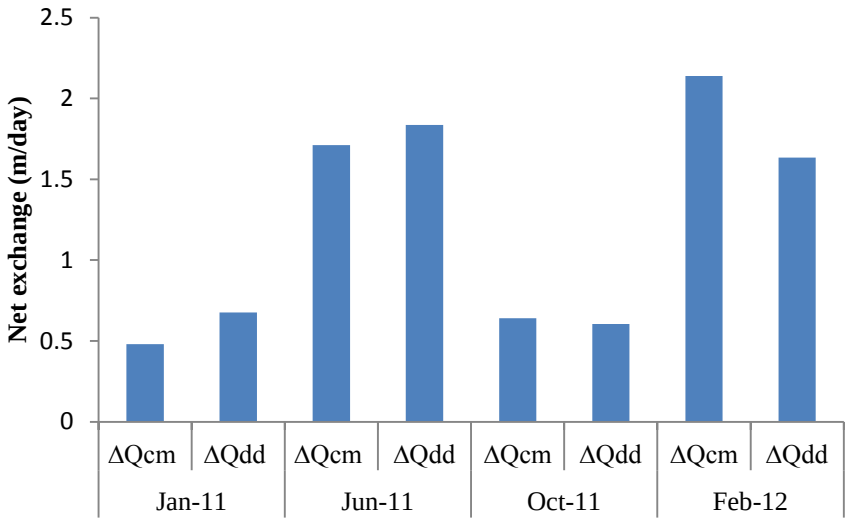

Figure 4.3. Reach-scale net exchange computed from velocity-area and dye dilution gauging.

Using the approach of Harvey and Wagner (2000), positive inflow values were obtained for all three sub-reaches at all time except for reach 3 in January 2011 (Fig. 4.4). The relatively small outflow in January is within measurement error. The difference between net exchange and inflow may be interpreted as a result of hyporheic exchange. At the reach scale, net exchange was equal to inflow in January and June 2011, indicating the only mode of exchange was groundwater inflow to the stream (Fig. 4.5). Net exchange exceeded inflow in October 2011 and February 2012.

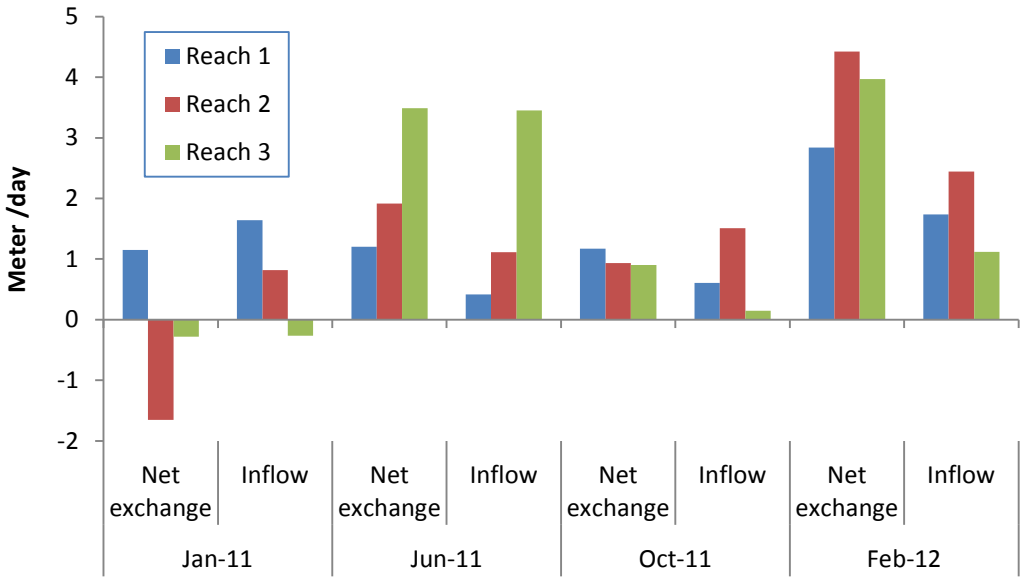

Figure 4.4. Sub-reach scale net exchange and inflow computed following Harvey and Wagner (2000).

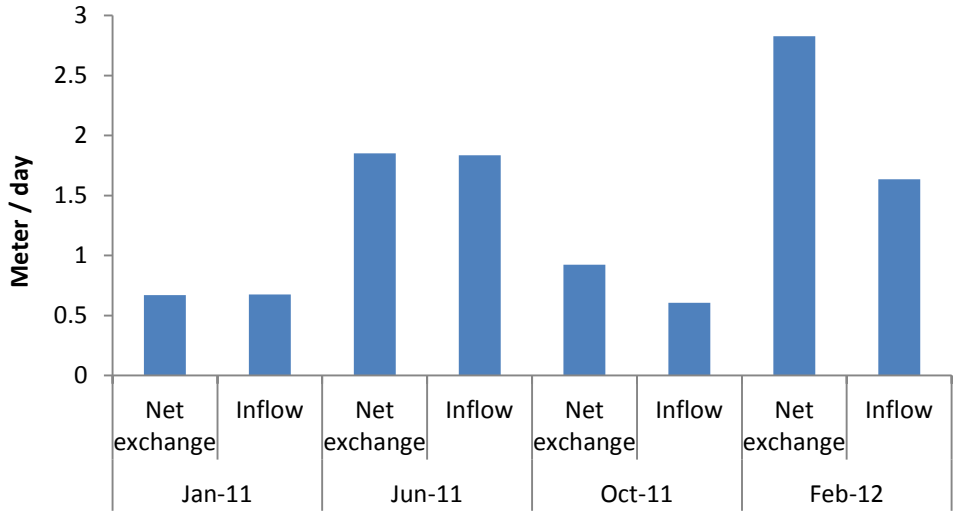

Figure 4.5. Reach-scale net exchange and inflow computed following Harvey and Wagner (2000).

4.2 Thermal investigation to assess spatial and temporal variability

Although the methods described can help to estimate sub-reach to reach-scale exchanges, it is not possible to identify specific discharge locations from such investigations. Thermal investigations along the surface water-groundwater interface have been able to identify and delineate the groundwater inflow locations in previous studies (Silliman et al., 1993; Conant, 2004; Keery et al., 2007; Lowry et al., 2007). Our thermal results have clearly isolated discrete, focused groundwater inflow zones along the study reach. The close spatial match of temperature anomalies with the observed springs in the field further supports the idea that the overall groundwater inflow along the study reach was dominated by focused discharge. Temperature distributions along the streambed were similar along the interface and at depth. However, temperature anomalies (close to spring water temperature [14 ± 3^{o} C]) were more prominent at depth, particularly those at ~ 0–20 m, ~ 60 m, ~ 100 m, ~ 140 m and ~ 220 m (Fig. 4.6). Temperature anomalies at the downstream end of reach 2, which were associated with EB5 and WB1.5, were distinct in the depth profile but were suppressed in the interface profile both in January and August. The anomaly at ~ 20–40 m along the west bank on both interface and depth maps in August was absent in January.

The same reach was investigated in August 2002 by measuring temperature at refusal depth following the same method at similar grid spacing (LaSage et al., 2008a). Refusal depth temperature profiles obtained for January and August 2011 were compared to the August 2002 temperature profile. In general, the temperature anomalies observed in 2002 were spatially persistent after 9 years (Fig. 4.7). However, some discharge locations have evolved over time by migrating several meters up- or downstream. The west bank spring WB0.5, which emerged at ~ 25 m in August 2011, was not evident in either August 2002

or January 2011. Conversely, the midstream spring MS2, located at ~ 180–200 m in 2002, may have migrated a few meters upstream.

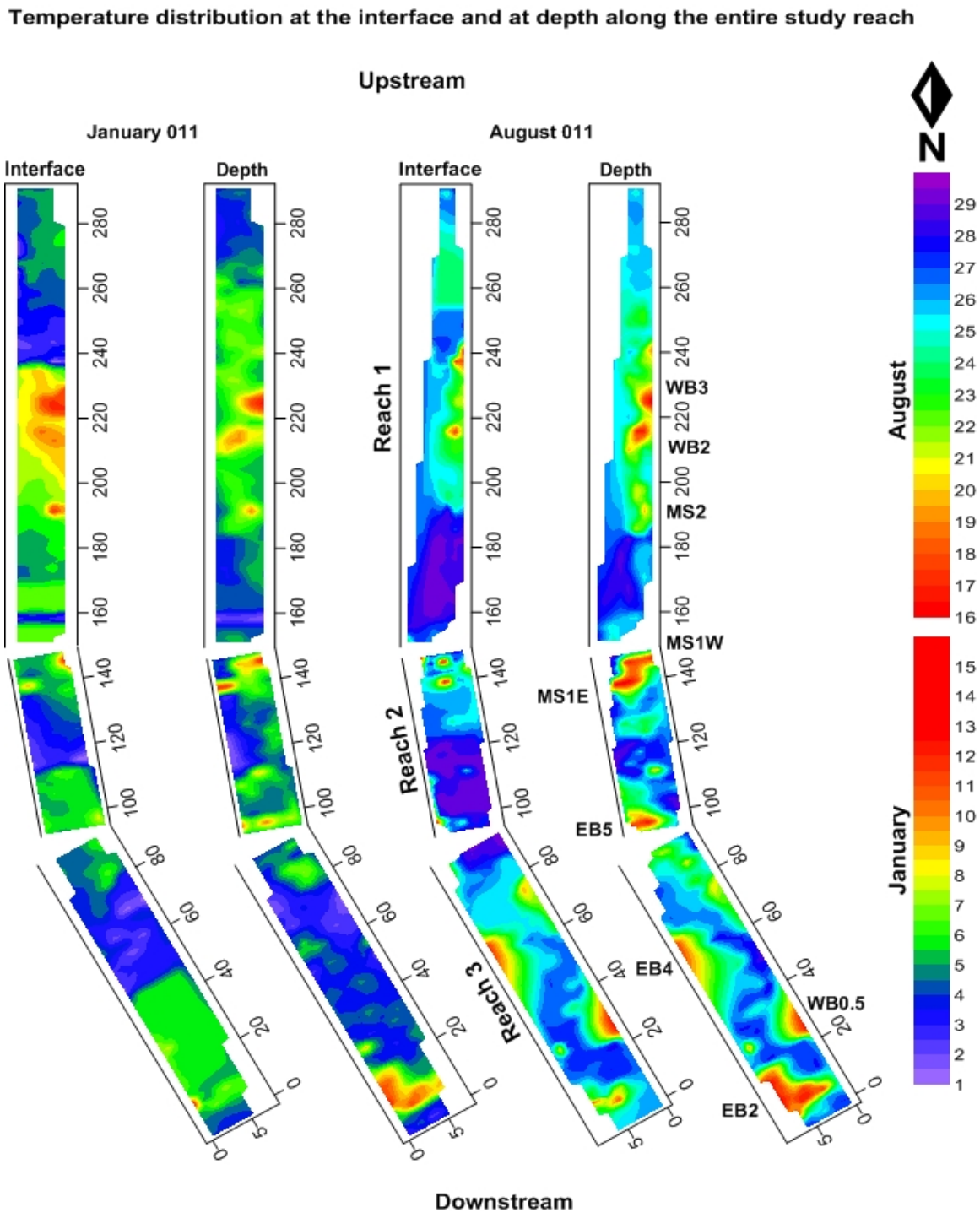

Figure 4.6. Spatial and temporal variation in temperature distribution at the interface and at depth.

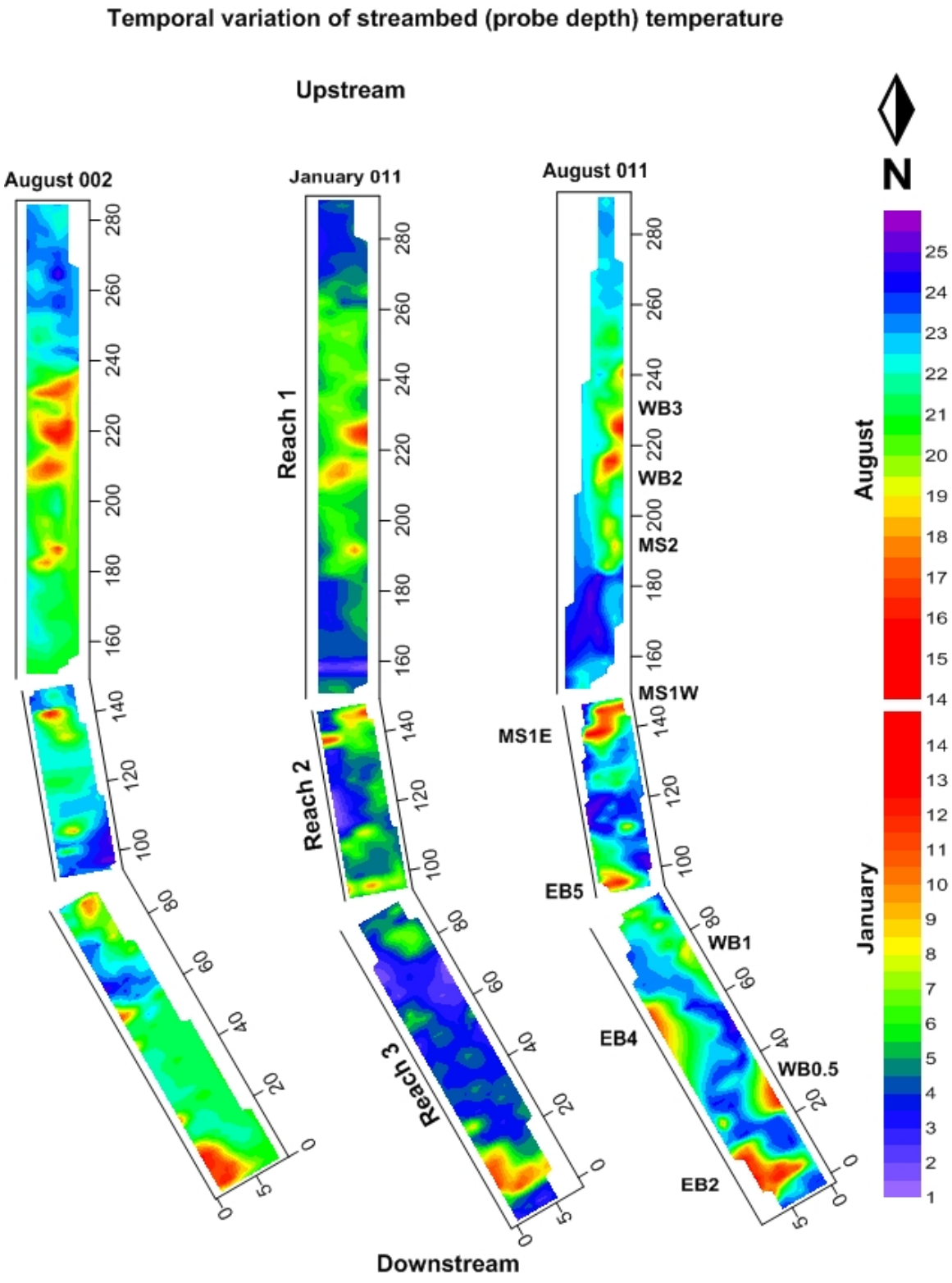

Figure 4.7. Comparison of streambed temperature distribution at depth between August 2002 and August 2011.

4.2.1 Comparison of distributed temperature sensing and temperature probing

4.2.1.1 Reach 1

DTS profiles along the east and west banks show temperature windows where diurnal temperature changes had been damped or moderated due to groundwater inflow. There were four distinct damped zones along the east bank, at ~ 115 m, between ~ 180–200 m, around 240 m and at ~ 265 m. Similarly, there were three damped zones along the west bank at ~ 185 m, ~ 220 m, and ~ 240 m. Anomalous zones on the DTS profile along the west bank match almost exactly with the anomalies on the temperature probe profile (Fig. 4.8) and correspond closely with observed springs along the west bank. Springs were not visible along the east bank of reach 1, but anomalous zones were identified along the east bank on the DTS profile and the temperature probe anomalies along the west bank seem to be propagating towards the east bank. The anomaly around 190 m on the temperature probe profile, which was not visible in the field, is reflected on the DTS west bank profile. In this case DTS was useful in validating the result obtained from the temperature probing.

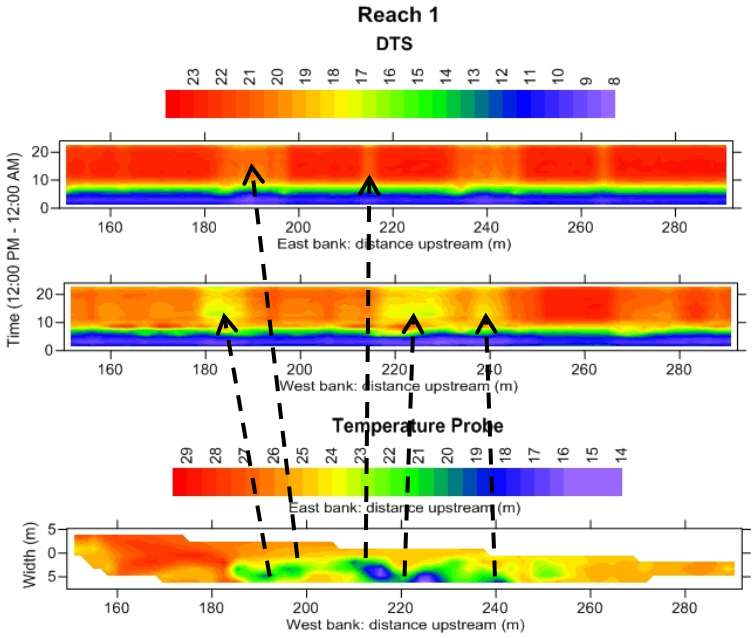

Figure 4.8. Comparison of anomalies on DTS profiles (top two figures) and temperature probe depth profile from August 2011 (bottom), reach 1.

4.2.1.2 Reach 2

The anomalies on the temperature probe map representing springs MS1W at 145 m and MS1E at 140 m were clearly reflected on the west and east bank DTS profiles (Fig. 4.9). Similarly, the anomaly identified between 125–130 m on the temperature probe depth map was captured on the west bank DTS profile. This location is important because it

coincided with the emergence of a new spring first observed in July 2012. The anomaly is not as pronounced as in other locations of identified groundwater inflow but it could represent the area in the process of new spring evolution.

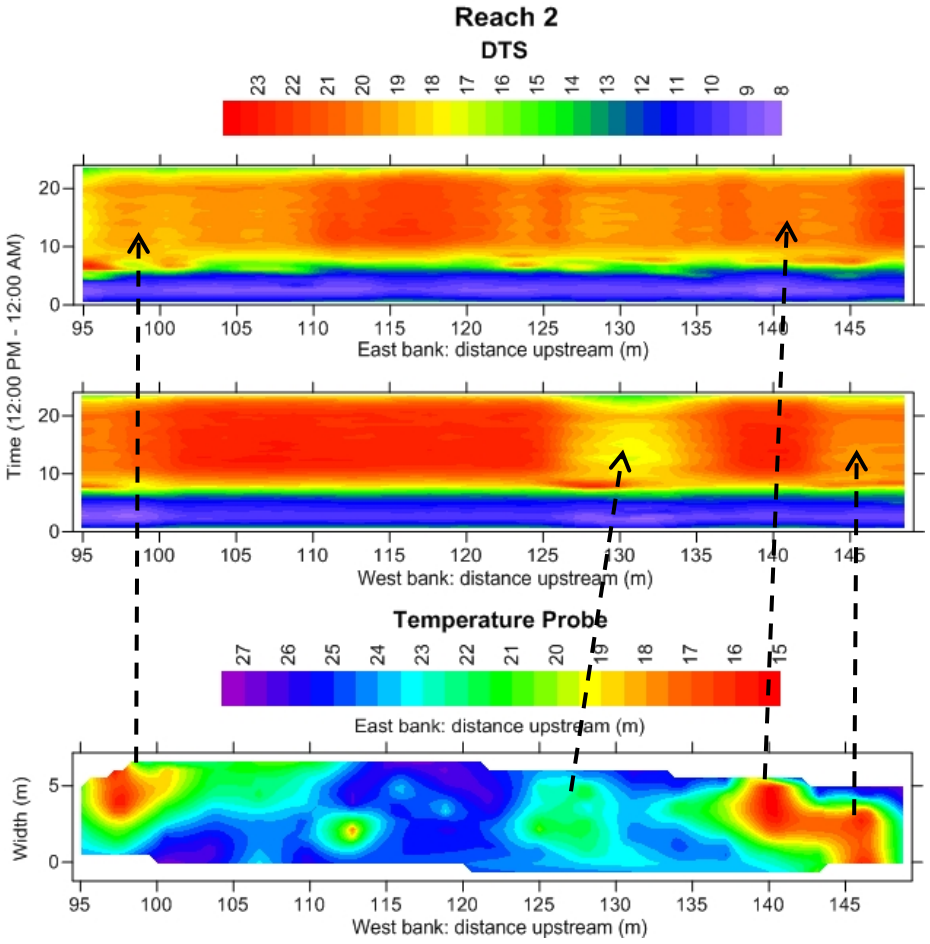

Figure 4.9. Comparison of anomalies on DTS profiles (top two figures) and temperature probe depth profile from August 2011 (bottom), reach 2.

4.2.1.3 Reach 3

A broad window between ~ 5–40 m on the east bank DTS profile (Fig. 4.10) and more discrete anomalies on the temperature probe map are likely to reflect a group of springs (EB2, EB3, and EB4) observed in the field. Fewer springs were visible along the west bank, as reflected on the DTS and temperature probe profiles (Fig. 4.10). Almost all of the anomalous zones identified along east and west banks by temperature probing were also observed along the DTS profiles. An exception is the anomaly observed on the east bank at ~ 60 m, which was not evident on the DTS profile. This anomaly corresponds with the east bank spring EB4, which was set back from the stream channel, and the DTS cable was laid out on the bank surface, i.e., out of the water.

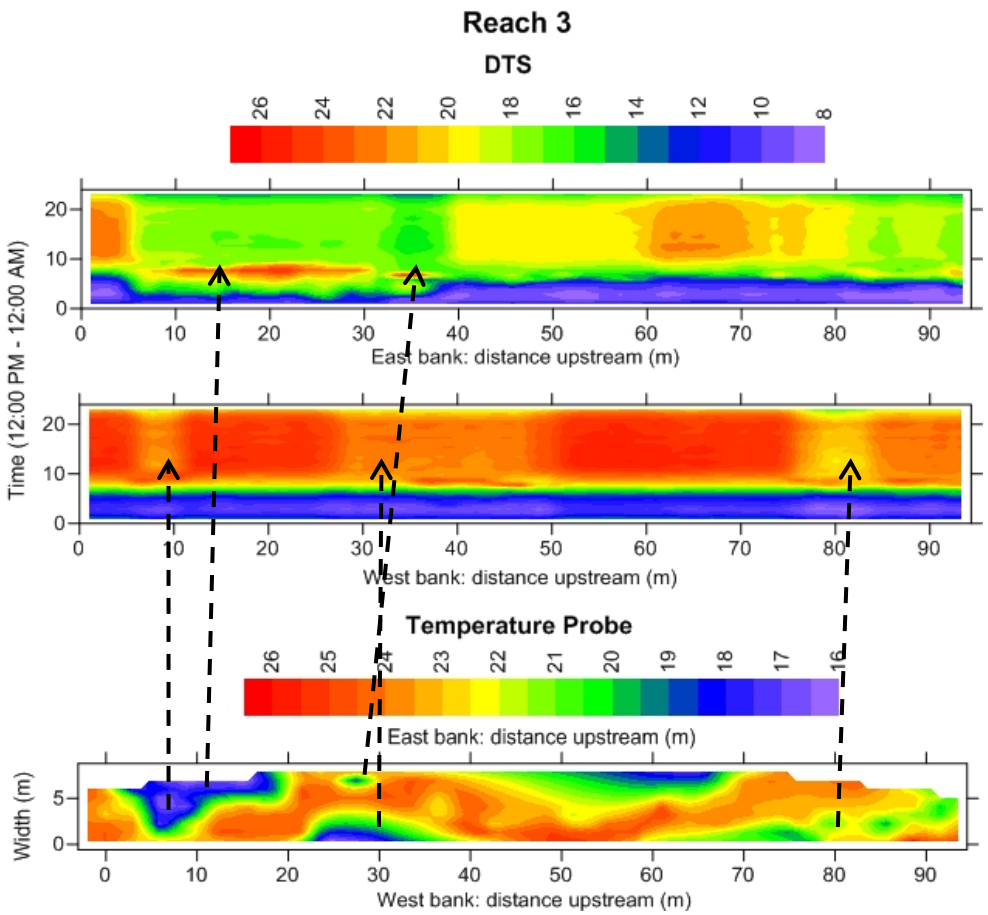

Figure 4.10. Comparison of anomalies on DTS profiles (top two figures) and temperature probe depth profile from August 2011 (bottom), reach 3.

4.3 Integrated methods of groundwater flux measurements

Hydraulic conductivity (K) values for the individual monitoring wells LB6Y and LB6Z were 0.9 and 1.8 m/day (3.0 and 5.9 ft/day), respectively. These K values were used to calculate the Darcy flux between wells using continuous hydraulic head monitoring data from September 23, 2011, to February 8, 2012. Using minimum and maximum values for K and Δh, the range of fluxes varied from 0.007 to 2.3 m/day with an average of 0.2 m/day. Taking an average K value for the wells and maximum Δh value for the monitoring period, the calculated flux was 1.7 m/day. Using the average K value and minimum Δh during the monitoring period, the calculated flux was 0.01 m/day.

Average groundwater fluxes calculated from four different methods were similar (Fig. 4.11), with 0.2 m/day standard deviation. Average Darcy flux calculated between the two monitoring wells was 1.16 m/day (3.8 ft/day). Average groundwater fluxes of 1.34, 1.19 and 1.55 m/day were estimated from velocity-area, dye-dilution and velocity/dye-dilution gauging methods, respectively, for the entire reach.

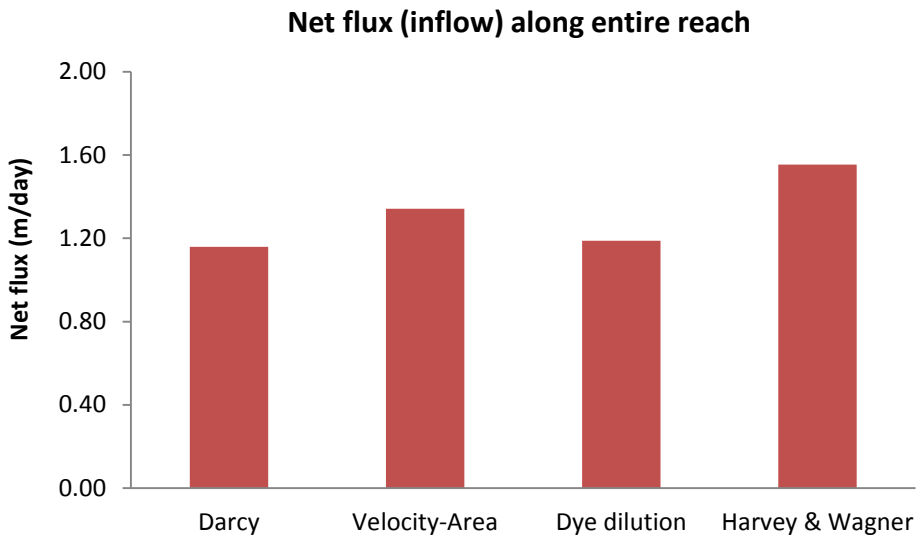

Figure 4.11. Reach-scale annual average of groundwater flux.

4.4 Sub-reach to reach-scale groundwater flux: total vs. focused

Results from temperature probing and DTS indicate that the groundwater discharge to the stream was primarily focused. The reach areas were computed from gaging data and the focused discharge areas were determined from the temperature probe maps at depth (Appendix V). The focused discharge zones were delineated based on the temperature envelope (range) obtained from 1-month continuous temperature monitoring for the springs along the study reach. Sub-reach scale focused discharge areas were calculated by adding up all individual discharge zones. Net discharge fluxes were computed by dividing ΔQ (obtained from gaging and dye dilution) by sub-reach and reach area as well as by the focused discharge area.

The temperature anomaly map generated from the January 2011 temperature probe data indicated that groundwater inflow zones occupied only about 2.6% of reach 1, 2.2% of reach 2, and 3.5% of reach 3. Similarly, in August 2011, temperature anomalies occupied only about 2.8% of reach 1, 8.0% of reach 2, and 7.4% of reach 3. The areas contributing to groundwater discharge were greater in summer than in winter. Overall, approximately 5.9% of the whole reach area was found to contribute to groundwater discharge in August, versus 2.9% in January.

Sub-reach to reach-scale groundwater fluxes were calculated assuming that all discharge coincides with temperature anomalies. The focused groundwater fluxes were estimated as an annual average integrating all four rounds of field measurements. The estimated flux varied least between velocity gauging and dye dilution estimates for reach 1, dye-dilution and Harvey and Wagner (velocity/dye-dilution) estimates for reach 2, and velocity gauging and Harvey and Wagner estimates for reach 3 (Fig. 4.12). The estimated annual

average of focused groundwater flux along the entire reach was 33.8 m/day for gauging, 35.6 m/day for dye tracing, and 42.5 m/day for the Harvey and Wagner method.

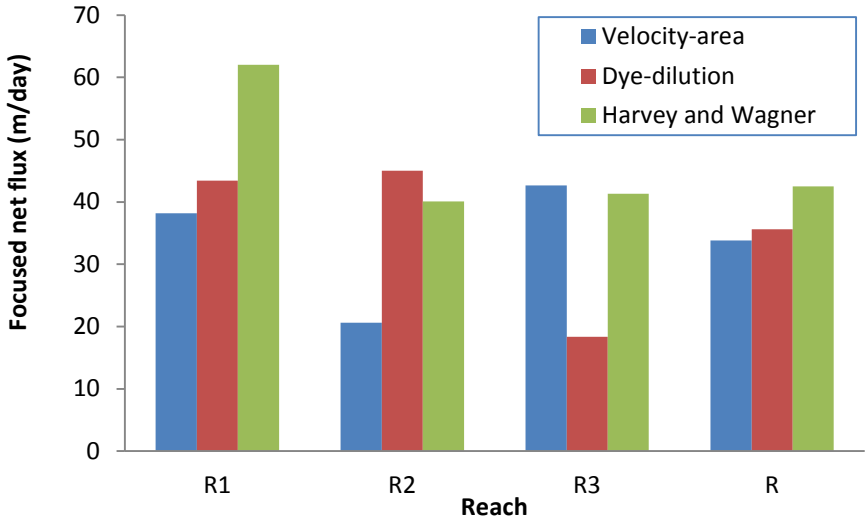

Figure 4.12. Sub-reach (R1 – R3) to reach-scale (R) focused groundwater discharge estimates.

4.5 Temporal variability in groundwater discharge and associated erosion

Temporal variability in spring discharge from 1999 to 2001 (LaSage et al., 2008a) was broadly similar to variability observed in this study. Discharge values at WB3 (and at WB2, prior to the emergence of WB3) were greatest during spring and early summer and smallest during autumn and early winter (Fig. 4.13). Discharge at WB1 was lower and not as variable during the year. As noted previously, measurement of spring discharge was limited by the shape and size of the orifice and its location relative to stream level.

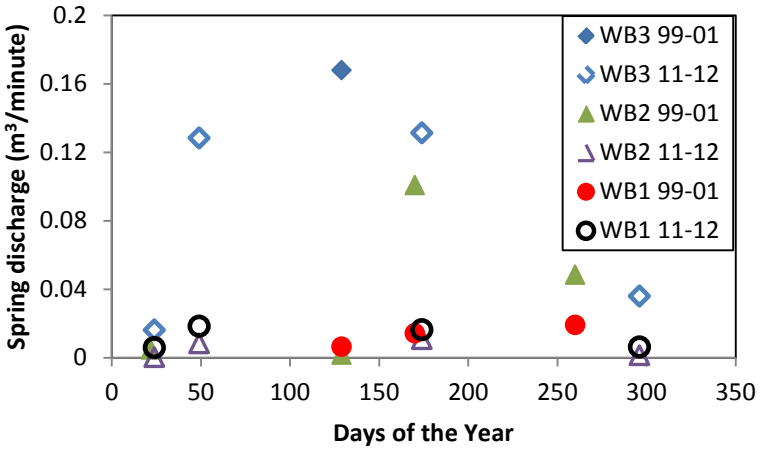

Figure 4.13. Measured discharge of springs WB1, WB2, and WB3, 1999-2001 and 2011-2012.

Figure 4.14. West bank spring,WB3 in 2002 and 2011.

Spring WB3 emerged between January and May 2000 (LaSage et al., 2008a) and persisted at approximately the same location through this study, but experienced bank collapse as a result of groundwater sapping and stream erosion (Fig. 4.14). Average bank elevation at the WB3 erosion stake varied by ±3 cm from January 2011 to February 2012. Besides WB1, WB2, and WB3, other springs observed by LaSage et al. (2008a) that persisted throughout this study included EB2, EB3, and EB4, although discharge from EB4 decreased. Springs observed by LaSage et al. (2008a) that were not visible in this study included EB1, WB1.5, MS2, and RR, although the temperature anomaly along reach 1 at ~ 190 m may coincide with the new location of MS2, as noted above. Similarly, MS1 appears to have evolved into orifices along the east bank (MS1E) and west bank (MS1W) between 2002 and 2010. Springs that emerged during this study included WB0.5, WB1.1, EB5, MS1EU, and the unnamed spring observed in July 2012 at 125–130 m along reach 2, where the August 2011 temperature probe map indicated a relatively weak anomaly. Spring discharge created a 0.82-m (2.7-ft) deep and 0.9-m (3-ft) wide hole in the streambed (Fig. 4.15).

Figure 4.15. Newly emerged streambed spring along reach 2.

4.6 Variability in contaminant concentrations

In general, as observed by LaSage et al. (2008b), concentrations of TCE and ^{99}Tc in stream water increased along the study reach from WB3U to EB2D; peak concentrations in springs commonly occurred at WB3; and TCE and ^{99}Tc were usually greater in west bank (upgradient) springs than in east bank springs. The surface water TCE and ^{99}Tc concentrations at the up- and downstream ends of the study reach were compared to the stream discharge for the periods June 1999 to May 2001 (LaSage et al., 2008b) and January 2011 to February 2012 (Fig. 4.16). Except for ^{99}Tc in October 2000 and ^{99}Tc and TCE in January 2001, contaminant concentrations in stream water and net contaminant fluxes (indicating mass loading to the stream) tended to vary seasonally with discharge. However, maximum contaminant concentrations in stream water and springs, and maximum values of net contaminant fluxes along the study reach (Fig. 4.17), were considerably higher during 1999–2001. In the present study, maximum concentrations were 160 µg/L for TCE at WB3 in January 2011 and 72.74 pCi/L for ^{99}Tc at RRS in October 2011, versus 450 µg/L for TCE and 461 pCi/L for ^{99}Tc previously (both at WB3 in May 2001). Contaminants were detected in all springs monitored during 1999–2001, whereas concentrations in springs downstream of MS1W were ususally at or below the detection limit of 5 µg/L for TCE, and were close to or within uncertainty for ^{99}Tc, during 2011–2012. In addition, ^{99}Tc concentrations decreased more than TCE concentrations did between two periods: the linear regression between two analytes in springs was TCE = 1.1^{99}Tc + 8.9 (r^2 = 0.86) for 1999–2001 and TCE = 2.7^{99}Tc – 3.8 (r^2 = 0.95) for 2011–2012. The relatively small differences in contaminant concentrations in stream water between WB3U and EB2D magnify the effects of measurement uncertainty on contaminant mass-flux calculations.

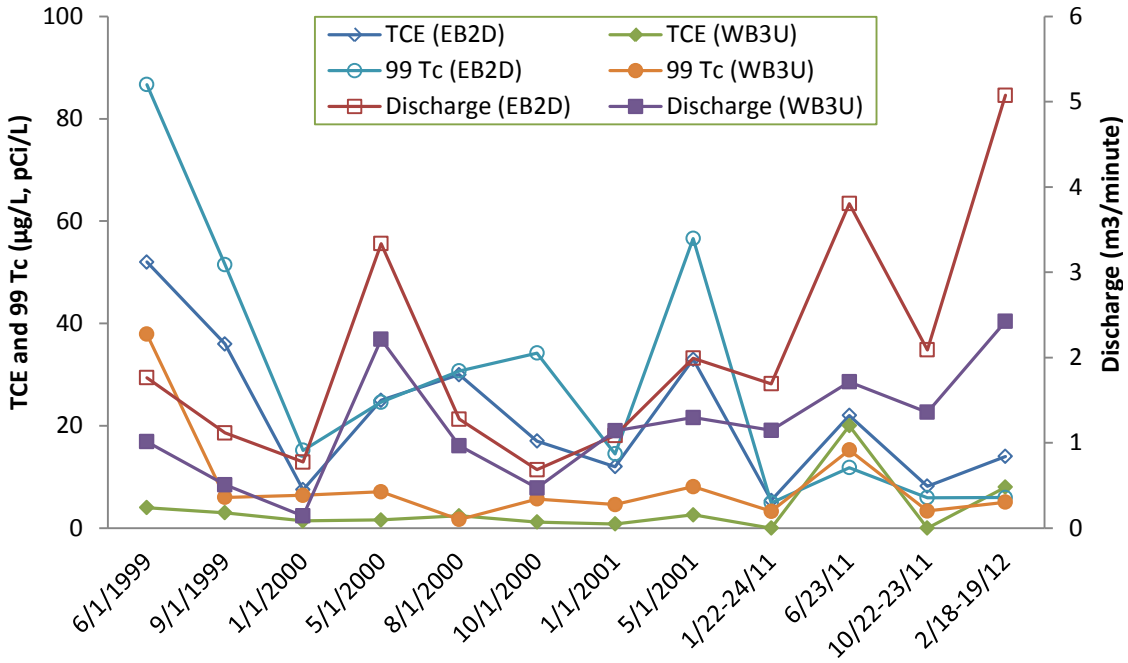

Figure 4.16. TCE and ^{99}Tc concentrations in surface water at the up- and downstream ends of the study reach compared with stream discharge.

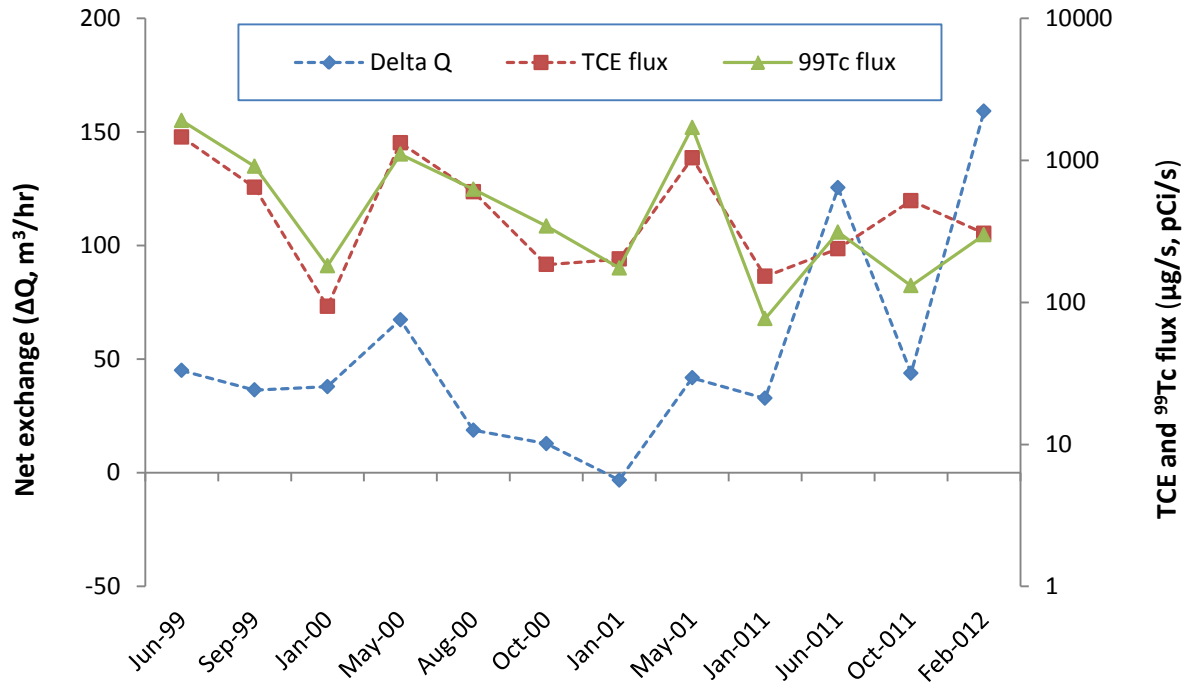

Figure 4.17. Net contaminant and seepage fluxes (from velocity-area gauging) along the study reach.

Results of quarterly to semiannual monitoring of WB3 by PGDP contractors (who referred to the spring as LBCSP5) help to bridge the temporal data gap between LaSage et al. (2008b) and this study. The contractors monitored ^{99}Tc from 2002 to 2010 and TCE from 2002 to 2012. Because samples were not collected simultaneously by us and by contractors or analyzed in the same laboratories, exact comparisons are limited. However, a plot of the combined data sets versus time indicates that contaminant concentrations have gradually decreased, albeit with fluctuations, during the past decade (Fig. 4.18). Dissolved oxygen results for springs in this study (2.60–4.77 mg/L, with values 2.9–4.2 mg/L for 28 of 32 samples) are similar to those of LaSage et al. (2008b) (2.92–5.10 mg/L, with values 3.3–4.5 mg/L for 45 of 47 samples). As observed by LaSage et al. (2008b), putative daughter products of anaerobic degradation of TCE (less-chlorinated ethenes, such as dichloroethenes and vinyl chloride) were largely undetectable in this study (the only exception was cis-1,2-dichloroethene, which occurred at 5.3 µg/L in RRS in October 2011). Therefore, the decrease in TCE concentrations between 2001 and 2011 is probably not a result of intrinsic reductive dechlorination, which is a common mechanism of TCE attenuation at other sites (LaSage et al., 2008b). Instead, the decrease in both ^{99}Tc and TCE concentrations is likely attributable to the interception of contaminant plumes by upgradient pumping wells between PGDP and Little Bayou Creek. Pumping wells were initially installed in August 1995 (Jolly, 1996), but portions of the plumes beyond the radius of influence of the wells would have continued to discharge to the creek for some period thereafter.

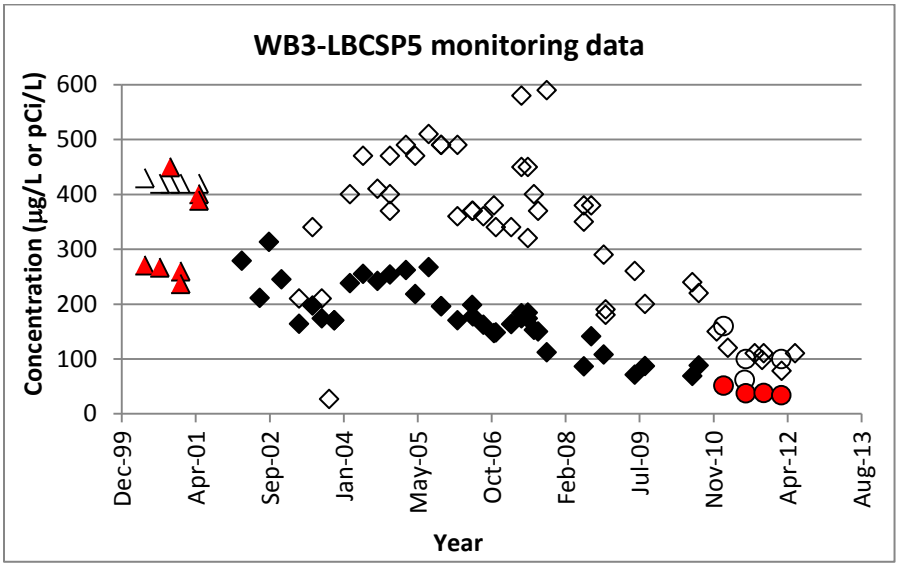

Figure 4.18. TCE concentrations (open symbols) and ^{99}Tc concentrations (filled symbols) in farthest upstream spring of the study reach. Data sources: triangles, LaSage et al. (2008b); diamonds, contractors; circles: present study.

Chapter 5. Summary and conclusions

The study has built upon previous studies in the Little Bayou Creek watershed (Fryar et al., 2000; Mukherjee et al., 2005; LaSage et al., 2008a, b), using a variety of approaches at different spatial scales, to document ongoing seasonality in groundwater discharge and the persistence and evolution of discharge zones along the creek. Synchronous changes in Ohio River stage and hydraulic heads in the monitoring wells at the study site indicate regional groundwater-surface water interconnection. Both systems responded similarly to precipitation events, albeit with some time lags. Stream discharge was measured from velocity-area and dye-dilution methods when there was no rainfall recorded at three nearby rainfall stations for at least the previous 24 hours. Discharge increased downstream for all four rounds of field measurements (January, June, and October 2011 and February 2012). The stream discharge was greater in June and February as a result of increased baseflow due to relatively high precipitation 30 days prior to the measurement period. Seasonality was observed in stream discharge during 1999–2001 and 2010–2012 measurement periods, with greatest values in February-June and minimum values in October-January. Spring discharge also varied seasonally in both study periods.

Velocity gauging (velocity-area) and dye-dilution discharge values indicated a net gain along the ~ 300 m study reach for all four rounds of measurement. This result is consistent with the 1999–2001 measurements. Net exchange was greater in June and February than in January and October for both gauging and dye dilution. At the sub-reach scale, the negative net exchange value, obtained from dye dilution measurement, for reach 3 in January 2011 may indicate a temporary losing condition. Similarly, the negative net exchange for gauging and positive net exchange for dye dilution along reach 2 in January and October may represent the potential area of hyporheic exchange.

Sub-reach to reach-scale net exchanges estimated from differential velocity-area and dye dilution gauging includes inflow and outflow components that cannot be isolated. We used a method proposed by Harvey and Wagner (2000) to isolate these components. The outflow component for both sub-reach and reach-scales was negative or near zero, indicating that net exchange was a result of inflow only. Average, area-normalized, annual net fluxes calculated from the velocity-area, dye dilution, and velocity/dye-dilution (Harvey and Wagner) methods at the reach scale (1.19 – 1.55 m/day) were similar to the value calculated from Darcy's law for the paired monitoring wells (1.16 m/day).

The tracer test data were used as an input in the OTIS-P software to simulate the dye breakthrough curve (BTC) and to estimate hydrologic parameters (dispersion coefficient, main channel cross-sectional area, storage zone cross-sectional area, and storage zone

exchange coefficient). Observed and simulated BTCs matched reasonably well, with r^2 0.99 for peak concentration and r^2 varying from 0.82–0.94 for peak time. Simulated average main channel cross-sectional area was almost equal to (4% less than) the measured area. Storage zone cross-sectional area also varied at the sub-reach scale, with an average reach scale area of 0.033 m^2, which accounts for approximately 3% of main channel cross-sectional area. The A_S/A ratio for the entire study period and for entire reach varied between 0.01 and 0.05. Our estimated ratio compares with the upper range value (0.04) calculated for an adjoining downstream reach by Mukherjee et al. (2005).

Manually measured spring temperatures in different seasons (11.7 to 15.3 ^oC) varied relatively narrowly compared to the stream (0.66 ^oC to 25.8 ^oC). Three springs along the study reach were continuously monitored at 5-minute intervals for ~ 5 months. Average temperature in all three springs during the first month (September 22–October 22, 2011) varied within a range of 14.8 to 15.5 ^oC. Minimum and maximum recorded temperatures in these springs during this period were 12.6 ^oC at MS1W and 18.6 ^oC at WB3, respectively. Subsequent variability in recorded temperatures was attributed to loggers becoming unmoored from the spring orifices. Temperature anomaly maps at the top of the stream bed and at maximum probe penetration depth were generated for each of three sub-reaches from the data acquired in January and August 2011. Locations of springs were inferred and, in most cases, observed where temperatures were markedly (5 to 8 ^oC) above background in winter or below background in summer. Most of the discharge locations delineated from temperature probing were also reflected along the DTS profile. The discharge zones delineated in January 2011 and August 2011 were compared against the August 2002 temperature anomaly map. Some discharge locations had not changed significantly since 2002, but upstream or downstream migration of some springs and emergence of new springs were observed and reflected in the temperature anomaly maps. Using the range of 12.6 to 17.1 ^oC (MS1W) to delineate focused discharge zones coinciding with mapped temperature anomalies, groundwater inflow occurred along ~ 2.9% of the entire reach area in January 2011 and ~ 5.9% of the entire reach area in August. Estimated annual average of focused groundwater flux through the entire reach varied from 34–43 m/day.

TCE and ^{99}Tc concentrations in stream water were higher along the upstream half of the study reach and were greater when baseflow was elevated (June and February). TCE and ^{99}Tc in stream water correlated poorly for individual sampling rounds (maximum r^2 = 0.38 in June 2011), but they correlated strongly for the entire dataset (r^2 = 0.89). As observed by LaSage et al. (2008b), contaminant concentrations in springs tended to decrease downstream. The TCE and ^{99}Tc were highest, 160 µg/L and 51.68 pCi/L respectively, for the farthest upstream spring (WB3) in January 2011. Concentrations were below detection limits for the farthest downstream spring (EB2). In general, contaminant concentrations were higher in west bank springs than in east bank springs.

TCE and ^{99}Tc concentrations in springs, unlike in the stream, correlate strongly for both individual sampling rounds as well as for all data collectively, with r^2 values ranging from 0.9–0.99. Regular monitoring of spring WB3 between 1999 and 2012 has shown a gradual decrease in concentration for both contaminants. Dissolved oxygen concentrations from 2.60 to 4.77 mg/L and lack of daughter products such as dichloroethenes, vinyl chloride and ethenes in the springs during the study period indicated unfavorable conditions for intrinsic reductive dechlorination of TCE, as observed by LaSage et al. (2008b). The decrease in both ^{99}Tc and TCE concentrations is likely attributable to the interception of contaminant plumes by upgradient pumping wells between PGDP and Little Bayou Creek. However, the persistence of TCE concentrations above the MCL in springs along the uppermost sub-reach suggests that additional remedial measures may be necessary.

APPENDICES

Appendix I

Little Bayou Creek stream gauged field data (current meter with top-setting rod)

Sample IDs indicate gauging locations downstream (D) and upstream (U) of east bank (EB), west bank (WB) and mid-stream (MS) springs.

October 22, 2010					
EB2D			EB2U		
Distance along transect	Depth (ft)	Velocity (ft/s)	Distance along transect	Depth (ft)	Velocity (ft/s)
0	0	0	0	0	0
0.6	0.76	0.01	0.6	0.32	0.01
1.6	1.08	0.01	1.6	0.68	0.05
2.6	1.24	0.02	2.6	0.78	0.05
3.6	1.3	0.04	3.6	0.8	0.05
4.6	1.33	0.04	4.6	0.86	0.05
5.6	1.4	0.03	5.6	0.78	0.07
6.6	1.35	0.04	6.6	0.7	0.07
7.6	1.32	0.04	7.6	0.65	0.06
8.6	1.28	0.03	8.6	0.6	0.07
9.6	1.22	0.04	9.6	0.49	0.03
10.6	1.18	0.05	10.6	0.4	0.07
11.6	1.06	0.07	11.6	0.29	0.04
12.6	1.05	0.1	12.6	0.4	0.03
13.6	1.04	0.08	13.6	0.23	0.02
14.6	0.99	0.07	14.6	0.24	0.05
15.6	0.95	0.05	15.6	0.27	0.08
16.6	1.01	0.04	16.6	0.33	0.06
17.6	1.1	0.01	17.6	0.32	0.06
18.6	0.9	0.04	18.6	0.33	0.11
19.6	0.68	0.02	19.6	0.41	0.1
20.6	0.4	0	20.6	0.51	0.11
21.7	0	0	21.6	0.61	0.1
			22.6	0.68	0.09
			23.6	0.43	0.05
			24.6	0.22	0.02
			25.3	0	0

October 22, 2010					
WB1.5D			WB1.5U		
Distance along transect	Depth (ft)	Velocity (ft/s)	Distance along transect	Depth (ft)	Velocity (ft/s)
0	0	0	0	0	0
1.1	0.23	0	1	0.22	0
2.1	0.32	0	2	0.38	0.01
3.1	0.45	0.01	3	0.55	0.01
4.1	0.47	0.04	4	0.69	0.04
5.1	0.56	0.08	5	0.88	0.04
6.1	0.66	0.07	6	0.84	0.06
7.1	0.69	0.1	7	0.91	0.07
8.1	0.68	0.1	8	0.83	0.07
9.1	0.74	0.12	9	0.81	0.1
10.1	0.82	0.11	10	0.73	0.12
11.1	0.87	0.12	11	0.8	0.12
12.1	0.7	0.1	12	0.75	0.11
13.1	0.62	0.11	13	0.88	0.11
14.1	0.55	0.11	14	0.87	0.07
15.1	0.47	0.09	15	0.91	0.03
16.1	0.42	0.08	16	0.86	0.01
17.1	0.38	0.08	17	0.47	0
18.1	0.18	0	18	0.62	0
19.1	0.17	0	19	0.36	0
20.1	0.2	0	20	0	0
21.1	0.28	0			
22.1	0.31	0.03			
23.1	0.28	0			
24	0	0			

October 22, 2010					
MS1D			MS1U		
Distance along transect	Depth (ft)	Velocity (ft/s)	Distance along transect	Depth (ft)	Velocity (ft/s)
0	0	0	0	0	0
1	0.23	0	0.4	0.32	0
2	0.32	0	1.4	0.33	0
3	0.46	0	2.4	0.42	0.02
4	0.59	0.05	3.4	0.47	0.02
5	0.7	0.02	4.4	0.4	0.03
6	0.84	0.03	5.4	0.39	0.04
7	0.72	0.06	6.4	0.45	0.06
8	0.68	0.06	7.4	0.51	0.07
9	0.68	0.08	8.4	0.62	0.07
10	0.6	0.08	9.4	0.72	0.06
11	0.65	0.08	10.4	0.83	0.06
12	0.69	0.09	11.4	0.8	0.07
13	0.74	0.09	12.4	0.86	0.06
14	0.74	0.08	13.4	0.89	0.08
15	0.78	0.08	14.4	0.92	0.06
16	0.87	0.07	15.4	0.67	0.07
17	0.88	0.07	16.4	0.55	0.07
18	0.87	0.06	17.4	0.56	0.06
19	1.2	0.03	18.4	0.4	0
20	0.65	0.04	19.4	0.27	0
21	0.63	0	20.7	0	0
21.9	0	0			

October 22, 2010					
WB3D			WB3U		
Distance along transect	Depth (ft)	Velocity (ft/s)	Distance along transect	Depth (ft)	Velocity (ft/s)
0	0	0	0	0	0
1	0.23	0	0.7	0.29	0
2	0.19	0	1.7	0.62	0.02
3	0.17	0	2.7	0.69	0.03
4	0.19	0	3.7	0.61	0.04
5	0.2	0	4.7	0.55	0.04
6	0.23	0.04	5.7	0.51	0.06
7	0.24	0	6.7	0.55	0.07
8	0.21	0	7.7	0.54	0.06
9	0.34	0.01	8.7	0.53	0.06
9.5	0.39	0.01	9.7	0.6	0.07
10	0.37	0.05	10.7	0.57	0.07
10.5	0.33	0.17	11.7	0.53	0.07
11	0.32	0.41	12.7	0.55	0.06
11.5	0.33	0.52	13.7	0.64	0.06
12	0.42	0.52	14.7	0.82	0.05
12.5	0.44	0.45	15.7	0.7	0.05
13	0.46	0.26	16.7	0.6	0.05
13.5	0.47	0.07	17.7	0.57	0.05
14	0.5	0.08	18.7	0.49	0.06
14.5	0.51	0.01	19.7	0.49	0.05
15	0.53	0	20.7	0.53	0.04
16	0.54	0	21.7	0.61	0.01
17	0.72	0	22.7	0.49	0
18	0.8	0.02			
19	0.85	0.04			
19.5	0.86	0.06			
20.6	0	0			

January 23, 2011					
EB2D			EB2U		
Distance along transect	Depth (ft)	Velocity (ft/s)	Distance along transect	Depth (ft)	Velocity (ft/s)
1.25	0	0	1.167	0	0
2	0.33	0	2	0.25	0.05
2.5	0.6	0	2.5	0.49	0.05
3	0.91	0	3	0.52	0.07
3.5	0.92	0.01	3.5	0.6	0.09
4	0.87	0	4	0.65	0.07
4.5	1.08	0.02	4.5	0.72	0.07
5	1.07	0.03	5	0.7	0.07
5.5	1.07	0.06	5.5	0.62	0.08
6	1.1	0.05	6	0.57	0.07
6.5	1.05	0.07	6.5	0.5	0.1
7	1.02	0.06	7	0.48	0.1
7.5	1.05	0.08	7.5	0.44	0.09
8	1.08	0.06	8	0.42	0.1
8.5	1.11	0.05	8.5	0.4	0.09
9	1.15	0.06	9	0.36	0.09
9.5	1.16	0.06	9.5	0.38	0.08
10	1.14	0.08	10	0.42	0.08
10.5	1.08	0.06	10.5	0.4	0.08
11	1.06	0.07	11	0.37	0.07
11.5	1.07	0.05	11.5	0.36	0.07
12	1.11	0.06	12	0.33	0.07
12.5	1.12	0.06	12.5	0.32	0.06
13	1.14	0.07	13	0.36	0.06
13.5	1.26	0.05	13.5	0.37	0.08
14	1.31	0.06	14	0.42	0.09
14.5	1.3	0.06	14.5	0.5	0.09
15	1.34	0.05	15	0.49	0.08
15.5	1.37	0.06	15.5	0.52	0.09
16	1.41	0.05	16	0.54	0.09
16.5	1.42	0.06	16.5	0.49	0.08
17	1.43	0.05	17	0.54	0.09
17.5	1.19	0.03	17.5	0.64	0.07
18	1.45	0.02	18	0.63	0.09
18.5	1.39	0.03	18.5	0.73	0.07
19	1.36	0.03	19	0.74	0.08
19.5	1.32	0.03	19.5	0.78	0.07
20	1.3	0.03	20	0.79	0.09
20.5	1.3	0.01	20.5	0.79	0.08
21	1.3	0	21	0.8	0.07
22	1.02	0	21.5	0.82	0.07
23	0	0	22	0.8	0.09
			22.5	0.84	0.05
			23	0.9	0.02
			23.5	0.86	0.02
			24	0.82	0.02
			24.5	0.91	0.01
			25	0.84	0
			26	0.48	0
			26.75	0	0

January 23, 2011					
WB1D			WB1U		
Distance along transect	Depth (ft)	Velocity (ft/s)	Distance along transect	Depth (ft)	Velocity (ft/s)
1.25	0	0	1.83	0	0
2	0.2	0.01	2.25	0.25	0
2.5	0.26	0.05	2.5	0.41	0.1
3	0.23	0.17	2.75	0.47	0.13
3.5	0.26	0.23	3	0.48	0.12
4	0.28	0.28	3.25	0.47	0.19
4.5	0.3	0.35	3.5	0.45	0.29
5	0.25	0.34	3.75	0.6	0.29
5.5	0.17	0.25	4	0.58	0.34
6	0.12	0.03	4.25	0.55	0.3
6.5	0.12	0.02	4.5	0.52	0.41
8	0.14	0	4.75	0.56	0.43
9	0.26	0	5	0.57	0.4
10	0.28	0	5.25	0.55	0.34
11	0.33	0.02	5.5	0.52	0.3
11.5	0.34	0.05	5.75	0.51	0.35
12	0.29	0.02	6	0.5	0.34
12.5	0.3	0.01	6.25	0.46	0.27
13	0.3	0	6.5	0.45	0.17
13.5	0.3	0.01	6.75	0.43	0.21
14	0.25	0.03	7	0.41	0.27
14.5	0.26	0.05	7.25	0.37	0.23
15	0.25	0.09	7.5	0.37	0.23
15.5	0.3	0.15	7.75	0.35	0.16
16	0.31	0.12	8	0.31	0.17
16.5	0.38	0.2	8.25	0.31	0.12
17	0.42	0.19	8.5	0.3	0.11
17.5	0.43	0.18	8.75	0.28	0.11
18	0.51	0.16	9	0.26	0.06
18.5	0.57	0.14	9.25	0.23	0.06
19	0.52	0.14	9.5	0.17	0
19.5	0.43	0.2	10	0.13	0
20	0.44	0.15	11	0.1	0
20.5	0.43	0.16	11.5	0	0
21	0.41	0.12			
21.5	0.44	0.08			
22	0.41	0.11			
22.5	0.32	0.1			
23	0.35	0.06			
23.5	0.32	0			
24	0.28	0			
24.5	0.23	0.01			
26	0	0			

January 23, 2011					
WB1.5D			WB1.5U		
Distance along transect	Depth (ft)	Velocity (ft/s)	Distance along transect	Depth (ft)	Velocity (ft/s)
2	0	0	1.25	0	0
3	0.25	0	2	0.25	0.03
3.5	0.3	0.02	2.5	0.46	0.03
4	0.37	0.04	3	0.53	0.02
4.5	0.33	0.01	3.5	0.57	0.02
5	0.2	0.01	4	0.62	0.02
5.5	0.21	0	4.5	0.64	0.05
6	0.23	0.01	5	0.68	0.04
6.5	0.22	0	5.5	0.83	0.03
7	0.22	0.01	6	1.1	0.03
7.5	0.2	0	6.5	1.08	0.02
8	0.25	0.03	7	1.02	0.05
8.5	0.25	0.04	7.5	1.02	0.07
9	0.27	0.01	8	0.97	0.1
9.5	0.36	0.02	8.5	0.96	0.1
10	0.43	0.09	9	0.91	0.09
10.5	0.47	0.08	9.5	0.9	0.11
11	0.51	0.07	10	0.83	0.1
11.5	0.56	0.09	10.5	0.86	0.08
12	0.58	0.1	11	0.84	0.1
12.5	0.58	0.1	11.5	0.8	0.11
13	0.7	0.11	12	0.81	0.08
13.5	0.74	0.1	12.5	0.84	0.09
14	0.78	0.1	13	0.87	0.08
14.5	0.79	0.11	13.5	0.8	0.06
15	0.77	0.11	14	0.85	0.06
15.5	0.79	0.11	14.5	0.81	0.05
16	0.78	0.1	15	0.68	0.03
16.5	0.73	0.1	15.5	0.68	0.03
17	0.68	0.08	16	0.74	0.03
17.5	0.67	0.09	16.5	0.73	0.02
18	0.69	0.09	17	0.7	0.01
18.5	0.69	0.1	17.5	0.62	0
19	0.66	0.09	18	0.51	0
19.5	0.68	0.09	19	0.47	0
20	0.6	0.1	20	0.23	0
20.5	0.54	0.07	21.33	0	0
21	0.55	0.04			
21.5	0.53	0.01			
22	0.48	0			
22.5	0.43	0			
23	0.38	0			
24	0.32	0			
25	0.26	0			
25.67	0	0			

January 23, 2011					
WB1D			WB1U		
Distance along transect	Depth (ft)	Velocity (ft/s)	Distance along transect	Depth (ft)	Velocity (ft/s)
0.58	0	0	0.5	0	0
1	0.18	0	1.5	0.26	0
1.5	0.36	0.04	2	0.31	0
2	0.52	0.05	2.5	0.41	0.01
2.5	0.65	0.05	3	0.48	0.02
3	0.79	0.04	3.5	0.51	0.02
3.5	0.95	0.05	4	0.47	0.03
4	0.9	0.06	4.5	0.51	0.03
4.5	0.9	0.05	5	0.49	0.05
5	0.84	0.06	5.5	0.54	0.06
5.5	0.85	0.05	6	0.63	0.06
6	0.88	0.05	6.5	0.65	0.08
6.5	0.91	0.05	7	0.72	0.08
7	0.9	0.06	7.5	0.86	0.07
7.5	0.92	0.06	8	0.96	0.09
8	0.9	0.06	8.5	0.91	0.09
8.5	0.91	0.07	9	0.84	0.1
9	0.93	0.07	9.5	0.83	0.09
9.5	0.9	0.07	10	0.81	0.09
10	0.88	0.08	10.5	0.81	0.07
10.5	0.87	0.06	11	0.8	0.09
11	0.83	0.06	11.5	0.75	0.1
11.5	0.82	0.08	12	0.72	0.09
12	0.81	0.06	12.5	0.74	0.09
12.5	0.77	0.07	13	0.69	0.08
13	0.75	0.08	13.5	0.65	0.08
13.5	0.69	0.08	14	0.65	0.09
14	0.66	0.07	14.5	0.62	0.08
14.5	0.59	0.07	15	0.52	0.1
15	0.61	0.08	15.5	0.51	0.08
15.5	0.58	0.06	16	0.5	0.08
16	0.8	0.02	16.5	0.52	0.08
16.5	0.83	0.05	17	0.56	0.09
17	0.81	0.03	17.5	0.53	0.07
17.5	0.86	0.02	18	0.51	0.06
18	0.8	0.01	18.5	0.49	0.06
18.5	0.73	0.02	19	0.44	0.06
19	0.61	0.02	19.5	0.43	0.06
19.5	0.55	0.01	20	0.44	0.05
20	0.56	0.01	20.5	0.41	0.02
21	0.28	0	21	0.36	0.01
22.67	0	0	21.5	0.28	0
			22.5	0	0

January 23, 2011					
WB3D			WB3U		
Distance along transect	Depth (ft)	Velocity (ft/s)	Distance along transect	Depth (ft)	Velocity (ft/s)
1.33	0	0	0.17	0	0
2	0.84	0.26	1	0.19	0
2.5	0.83	0.26	1.5	0.4	0
3	0.76	0.23	2	0.61	0.01
3.5	0.73	0.23	3	0.51	0.03
4	0.71	0.22	3.5	0.47	0.02
4.5	0.68	0.21	4	0.43	0.04
5	0.62	0.14	4.5	0.42	0.04
5.5	0.56	0.05	5	0.51	0.04
6	0.61	0.14	5.5	0.58	0.05
6.5	0.64	0.13	6	0.65	0.06
7	0.65	0.1	6.5	0.64	0.03
7.5	0.67	0.06	7	0.66	0.04
8	0.62	0.05	7.5	0.68	0.07
8.5	0.59	0.05	8	0.72	0.07
9	0.6	0.03	8.5	0.75	0.05
9.5	0.51	0.02	9	0.7	0.05
10	0.52	0.01	9.5	0.68	0.06
10.5	0.38	0.01	10	0.67	0.05
11	0.35	0	10.5	0.66	0.05
11.5	0.33	0	11	0.63	0.05
12	0.38	0	11.5	0.61	0.07
13	0.32	0	12	0.61	0.06
14	0.26	0	12.5	0.6	0.09
15	0.22	0	13	0.61	0.08
16	0.19	0	13.5	0.57	0.07
17	0.2	0	14	0.52	0.08
18	0.22	0	14.5	0.52	0.08
19	0.23	0	15	0.49	0.08
20.75	0	0	15.5	0.48	0.06
			16	0.47	0.07
			16.5	0.43	0.08
			17	0.47	0.08
			17.5	0.43	0.06
			18	0.42	0.09
			18.5	0.46	0.08
			19	0.43	0.08
			19.5	0.42	0.08
			20	0.45	0.08
			20.5	0.51	0.07
			21	0.54	0.07
			21.5	0.56	0.06
			22	0.55	0.05
			22.5	0.42	0.03
			23	0.28	0

June 23, 2011					
EB2D			EB2U		
Distance along transect	Depth (ft)	Velocity (ft/s)	Distance along transect	Depth (ft)	Velocity (ft/s)
1	0	0	1	0	0
2	0.35	0.02	2	0.16	0.59
3	0.44	0.02	3	0.23	0.83
4	0.67	0.33	4	0.29	0.63
5	0.62	0.38	5	0.24	0.83
6	0.68	0.47	6	0.22	0.77
7	0.68	0.52	7	0.25	0.82
8	0.69	0.31	8	0.23	0.87
9	0.66	0.41	9	0.27	0.77
10	0.68	0.31	10	0.28	0.73
11	0.67	0.26	11	0.3	0.93
12	0.53	0.09	11.5	0.32	0.87
13	0.64	0.08	12	0.29	0.69
14	0.65	0.1	12.5	0	0
15	0.79	0.04			
16	0.63	0.01			
17	0.64	0.02			
18	0.68	0			
19	0.62	0			
20	0.63	0			
21	0.35	0			
21.42	0	0			

June 23, 2011					
WB1D			WB1U		
Distance along transect	Depth (ft)	Velocity (ft/s)	Distance along transect	Depth (ft)	Velocity (ft/s)
0.67	0	0	0.75	0	0
2	0.15	0	1	0.18	0
3	0.18	0.16	2	0.62	0.52
4	0.15	0.37	2.5	0.65	0.52
5	0.1	0	3	0.55	0.34
6	0.16	1.55	3.5	0.48	0.5
7	0.17	1.31	4	0.54	0.6
8	0.16	1.7	4.5	0.55	0.49
9	0.27	1.95	5	0.53	0.48
10	0.25	1.88	5.5	0.54	0.56
11	0.22	1.86	6	0.6	0.56
12	0.24	1.89	6.5	0.57	0.41
13	0.19	1.27	7	0.52	0.41
14	0.1	0.54	7.5	0.53	0.38
15	0	0	8	0.43	0.24
16	0	0	8.5	0.46	0.08
17	0.2	0.28	9	0.31	0
18	0.25	0.31	10	0	0
19	0.47	0.23			
20	0.2	0.1			
20.33	0	0			

June 23, 2011					
WB1.5D			WB1.5U		
Distance along transect	Depth (ft)	Velocity (ft/s)	Distance along transect	Depth (ft)	Velocity (ft/s)
3.33	0	0	1.08	0	0
8	0.11	0	2	0.8	0.04
9	0.15	0.04	3	0.63	0.06
10	0.22	0.19	4	0.63	0.08
11	0.22	0.25	5	0.62	0.03
12	0.27	0.27	6	0.64	0.04
13	0.23	0.33	7	0.75	0.06
14	0.26	0.38	8	0.82	0.12
15	0.32	0.3	9	0.76	0.24
16	0.4	0.34	10	0.74	0.29
17	0.45	0.37	11	0.76	0.3
18	0.53	0.33	12	0.75	0.27
19	0.58	0.35	13	0.73	0.24
20	0.59	0.26	14	0.74	0.19
21	0.6	0.09	15	0.73	0.18
22	0.53	0.1	16	0.61	0.16
23	0.38	0	17	0.57	0.12
24	0	0	18	0.52	0.08
			19	0.43	0.05
			20	0.23	0
			21	0	0

June 23, 2011					
MS1D			MS1U		
Distance along transect	Depth (ft)	Velocity (ft/s)	Distance along transect	Depth (ft)	Velocity (ft/s)
0	0	0	1.33	0	0
1	0.4	0.03	2	0.28	0.04
2	0.51	0.07	3	0.34	0.09
3	0.69	0.13	4	0.58	0.12
4	1.16	0.15	5	0.63	0.08
5	0.82	0.13	6	0.7	0.1
6	1.01	0.12	7	0.64	0.21
7	1.05	0.13	8	1.05	0.16
8	1.09	0.13	9	1.01	0.23
9	0.95	0.15	10	0.9	0.19
10	0.92	0.13	11	0.75	0.19
11	0.83	0.12	12	0.8	0.18
12	0.76	0.12	13	0.7	0.11
13	0.7	0.17	14	0.55	0.03
14	0.78	0.15	15	0.24	0
15	0.79	0.07	16	0	0
16	0.83	0.03			
17	0.65	0.03			
18	0.33	0.02			
19.25	0	0			

January 23, 2011					
WB3D			WB3U		
Distance along transect	Depth (ft)	Velocity (ft/s)	Distance along transect	Depth (ft)	Velocity (ft/s)
0.42	0	0	0.33	0	0
1	1.01	0	1	0.31	0
2	1.03	0	2	0.55	0
3	0.72	0.4	3	0.7	0.01
4	0.52	0.46	4	0.52	0.03
5	0.33	0.61	5	0.41	0.08
6	0.32	0.6	6	0.51	0.06
7	0.22	0.58	7	0.52	0.06
8	0.25	0.56	8	0.56	0.05
9	0.21	0.61	9	0.57	0.07
10	0.17	0.11	10	0.58	0.09
11	0.2	0.31	11	0.56	0.1
12	0.13	0.04	12	0.56	0.11
13	0	0	13	0.51	0.12
13.83	0	0	14	0.45	0.16
			15	0.5	0.16
			16	0.33	0.17
			17	0.35	0.16
			18	0.47	0.16
			19	0.5	0.13
			20	0.44	0.14
			21	0.48	0.15
			22	0.47	0.11
			23	0.13	0.05
			23.16	0	0

October 22, 2011					
EB2D			**EB2U**		
Distance along transect	Depth (ft)	Velocity (ft/s)	Distance along transect	Depth (ft)	Velocity (ft/s)
0.6	0	0	1.17	0	0
1	0.33	0	1.5	0.13	0.11
2	0.51	0.01	2	0.23	0.31
3	0.79	0.04	2.5	0.35	0.38
4	0.86	0.06	3	0.34	0.42
5	0.8	0.02	3.5	0.27	0.43
6	0.68	0.03	4	0.25	0.42
7	0.72	0.05	4.5	0.31	0.32
8	0.81	0.03	5	0.29	0.2
8.5	0.83	0.1	5.5	0.34	0.27
9	0.84	0.08	6	0.28	0.39
9.5	0.8	0.09	6.5	0.27	0.33
10	0.81	0.12	7	0.25	0.43
10.5	0.84	0.09	7.5	0.23	0.42
11	0.85	0.11	8	0.24	0.45
11.5	0.82	0.1	8.5	0.23	0.46
12	0.81	0.13	9	0.23	0.45
12.5	0.73	0.11	9.5	0.23	0.31
13	0.9	0.12	10	0.25	0.21
13.5	0.92	0.15	10.5	0.22	0.16
14	0.98	0.11	11	0.24	0.12
14.5	1	0.12	11.5	0.16	0.14
15	0.99	0.1	12	0.13	0.02
15.5	0.98	0.11	12.5	0.14	0.02
16	1	0.11	13	0.16	0.01
16.5	0.96	0.12	13.5	0.13	0
17	0.96	0.11	14	0.16	0
17.5	1.1	0.09	15	0.21	0.01
18	1.2	0.05	16.33	0	0
18.5	1.2	0.05	22.25	0	0
19	1.3	0.05	23.5	0.2	0
19.5	1.1	0.03	24	0.26	0
20	0.89	0.02	25	0.18	0
21	0.46	0	26	0.2	0
21.9	0.46	0	27.25	0	0

October 22, 2011					
WB1D			WB1U		
Distance along transect	Depth (ft)	Velocity (ft/s)	Distance along transect	Depth (ft)	Velocity (ft/s)
19	0	0	0.25	0	0
20	0.15	0.1	1	0.26	0.01
20.5	0.17	0.04	2	0.24	0
21	0.2	0.2	3	0.23	0
21.5	0.18	0.16	4	0.27	0
22	0.22	0.2	5	0.28	0.01
22.5	0.28	0.41	6	0.2	0
23	0.3	0.51	6.66	0	0
23.5	0.31	0.54	11	0	0
24	0.3	0.57	12.5	0.31	0.51
24.5	0.34	0.47	13	0.35	1.04
25	0.35	0.72	13.5	0.35	1.2
25.5	0.34	0.79	14	0.33	1.05
26	0.24	0.83	14.5	0.34	0.86
26.5	0.18	0.79	15	0.29	0.72
26.83	0.16	0.73	15.5	0.22	0.2
27.42	0	0	16	0.13	0.04
			16.58	0	0

October 22, 2011					
WB1.5D			WB1.5U		
Distance along transect	Depth (ft)	Velocity (ft/s)	Distance along transect	Depth (ft)	Velocity (ft/s)
11.42	0	0	0.42	0	0
13	0.21	0	2	0.21	0
13.5	0.26	0.01	3	0.37	0.01
14	0.33	0.01	4	0.46	0.01
14.5	0.34	0	5	0.51	0.09
15	0.33	0	6	0.55	0.11
15.5	0.36	0.01	7	0.53	0.17
16	0.37	0.04	8	0.55	0.19
16.5	0.41	0.07	9	0.51	0.19
17	0.38	0.11	10	0.46	0.21
17.5	0.41	0.16	11	0.45	0.2
18	0.46	0.15	12	0.42	0.23
18.5	0.5	0.25	13	0.41	0.23
19	0.52	0.39	14	0.36	0.19
19.5	0.54	0.5	15	0.32	0.15
20	0.6	0.45	16	0.37	0.14
20.5	0.63	0.45	17	0.28	0.08
21	0.61	0.32	18	0.22	0.09
21.5	0.59	0.15	18.5	0.16	0.03
22	0.53	0.12	21	0.16	0
22.5	0.44	0.1	22	0.34	0
23	0.4	0.06	23	0.37	0
23.5	0.35	0.02	24	0.27	0
24	0.31	0	24.5	0	0
24.5	0.32	0			
25	0.36	0			
26.16	0	0			

October 22, 2011					
MS1D			MS1U		
Distance along transect	Depth (ft)	Velocity (ft/s)	Distance along transect	Depth (ft)	Velocity (ft/s)
0	0	0	1.25	0	0
1	0.24	0	2.5	0.24	0.04
2	0.31	0.04	3	0.35	0.08
3	0.42	0.07	3.5	0.36	0.08
4	0.73	0.06	4	0.47	0.07
5	0.56	0.07	4.5	0.43	0.02
5.5	0.56	0.07	5	0.34	0.03
6	0.54	0.08	5.5	0.32	0.06
6.5	0.55	0.07	6	0.4	0.04
7	0.59	0.1	6.5	0.3	0.15
7.5	0.65	0.09	7	0.5	0.19
8	0.62	0.09	7.66	0.87	0.21
8.5	0.6	0.1	8	0.87	0.22
9	0.62	0.11	8.5	0.88	0.25
9.5	0.63	0.11	9	0.71	0.22
10	0.65	0.14	9.5	0.63	0.24
10.5	0.69	0.11	10	0.59	0.23
11	0.7	0.12	10.5	0.67	0.17
11.5	0.78	0.11	11	0.73	0.2
12	0.79	0.12	11.5	0.76	0.1
12.5	0.8	0.14	12	0.91	0.01
13	0.81	0.12	12.5	0.87	0.01
13.5	0.77	0.12	13	0.76	0.1
14	0.72	0.11	13.5	0.73	0.08
14.5	0.67	0.1	14	0.67	0.02
15	0.69	0.11	14.5	0.56	0
15.5	0.74	0.07	15	0.46	0
16	0.52	0.03	15.5	0.35	0
17	0.56	0.06	16.75	0	0
18	0.63	0.02			
19	0.26	0			

October 22, 2011					
WB3D			WB3U		
Distance along transect	Depth (ft)	Velocity (ft/s)	Distance along transect	Depth (ft)	Velocity (ft/s)
0.83	0	0	0	0	0
1.5	0.9	0.06	1	0.64	0
2	0.91	0.17	2	0.74	0
2.5	0.92	0.17	3	0.77	0.01
3	0.82	0.21	4	1.05	0.02
3.5	0.81	0.24	5	0.96	0.02
4	0.8	0.31	6	0.79	0.02
4.5	0.79	0.22	7	0.65	0.04
5	0.71	0.25	8	0.64	0.03
5.5	0.66	0.17	9	0.72	0.04
6	0.68	0.16	10	0.73	0.04
6.5	0.65	0.13	11	0.72	0.07
7	0.57	0.04	11.5	0.75	0.07
7.5	0.65	0.02	12	0.78	0.08
8	0.47	0	12.5	0.8	0.07
9	0.41	0	13	0.8	0.07
10	0.45	0	13.5	0.81	0.09
11	0.44	0	14	0.82	0.1
12	0.36	0	14.5	0.81	0.1
13	0.22	0	15	0.82	0.09
14.9	0	0	15.5	0.81	0.09
19	0	0	16	0.83	0.11
20.66	0	0	16.5	0.86	0.1
			17	0.86	0.09
			17.5	0.84	0.07
			18	0.86	0.07
			18.5	0.81	0.04
			19	0.78	0.06
			19.5	0.76	0.05
			20	0.7	0.05
			20.5	0.69	0.05
			21	0.61	0.03
			22	0.48	0
			23	0.21	0
			23.66	0	0

February 19, 2012					
EB2D			EB2U		
Distance along transect	Depth (ft)	Velocity (ft/s)	Distance along transect	Depth (ft)	Velocity (ft/s)
1.16	0	0	16	0	0
2	0.28	0.25	18	0.14	0
2.5	0.26	0.38	18.5	0.16	0.08
3	0.23	0.52	19	0.15	0.22
3.5	0.3	0.52	19.5	0.14	0.36
4	0.31	0.77	20	0.15	0.33
4.5	0.33	0.83	20.5	0.12	0.44
5	0.35	0.77	21	0.16	0.54
5.5	0.36	0.67	21.25	0.14	0.45
6	0.37	0.78	21.5	0.16	0.52
6.5	0.32	0.77	21.75	0.18	0.52
7	0.35	0.76	22	0.2	0.62
7.5	0.42	0.73	22.25	0.22	0.75
8	0.41	0.69	22.5	0.24	0.85
8.5	0.43	0.7	22.75	0.27	0.97
9	0.4	0.65	23	0.28	0.91
9.5	0.35	0.53	23.25	0.3	1.07
10	0.26	0.45	23.5	0.32	0.96
10.5	0.14	0.28	23.75	0.38	1.08
11.5	0.16	0.39	24	0.47	1.18
12	0.17	0.32	24.25	0.47	1.16
12.5	0.15	0.34	24.5	0.51	1.26
13	0.18	0.45	24.75	0.58	1.34
13.5	0.2	0.49	25	0.57	1.35
14	0.16	0.51	25.25	0.59	1.34
14.5	0.16	0.44	25.5	0.6	1.33
15	0.18	0.53	25.75	0.53	1.39
15.5	0.18	0.38	26	0.49	1.34
16	0.14	0.56	26.25	0.5	1.38
16.5	0.15	0.44	26.5	0.45	1.31
17	0.15	0.51	26.75	0.36	1.2
17.5	0.16	0.61	27	0.25	1.27
18	0.18	0.51	27.25	0.18	1.03
18.5	0.21	0.57	27.5	0	0
19	0.24	0.57			
19.5	0.22	0.56			
20	0.28	0.64			
20.5	0.27	0.67			
21	0.26	0.68			
21.5	0.26	0.39			
22.5	0	0			

February 19, 2012					
WB1D			WB1U		
Distance along transect	Depth (ft)	Velocity (ft/s)	Distance along transect	Depth (ft)	Velocity (ft/s)
16.83	0	0	0.58	0	0
18.25	0.23	0.7	1	0.26	0
18.5	0.25	1.07	1.5	0.49	0
18.75	0.33	0.91	2	0.63	0.17
19	0.28	1.03	2.5	0.62	0.26
19.25	0.23	0.71	3	0.53	0.17
19.5	0.24	0.65	3.5	0.5	0.13
19.75	0.21	0.2	4	0.59	0.12
20	0.18	0.12	4.5	0.5	0.13
20.25	0.17	0.04	5	0.5	0.19
20.5	0.18	0.15	5.5	0.46	0.24
20.75	0.22	0.16	6	0.42	0.43
21	0.18	0.51	6.5	0.4	0.46
21.25	0.23	0.6	7	0.43	0.45
21.5	0.24	0.63	7.5	0.44	0.49
21.75	0.2	0.74	8	0.39	0.52
22	0.31	0.85	8.5	0.37	0.53
22.25	0.32	1.05	9	0.37	0.63
22.5	0.31	1.1	9.5	0.36	0.65
22.75	0.32	1.13	10	0.35	0.69
23	0.33	0.92	10.5	0.35	0.68
23.25	0.37	0.54	11	0.4	0.73
23.5	0.42	0.51	11.5	0.37	0.81
23.75	0.5	0.53	12	0.37	0.74
24	0.58	1.23	12.5	0.39	0.73
24.25	0.59	1.51	13	0.4	0.71
24.5	0.58	1.62	13.5	0.43	0.74
24.75	0.48	1.68	14	0.41	0.71
25	0.46	1.82	14.5	0.41	0.72
25.25	0.44	1.86	15	0.43	0.61
25.5	0.41	1.75	15.5	0.42	0.42
25.75	0.36	1.51	16	0.33	0.11
26	0.31	1.24	16.5	0.22	0
26.25	0.32	1.33	17	0.17	0
26.5	0.34	1.29	17.5	0.15	0
26.75	0.14	0.9	18	0	0
27.17	0	0	18.75	0	0
			28.5	Cut bank	

February 19, 2012					
WB1.5D			WB1.5U		
Distance along transect	Depth (ft)	Velocity (ft/s)	Distance along transect	Depth (ft)	Velocity (ft/s)
1.33	0	0	0.5	0	0
3	0.28	0	1.5	0.51	0
3.5	0.35	0	2	0.5	0.03
4	0.3	0.01	2.5	0.53	0.05
4.5	0.33	0.04	3	0.57	0.07
5	0.29	0.1	3.5	0.57	0.08
5.5	0.3	0.11	4	0.66	0.13
6	0.28	0.11	4.5	0.66	0.18
6.5	0.32	0.16	5	0.68	0.18
7	0.29	0.22	5.5	0.7	0.23
7.5	0.3	0.18	6	0.79	0.24
8	0.29	0.22	6.5	0.76	0.18
8.5	0.31	0.18	7	0.75	0.19
9	0.34	0.22	7.5	0.77	0.18
9.5	0.32	0.16	8	0.74	0.21
10	0.33	0.23	8.5	0.76	0.17
10.5	0.31	0.22	9	0.77	0.18
11	0.33	0.23	9.5	0.73	0.19
11.5	0.36	0.26	10	0.72	0.22
12	0.44	0.21	10.5	0.7	0.23
12.5	0.43	0.2	11	0.65	0.2
13	0.46	0.22	11.5	0.67	0.19
13.5	0.4	0.26	12	0.68	0.2
14	0.47	0.16	12.5	0.7	0.23
14.5	0.48	0.25	13	0.7	0.17
15	0.5	0.24	13.5	0.63	0.2
15.5	0.53	0.21	14	0.65	0.15
16	0.55	0.25	14.5	0.78	0.13
16.5	0.57	0.22	15	0.77	0.16
17	0.6	0.27	15.5	0.7	0.14
17.5	0.6	0.28	16	0.65	0.13
18	0.63	0.31	16.5	0.66	0.08
18.5	0.65	0.31	17	0.67	0.04
19	0.63	0.27	17.5	0.61	0.05
19.5	0.7	0.31	18	0.58	0.02
20	0.73	0.3	18.5	0.56	0.01
20.5	0.83	0.29	19	0.5	0.01
21	0.79	0.23	19.5	0.51	0
21.5	0.74	0.2	20	0.51	0
22	0.66	0.17	21	0.46	0
22.5	0.64	0.16	22	0.35	0
23	0.61	0.18	23	0.33	0
23.5	0.51	0.21	24	0.19	0
24	0.46	0.11	24.75	0	0
24.5	0.45	0.08			
25	0.34	0			
25.5	0.28	0			
26	0.21	0			
26.58	0	0			

February 19, 2012					
MS1D			MS1U		
Distance along transect	Depth (ft)	Velocity (ft/s)	Distance along transect	Depth (ft)	Velocity (ft/s)
0.33	0	0	0.33	0	0
1	0.5	0	1.5	0.24	0
2	0.67	0.02	2	0.29	0.1
2.5	0.71	0	2.5	0.43	0.11
3	0.84	0.05	3	0.56	0.1
4	1.06	0	3.5	0.57	0.17
5	0.86	0.03	4	0.65	0.26
6	1.02	0.08	4.5	0.63	0.11
6.5	0.94	0.09	5	0.48	0.12
7	1.1	0.08	5.5	0.56	0.13
7.5	1.16	0.13	6	0.6	0.16
8	1.27	0.17	6.5	0.5	0.23
8.5	1.26	0.17	7	0.67	0.25
9	1.24	0.14	7.5	0.77	0.27
9.5	1.16	0.18	8	1.1	0.28
10	1.15	0.21	8.5	1.19	0.33
10.5	1.06	0.23	9	1.09	0.28
11	0.98	0.21	9.5	1.22	0.29
11.5	0.98	0.2	10	1.18	0.24
12	1.01	0.19	10.5	1.09	0.22
12.5	1	0.18	11	0.96	0.2
13	1.01	0.19	11.5	0.87	0.16
13.5	1	0.18	12	0.7	0.15
14	1.01	0.18	12.5	0.65	0.11
14.5	0.9	0.15	13	0.55	0.07
15	0.97	0.07	13.5	0.44	0.07
16	0.95	0.17	14	0.32	0
16.5	0.97	0.08	15	0.16	0
17	0.9	0.03			
17.5	0.82	0			
18	0.82	0			
19	0.7	0			
20	0.55	0			

February 19, 2012					
WB3D			WB3U		
Distance along transect	Depth (ft)	Velocity (ft/s)	Distance along transect	Depth (ft)	Velocity (ft/s)
0.33	0	0	0	0	0
1	1.18	0.05	1	0.56	0.01
1.5	1.04	0.31	1.5	0.46	0.06
2	0.97	0.37	2	1.06	0.07
2.5	0.9	0.29	2.5	0.92	0.06
3	0.68	0.23	3	0.98	0.02
3.5	0.63	0.22	3.5	1.05	0
4	0.56	0.3	4	1.08	0
4.5	0.52	0.44	4.5	0.97	0
5	0.43	0.61	5	0.84	0
5.5	0.37	0.53	5.5	0.76	0
6	0.31	0.51	6	0.72	0
6.5	0.35	0.39	6.5	0.7	0
7	0.34	0.48	7	0.71	0
7.5	0.31	0.44	7.5	0.73	0
8	0.33	0.27	8	0.74	0.02
8.5	0.34	0.31	8.5	0.64	0.15
9	0.32	0.25	9	0.72	0.11
9.5	0.33	0.31	9.5	0.71	0.05
10	0.28	0.32	10	0.56	0.06
10.5	0.26	0.29	10.5	0.52	0.11
11	0.23	0.33	11	0.43	0.23
11.5	0.24	0.36	11.5	0.37	0.36
12	0.19	0.44	12	0.37	0.26
12.5	0.18	0.36	12.5	0.32	0.25
13	0.16	0.31	13	0.3	0.3
13.5	0.15	0.15	13.5	0.31	0.38
14	0.14	0.01	14	0.33	0.31
16	0.14	0	14.5	0.34	0.27
17	0.16	0	15	0.34	0.31
18	0.25	0	15.5	0.32	0.3
19	0.56	0	16	0.28	0.3
20	0.47	0	16.5	0.29	0.31
			17	0.32	0.29
			17.5	0.29	0.28
			18	0.3	0.19
			18.5	0.28	0.25
			19	0.3	0.25
			19.5	0.33	0.31
			20	0.35	0.29
			20.5	0.4	0.32
			21	0.42	0.29
			21.5	0.4	0.32
			22	0.43	0.25
			22.5	0.27	0.23
			23	0.16	0.22
			23.4	0	0

Appendix II

Measurement error calculated for gauged stream discharge using current meter and top-setting rod (velocity-area method)

Gaging location	Oct-10		Jan-11		Jun-11		Oct-11		Feb-12	
	Error		Error		Error		Error		Error	
	(+) %	(-) %	(+) %	(-) %	(+) %	(-) %	(+) %	(-) %	(+) %	(-) %
EB2D	29.8	27.9	29.1	26.5	13.5	12.9	20.6	18.7	20.7	22.5
EB2U	34.9	23.0	25.9	24.7	21.3	30.8	25.2	25.7	14.6	14.3
WB1D			26.0	23.3	25.0	25.0	21.1	21.1	15.1	19.9
WB1U			15.5	15.2	11.7	23.5	18.9	17.1	15.0	14.3
WB1.5D	22.4	19.0	24.4	21.2	18.0	16.8	16.3	14.5	15.5	14.2
WB1.5U	24.5	21.7	26.2	24.4	14.4	16.1	21.3	18.7	15.8	14.5
MS1D	26.4	23.1	27.3	25.0	15.3	16.3	20.6	19.2	14.8	13.9
MS1U	28.2	23.9	23.5	20.6	14.0	15.1	17.5	17.5	11.6	11.3
WB3D	27.2	23.2	18.5	40.0	19.2	17.0	16.3	25.1	16.7	25.1
WB3U	31.1	28.1	28.6	24.8	22.5	19.6	28.9	24.4	22.9	21.9

Appendix III

A. Dye (Rhodamine WT) concentrations at four sampling sites downstream of dye injection location for all four rounds of field experiments.

WB3U, MS1U, WB1.5D and EB2D – sampling locations upstream (U) and downstream (D) of major springs.

January 22, 2011							
WB3U		**MS1U**		**WB1.5D**		**EB2D**	
Time (min)	Concentration (µg/L)	Time (min)	Concentration (µg/L)	Time (min)	Concentration (µg/L)	Time (min)	Concentration (µg/L)
0	10.75	0	12.53	122	8.36	0	10.37
2	13.55	4	40.21	127	33.40	137	10.38
5	580.16	8	168.87	132	77.01	175	30.36
8	1168.96	12	286.86	137	154.86	180	56.88
11.25	610.24	16	390.47	142	184.99	185	104.61
14	535.04	20	358.02	147	193.55	190	137.60
17	403.23	24	294.58	152	188.42	195	163.19
20	293.53	28	241.83	157	165.53	200	179.21
23	191.32	32	207.56	162	137.32	205	174.02
26	122.51	36	155.00	167	122.83	210	176.20
31	77.05	41	126.75	172	123.25	215	158.19
36	112.53	46	102.96	177	96.13	225	128.80
41	104.23	51	82.67	182	90.81	230	109.80
46	176.51	56	68.17	187	79.71	240	90.27
51	125.04	61	60.05	192	66.73	245	87.81
56	124.18	66	51.22	197	61.49	250	84.42
61	88.21	71	37.62	202	52.70	255	80.80
66	99.84	76	41.07	207	48.64	270	56.01
71	121.15	81	36.44	212	48.28	280	41.36
76	109.72	86	31.65	217	38.36		
86	62.99	96	16.56	227	32.08		
96	51.46	106	14.26	237	24.99		
106	31.36	116	20.54	247	23.10		
116	26.09	126	12.98	257	19.39		
126	21.59	136	14.20	267	14.40		
136	23.12	146	10.75	277	15.02		
146	26.67	156	11.12				
156	23.34	166	13.44				
166	17.57	176	14.31				
176	19.82						

June 24, 2011							
WB3U		**MS1U**		**WB1.5D**		**EB2D**	
Time (min)	Concentration (µg/L)	Time (min)	Concentration (µg/L)	Time (min)	Concentration (µg/L)	Time (min)	Concentration (µg/L)
0	29.98	0	19.21	0	25.79	0	21.41
3	30.77	1	41.00	5	44.88	5	62.28
6	907.56	2	72.41	10	129.78	10	148.47
9	1482.93	5	132.06	15	235.90	15	181.06
12	952.42	8	263.64	20	268.88	20	176.56
15	388.05	11	394.38	25	250.21	25	165.83
18	284.51	14	396.19	30	230.59	30	155.36
21	326.16	17	369.11	35	184.04	35	132.60
24	243.15	20	334.36	40	139.10	40	114.38
27	293.78	23	287.73	45	117.83	45	90.50
32	151.04	28	239.10	55	81.05	55	68.22
37	144.54	33	184.59	65	58.28	65	40.15
42	85.33	38	152.51	75	46.64	75	34.10
47	57.45	43	127.95	85	32.02	85	27.46
52	43.39	48	98.58	95	28.26	95	28.29
57	44.22	53	84.40	105	21.15	105	27.47
62	36.03	58	66.42	115	28.35	115	25.28
67	28.33	63	48.91	125	23.11	125	20.89
72	40.41	68	45.21	135	26.82	135	20.01
77	35.45	73	44.58	145	18.33	145	16.14
87	27.15	83	37.44	155	18.17	155	22.13
97	28.51	93	34.91	165	22.29	165	20.79
107	34.56	103	32.66	175	19.79	175	20.72
117	25.43	113	28.78	185	22.93	185	21.47
127	24.79	123	24.52	195	19.75	195	16.81
137	24.73	133	28.21				
147	29.12	143	27.63				
157	25.45	153	33.45				
167	24.36	163	25.95				
177	24.63	173	22.86				

October 24, 2011							
WB3U		MS1U		WB1.5D		EB2D	
Time (min)	Concentration (µg/L)	Time (min)	Concentration (µg/L)	Time (min)	Concentration (µg/L)	Time (min)	Concentration (µg/L)
0	7.69	0	17.33	0	21.93	0	17.28
2	15.45	4	21.99	5	117.18	5	40.64
5	1273.66	8	102.25	10	174.90	10	97.30
8	1181.21	12	180.71	15	196.17	15	140.23
11	908.78	16	252.73	20	216.28	20	137.04
14	425.52	20	293.02	25	221.11	25	172.64
17	367.66	24	291.36	30	207.18	30	183.96
20	218.14	28	280.49	35	179.07	35	169.55
23	120.17	32	267.18	40	173.98	40	166.40
26	148.56	36	226.53	45	140.20	45	143.87
31	123.06	41	233.60	55	121.89	55	126.60
36	91.82	46	200.43	65	94.34	65	105.98
41	67.99	51	163.07	75	79.97	75	78.89
46	96.93	56	156.95	85	50.66	85	72.74
51	45.25	61	119.08	95	41.00	95	46.76
56	43.47	66	93.62	105	38.88	105	46.78
61	66.84	71	83.80	115	45.68	115	43.01
66	38.08	76	82.14	125	28.22	125	47.66
71	34.85	81	63.17	135	23.76	135	28.79
76	21.03	86	66.90	145	20.69	145	28.99
86	28.57	91	51.20	155	21.85	155	25.15
96	21.50	96	47.03	165	23.17	165	19.77
106	9.54	106	45.72	175	18.53	175	22.68
116	15.41	116	31.36	185	21.92	185	15.51
126	15.60	126	26.14	195	19.16	195	18.55
136	10.08	136	27.86	205	20.83	205	16.55
146	15.54	146	23.10	215	11.68	215	14.93
156	12.59	156	23.63	225	15.64	225	14.80
166	8.92	166	16.70	235	14.96	235	10.69
176	10.10	176	19.08	245	12.20	245	14.80

February 20, 2012							
WB3U		**MS1U**		**WB1.5 D**		**EB2D**	
Time (min)	Concentration (µg/L)	Time (min)	Concentration (µg/L)	Time (min)	Concentration (µg/L)	Time (min)	Concentration (µg/L)
0	34.00	0	25.70	0	29.86	0	25.12
5	60.16	5	38.23	5	193.92	5	57.89
7	834.72	7	60.26	10	307.67	10	173.01
9	783.25	9	145.53	15	286.56	15	237.82
11	1271.86	12	361.37	20	202.42	20	215.47
14	733.60	15	448.68	25	110.28	22	185.14
17	105.89	18	419.68	30	72.03	27	153.21
20	137.36	21	292.61	35	63.54	32	99.37
23	76.92	24	215.24	40	46.96	37	73.16
26	45.22	27	167.96	45	31.15	42	66.62
30	45.97	31	103.02	55	40.53	52	38.74
34	66.67	35	72.64	65	24.41	62	33.94
38	34.83	39	52.10	75	23.03	72	29.56
42	47.54	43	54.83	85	30.04	82	22.70
46	39.85	47	42.98	95	21.57	92	22.17
50	35.08	51	37.86	105	25.53	102	18.51
55	32.79	55	36.81	115	23.08	112	21.35
60	36.92	59	40.92	125	25.71	122	19.90
65	27.61	63	28.29	135	20.93	132	20.59
70	34.51	67	28.45	145	24.28	142	22.22
75	30.92	73	34.43	155	25.63	152	29.18
80	26.12	79	27.90	165	22.89	162	21.27
85	29.87	85	28.88	175	22.88	172	23.60
95	31.51	91	21.17	185	20.38	182	24.48
105	28.31	97	31.02	190	21.00	192	27.53
115	35.88	107	28.27	195	23.71		
125	26.92	117	25.19	200	20.86		
135	32.21	132	25.96				
145	30.99	152	26.97				
155	32.72	172	23.31				

B. Matlab function used to calculate centroid of the breakthrough curves

1. Function file

User defined Matlab function **centroid.m** (Mukherjee,2003) from Johnson, (1995) (http://web.ccr.jussieu.fr/ccr/Documentation/Calcul/matlab5v11/docs/ftp.mathworks.com /pub/contrib/v4/misc/centroid.m)**.**

```
function [x0,y0] = centroid(x,y)
% CENTROID Center of mass of a polygon.
% [X0,Y0] = CENTROID(X,Y) Calculates centroid
% (center of mass) of planar polygon with vertices
% coordinates X, Y.
% Z0 = CENTROID(X+i*Y) returns Z0=X0+i*Y0 the same
% as CENTROID(X,Y).
% Algorithm:
% X0 = Int{x*ds}/Int{ds}, where ds - area element
% so that Int{ds} is total area of a polygon.
% Using Green's theorem the area integral can be
% reduced to a contour integral:
% Int{x*ds} = -Int{x^2*dy}, Int{ds} = Int{x*dy} along
% the perimeter of a polygon.
% For a polygon as a sequence of line segments
% this can be reduced exactly to a sum:
% Int{x^2*dy} = Sum{ (x_{i}^2+x_{i+1}^2+x_{i}*x_{i+1})*
% (y_{i+1}-y_{i})}/3;
% Int{x*dy} = Sum{(x_{i}+x_{i+1})(y_{i+1}-y_{i})}/2.
% Similarly
% Y0 = Int{y*ds}/Int{ds}, where
% Int{y*ds} = Int{y^2*dx} =
% = Sum{ (y_{i}^2+y_{i+1}^2+y_{i}*y_{i+1})*
% (x_{i+1}-x_{i})}/3.
% Handle input .....................
if nargin==0, help centroid, return, end
if nargin==1
143
sz = size(x);
if sz(1)==2 % Matrix 2 by n
y = x(2,:); x = x(1,:);
elseif sz(2)==2 % Matrix n by 2
y = x(:,2); x = x(:,1);
else
y = imag(x);
x = real(x);
end
end
% Make a polygon closed ..............
x = [x(:); x(1)];
y = [y(:); y(1)];
% Check length .....................
l = length(x);
if length(y)~=l
error(' Vectors x and y must have the same length')
end
```

```
% X-mean: Int{x^2*dy} ..............
del = y(2:l)-y(1:l-1);
v = x(1:l-1).^2+x(2:l).^2+x(1:l-1).*x(2:l);
x0 = v'*del;
% Y-mean: Int{y^2*dx} ..............
del = x(2:l)-x(1:l-1);
v = y(1:l-1).^2+y(2:l).^2+y(1:l-1).*y(2:l);
y0 = v'*del;
% Calculate area: Int{y*dx} ..........
a = (y(1:l-1)+y(2:l))'*del;
tol= 2*eps;
if abs(a)<tol
disp(' Warning: area of polygon is close to 0')
a = a+sign(a)*tol+(~a)*tol;
end
% Multiplier
a = 1/3/a;
% Divide by area .....................
x0 = -x0*a;
y0 = y0*a;
if nargout < 2, x0 = x0+i*y0; end
```

2. Matlab input command file to calculate centroid for each successive downstream locations

```
X =
xlsread('\\128.163.123.137\ees\gntrip2\Documents\MATLAB\TraveltimeFeb01
2\Traveltime012.xlsx');
X1 = X(:,1) %sampling time for WB3U
Y1 = X(:,2) %dye concentration
X2 = X(1:29,3) %sampling time for MS1 U
Y2 = X(1:29,4) %dye concentration
X3 = X(1:26,5) %sampling time for WB1.5 D
Y3 = X(1:26,6) %dye concentration
X4 = X(1:18,7) %sampling time for EB2 D
Y4 = X(1:18,8) %dye concentration
[a1,a2]=centroid(X1,Y1)
[b1,b2]=centroid(X2,Y2)
[c1,c2]=centroid(X3,Y3)
[d1,d2]=centroid(X4,Y4)
```

C. Instrument calibration

February 2012

Instrument Parameters

Instrument	Cary Eclipse
Instrument Serial Number	el01104984
Data mode	Fluorescence
Excitation wavelength (nm)	400.00
Emission wavelength (nm)	600.00
Ex. Slit (nm)	5
Em. Slit (nm)	5
Excitation filter	Auto
Emission filter	Open
Ave time (sec)	0.10000
PMT voltage (V)	Medium
Standard replicates	1
Standard averaging	OFF
Sample replicates	1
Sample averaging	OFF
Weight and volume corrections	OFF
Fit type	Linear direct
Min R^2	0.95000
Concentration units	µg/L
Comments:	

Calibration

Collection time 2/22/2012 11:48:48 AM

Standard	Concentration µg/L	F	Readings
Std 1	0.4		0.022
Std 2	1.0		0.022
Std 3	2.0		-0.007
Std 4	4.0		0.029
Std 5	8.0		0.119
Std 6	16.0		0.178
Std 7	24.0		0.347
Std 8	40.0		0.391
Std 9	60.0		0.712
Std 10	100.0		1.180
Std 11	200.0		2.199
Std 12	300.0		3.190
Std 13	400.0		4.468

Calibration eqn	Int = 0.01102*Conc
Correlation coefficient	0.99847
Calibration time	2/22/2012 11:52:38 AM

WB3U

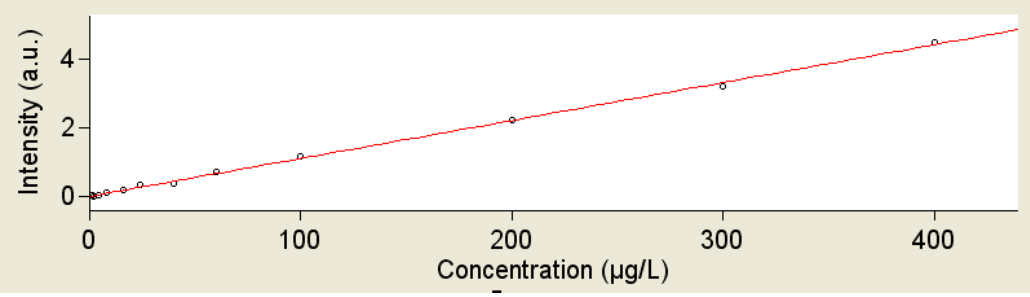

MS1U

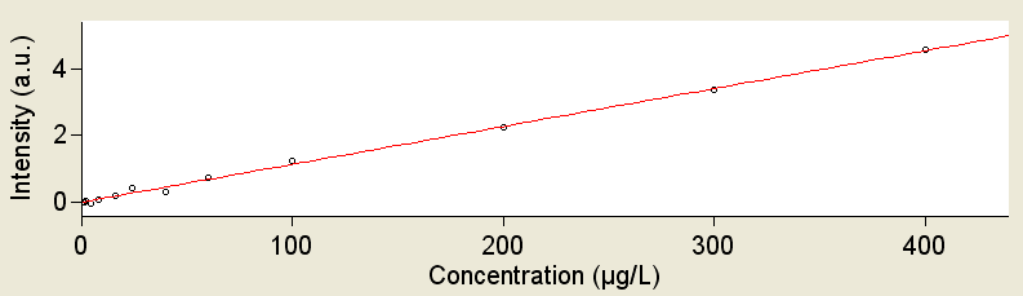

WB1.5D

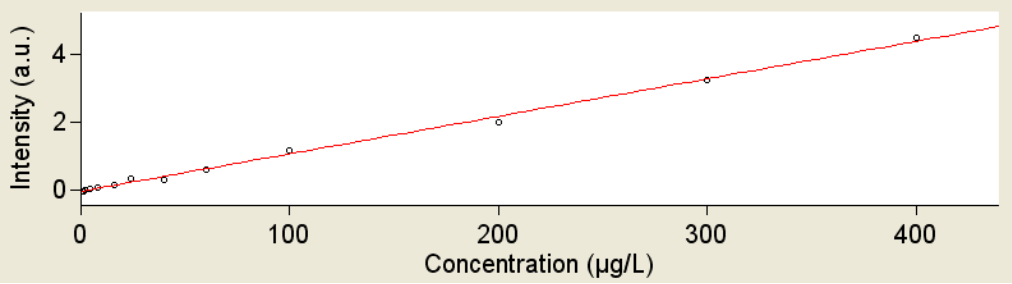

EB2D

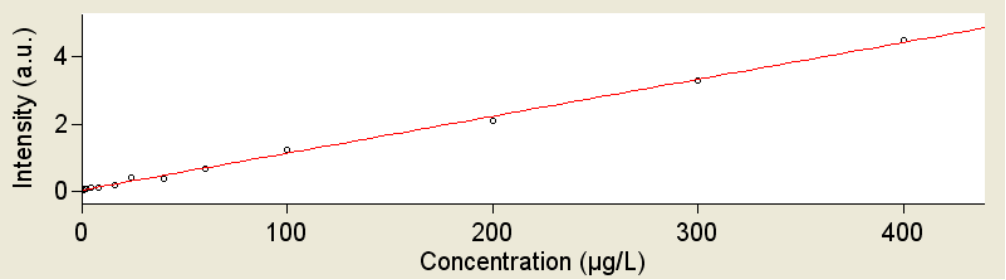

October 2011

Instrument Parameters

Instrument	Cary Eclipse
Instrument Serial Number	el01104984
Data mode	Fluorescence
Excitation wavelength (nm)	400.00
Emission wavelength (nm)	600.00
Ex. Slit (nm)	5
Em. Slit (nm)	5
Excitation filter	Auto
Emission filter	Open
Ave time (sec)	0.10000
PMT voltage (V)	Medium
Standard replicates	1
Standard averaging	OFF
Sample replicates	1
Sample averaging	OFF
Weight and volume corrections	OFF
Fit type	Linear direct
Min R^2	0.95000
Concentration units	µg/L
Comments:	

Calibration

Collection time	10/28/2011 12:32:45 PM

Standard	Concentration µg/L	F	Readings
Std 1	0.4		0.037
Std 2	1.0		-0.060
Std 3	2.0		-0.023
Std 4	4.0		0.014
Std 5	8.0		0.059
Std 6	16.0		0.097
Std 7	24.0		0.276
Std 8	40.0		0.377
Std 9	60.0		0.716
Std 10	100.0		1.292
Std 11	200.0		2.608
Std 12	300.0		3.484
Std 13	400.0		5.179

Calibration eqn	Int = 0.01252*Conc
Correlation coefficient	0.99531
Calibration time	10/28/2011 12:35:07 PM

WB3U

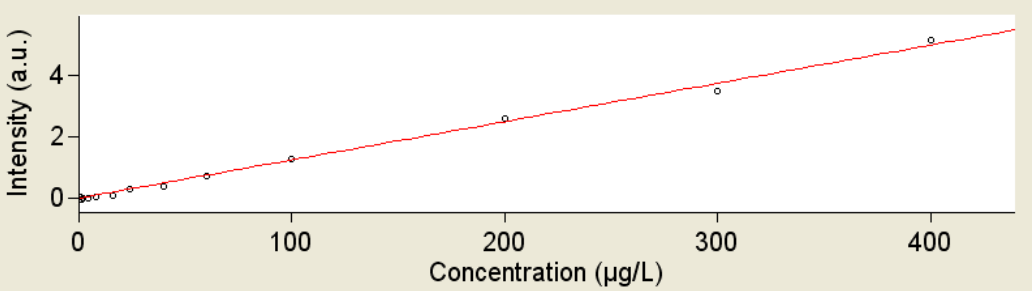

MS1U

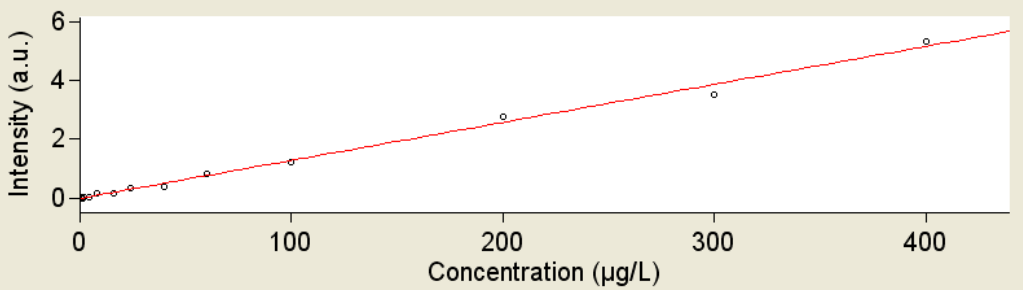

WB1.5D

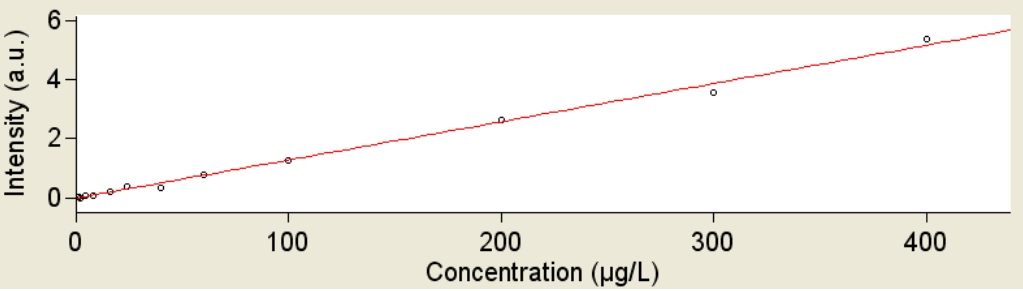

EB2D

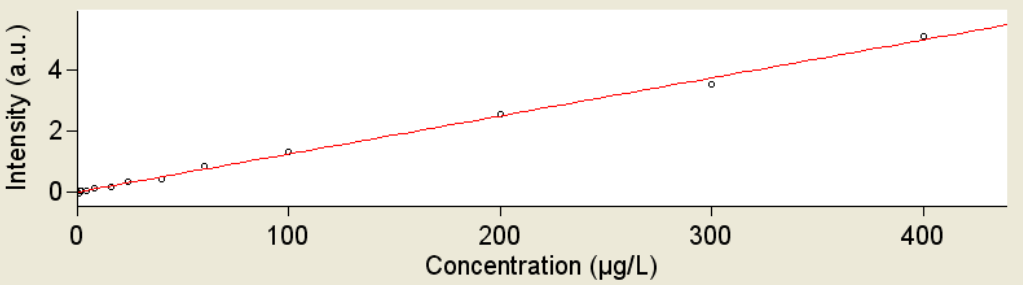

June 2011

Instrument Parameters

Instrument	Cary Eclipse
Instrument Serial Number	el01104984
Data mode	Fluorescence
Excitation wavelength (nm)	400.00
Emission wavelength (nm)	600.00
Ex. Slit (nm)	5
Em. Slit (nm)	5
Excitation filter	Auto
Emission filter	Open
Ave time (sec)	0.10000
PMT voltage (V)	Medium
Standard replicates	1
Standard averaging	OFF
Sample replicates	1
Sample averaging	OFF
Weight and volume corrections	OFF
Fit type	Linear
Min R^2	0.95000
Concentration units	µg/L
Comments:	

Calibration

Collection time 7/15/2011 12:40:34 PM

Standard	Concentration µg/L	F	Readings
Std 1	0.4		-0.007
Std 2	1.0		-0.030
Std 3	2.0		0.024
Std 4	4.0		0.015
Std 5	8.0		0.091
Std 6	16.0		0.046
Std 7	24.0		0.190
Std 8	40.0		0.336
Std 9	60.0		0.486
Std 10	100.0		0.975
Std 11	200.0		1.910
Std 12	300.0		2.930
Std 13	400.0		4.244

Calibration eqn	Int = 0.01036*Conc -0.05894
Correlation coefficient	0.99672
Calibration time	7/15/2011 12:44:35 PM

WB3U

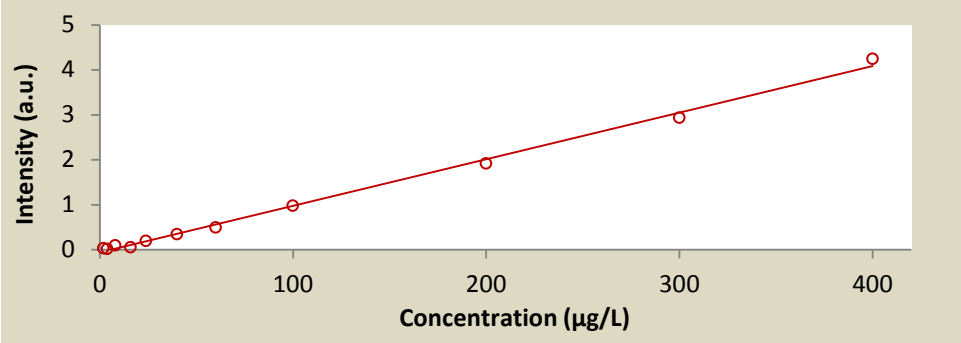

MS1U

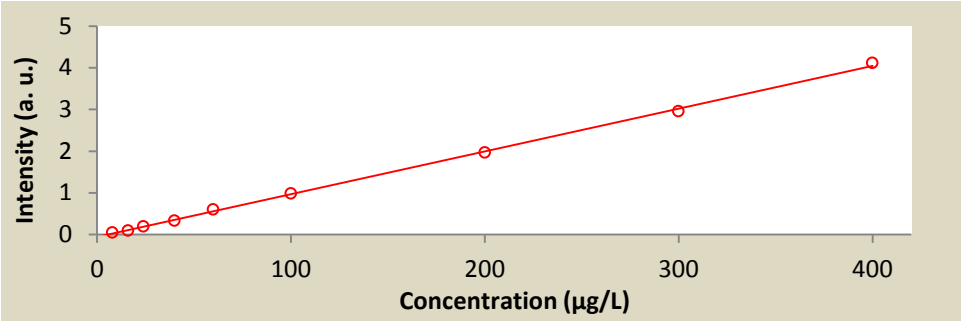

WB1.5D

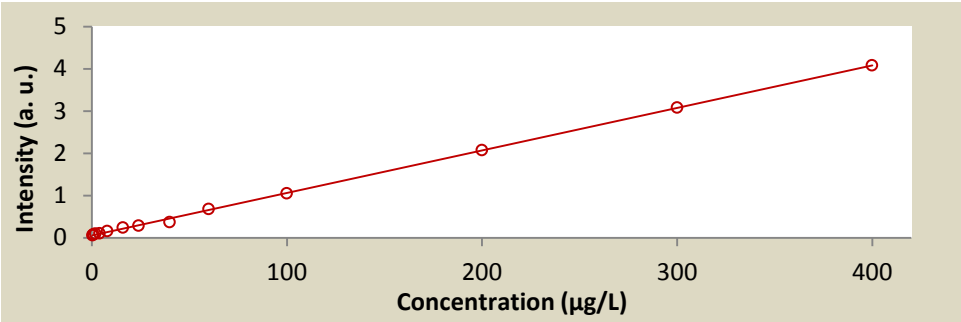

EB2U

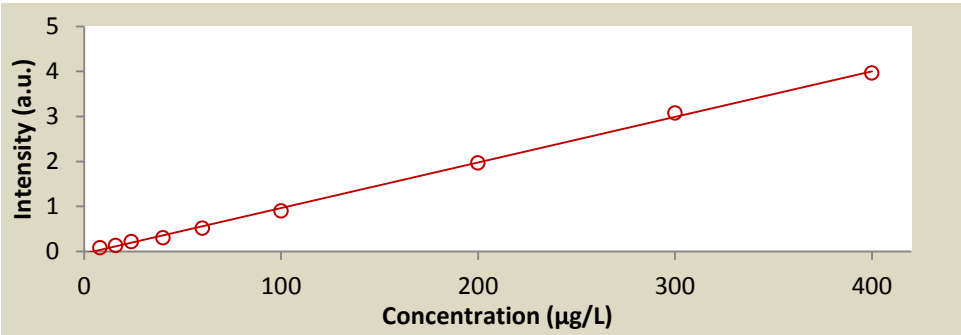

January 2011

Instrument Parameters

Instrument	Cary Eclipse
Instrument Serial Number	el01104984
Data mode	Fluorescence
Excitation wavelength (nm)	400.00
Emission wavelength (nm)	600.00
Ex. Slit (nm)	5
Em. Slit (nm)	5
Excitation filter	Auto
Emission filter	Open
Ave time (sec)	0.10000
PMT voltage (V)	Medium
Standard replicates	1
Standard averaging	OFF
Sample replicates	1
Sample averaging	OFF
Weight and volume corrections	OFF
Fit type	Linear
Min R^2	0.95000
Concentration units	µg/L

Comments:
Dye samples WB3 Upstream, Little Bayou Creek, Paducah

Calibration

Collection time	2/4/2011 2:01:23 PM

Standard	Concentration µg/L	F	Readings
Std 1	0.4		0.023
Std 2	1.0		0.015
Std 3	2.0		0.059
Std 4	4.0		0.127
Std 5	8.0		0.142
Std 6	16.0		0.201
Std 7	24.0		0.299
Std 8	40.0		0.625
Std 9	60.0		0.951
Std 10	100.0		1.648
Std 11	200.0		3.146
Std 12	300.0		4.969
Std 13	400.0		6.733

Calibration eqn	Int = 0.01666*Conc -0.02394
Correlation coefficient	0.99900
Calibration time	2/4/2011 2:04:36 PM

WB3U

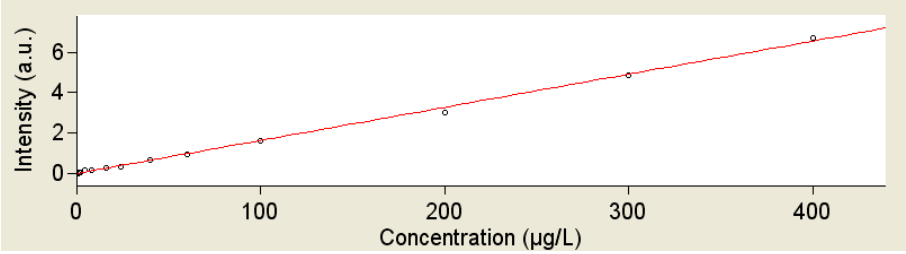

MS1U

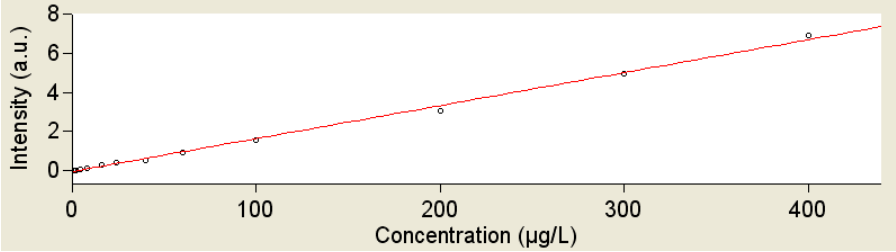

WB1.5D

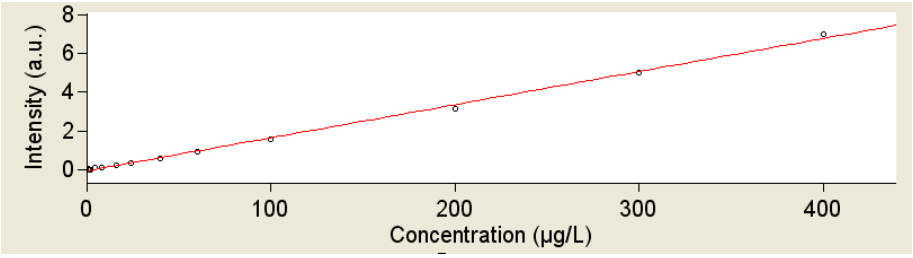

EB2D

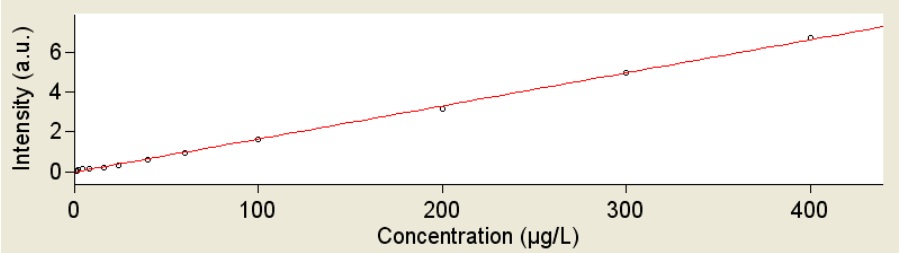

D. One-dimensional Transport with Inflow and Storage (OTIS)

Example Input files (OTIS-P):

1. Control file

```
#####################################################################
#######
#
#                         OTIS-P control file
#
#
#    line              name of the:
#    ----              --------------
#     1                parameter file
#     2                flow file
#     3                data file
#     4                STARPAC input file
#     5                parameter output file
#     6                STARPAC output file
#     7                solute output file
#     8                sorption output file (ISORB=1 only)
#
#####################################################################
   #######
LBCParam
LBCQ
data.inp
star.inp
params.out
star.out
RWTLbc

_
```

2. Parameter file

```
#################################################################
#
#  OTIS parameter file
#
#  Created 2012/04/17 20:15:08
#
#  http://water.usgs.gov/software/OTIS/
#
#################################################################
LBC011
1             |      PRTOPT
0.030000      |      PSTEP  [time]
0.010000      |      TSTEP  [time]
9.7200000     |      TSTART [time]
10.460000     |      TFINAL [time]
0.000000      |      XSTART [L]
0.000000      |      DSBOUND [(L/sec)CU]
3             |      NREACH
#################################################################
#
#  Physical Parameters
#
#                    for I = 1, NREACH
#
#NSEG RCHLEN       DISP         AREA2        ALPHA
#    |            |            |            |
#################################################################
106  106.000000   0.050000     0.050000     0.000011e+00
54   54.000000    0.050000     0.050000     0.000011e+00
194  194.000000   0.050000     0.050000     0.000011e+00
#################################################################
#
# Number of Solutes and flags for decay,sorption and gas exchange
#
# NSOLUTE (col.1-5) IDECAY(col.6-10) ISORB(col.11-15) IGAS(16-20)
#
#    |    |
#################################################################
1    0    0    0
#################################################################
#  Print Information
#################################################################
4    1              NPRINT (col.1-5)  IOPT (col.6-10)
1.00000000          (PRTLOC  for I = 1, NPRINT)
106.000000          (PRTLOC  for I = 1, NPRINT)
160.000000          (PRTLOC  for I = 1, NPRINT)
254.000000          (PRTLOC  for I = 1, NPRINT)
#################################################################
#
```

```
#  Boundary Conditions
#
#############################################################
16   3                  NBOUND (col.1-5)  IBOUND (col.6-10)
#############################################################
#               for I = 1,NBOUND
#
#USTIME       USBC (for i=1,NSOLUTE)
#            |            |            |
#############################################################
9.7200000    0.000000e+00
9.7500000    2.616300e-02
9.7800000    8.007200e-01
9.8100000    7.492600e-01
9.8400000    1.237900e+00
9.8900000    6.996000e-01
9.9400000    7.189900e-02
9.9900000    1.033600e-01
10.040000    4.292200e-02
10.090000    1.122200e-02
10.150000    1.197400e-02
10.210000    3.267800e-02
10.270000    8.360000e-04
10.330000    1.354700e-02
10.390000    5.858000e-03
10.460000    1.087000e-03
```

3. Flow file

```
#############################################################
#
#  OTIS steady flow file
#
#  Created 2012/04/17 20:15:08
#
#  http://water.usgs.gov/software/OTIS/
#
#############################################################
0.00                            QSTEP [hour]
5.253200e-02                    QSTART [L^3/second]
#############################################################
#                    for I = 1, NREACH
#
#QLATIN       QLATOUT      AREA         (CLATIN J=1,NSOLUTE)
#            |            |            |            |
#############################################################
0.000929e+00 0.000000e+00 1.120000     0.000000e+00
0.000934e+00 0.000000e+00 0.955000     0.000000e+00
0.000460e+00 0.000000e+00 0.755000     0.000000e+00
```

4. Data file

```
#######################################################################
#######
#
#                          OTIS-P data file
#
#
#    line     for J = 1, NREACH
#    ----
#     1       N - Number of observations for reach J.
#     2-N+1   TIME (time-variable) or DIST (steady-state)
associated
#             with each observation (col. 1-15) and CONC (col.
16-30)
#
#
#
#
#######################################################################
######
#
#  Reach 1 0-106m
#
23
9.9600000      0.000000
9.9900000      0.012500
10.020000      0.034600
10.050000      0.119800
10.100000      0.335700
10.150000      0.423000
10.200000      0.394000
10.250000      0.266900
10.300000      0.189500
10.350000      0.142200
10.410000      0.077300
10.470000      0.046900
10.530000      0.026400
10.600000      0.029100
10.660000      0.017300
10.720000      0.012100
10.780000      0.011100
10.850000      0.015200
10.920000      0.002600
10.980000      0.002700
11.080000      0.008700
11.180000      0.002200
11.280000      0.003200
#
#  Reach 2 106-160m
#
```

```
11
10.200000      0.000000
10.280000      0.164100
10.360000      0.277800
10.440000      0.256700
10.520000      0.172500
10.600000      0.080400
10.680000      0.042200
10.760000      0.033700
10.850000      0.017100
10.930000      0.001300
11.010000      0.011000
#
#  Reach 3 160-254m
#
13
10.320000      0.000000
10.400000      0.032800
10.480000      0.147900
10.560000      0.212700
10.640000      0.190300
10.720000      0.160000
10.800000      0.128100
10.880000      0.074200
10.960000      0.048000
11.050000      0.041500
11.210000      0.013600
11.370000      0.008800
11.540000      0.004400
_
```

5.STARPAC input file

```
#####################################################################
#########
#
#
#                     STARPAC Parameter Input File
#                                                          Rob
Runkel 3/11/95
#
#####################################################################
#########
#
#  Record Types 1-4, Integer values in Columns 1-5
#  -----------------------------------------------
#  IWEIGHT   Weight Revision Option
#  IVAPRX    Variance/Covariance Option
#  MIT       Maximum Number of Iterations
#  NPRT      STARPAC Print Option
```

```
#
0
1
100
22222
#
#  Record Types 5-7, Double precision values in Columns 1-13
#  ----------------------------------------------------------
#  DELTA     Maximum Scaled Change, First Iteration
#  STOPP     Stopping Value for Parameter Convergence
#  STOPSS    Stopping Value for Sum of Square Convergence
#
1.0
1.D-5
1.D-5
# For each of the ten model parameters, enter IFIXED (Integer,
Col. 1-5),
# SCALE (Floating Point, Column 6-18)
#
#IFXD SCALE
#    |                        | IFIXED and SCALE for:
#-------------------------------------------------------------------
--------
0    0.0D0             |Dispersion Coefficient, DISP
0    0.0D0             |M.C.Cross-Sectional Area, AREA
0    0.0D0             |S.Z.Cross-Sectional Area, AREA2
0    0.0D0             |S.Z.Exchange Coeffiecient, ALPHA
1    0.0D0             |M.C.1-Order Decay Coeff., LAMBDA
1    0.0D0             |S.Z.1-Order Decay Coeff., LAMBDA2
1    0.0D0             |Accessible Sed/Vol Water, RHO
1    0.0D0             |Distribution Coefficient, KD
1    0.0D0             |M.C.Sorption Rate Coeff., LAMHAT
1    0.0D0             |S.Z.Sorption Rate Coeff., LAMHAT2
```

Appendix IV

Stream stage and stream bank elevation obtained from laser survey (laser ranging instrument Impulse 200LR)

Survey date	Stake Locations	Top of the rod above stream stage (ft)	Top of the rod above bank (ft)	Stream stage corrected with survey data (ft, amsl)	Bank elevation corrected with survey data (ft, amsl)
22-Jan-11	EB2	1.54	1.41	314.11	314.24
	EB4	1.51	1.44	314.40	314.47
	WB1	1.15	0.7	316.11	316.56
	EB5	2.48	1.25	316.29	317.52
	WB1.5	2.32	1.52	318.52	319.32
	MS1W	2.47	1.65	319.58	320.40
	WB2	1.76	1.12	320.14	320.78
	WB3	2.06	1.65	319.87	320.28
6-Jun-11	EB2	2.03	1.3	313.62	314.35
	EB4	1.6	1.3	314.31	314.61
	WB1	1.31	0.55	315.95	316.71
	EB5	2.35	1.28	316.42	317.49
	WB1.5	2.21	1.29	318.63	319.55
	MS1W	2.52	0.8	319.53	321.25
	WB2	1.92	1	319.98	320.90
	WB3	1.91	1.66	320.02	320.27
23-Oct-11	EB2	2.03	1.37	313.62	314.28
	EB4	2.06	1.06	313.85	314.85
	WB1	1.46	1.18	315.80	316.08
	EB5	2.62	1.39	316.15	317.38
	WB1.5	2.33	1.73	318.51	319.11
	MS1W	2.65	1.55	319.40	320.50
	WB2	2.05	1.35	319.85	320.55
	WB3	2.14	1.79	319.79	320.14
18-Feb-12	EB2	1.82	1.4	313.83	314.25
	EB4	1.53	0.99	314.38	314.92
	WB1	0.95	0.65	316.31	316.61
	EB5	2.31	1.37	316.46	317.40
	WB1.5	2.13	1.56	318.71	319.28
	MS1W	2.44	1.62	319.61	320.43
	WB2	1.86	1.3	320.04	320.60
	WB3	1.94	1.89	319.99	320.04

Appendix V

Focused discharge area: January 2011

Reach 1

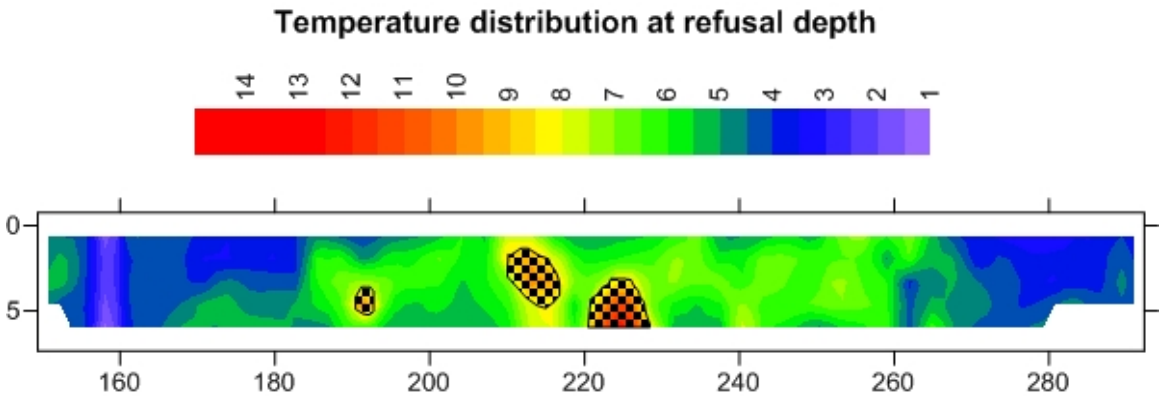

Reach 2

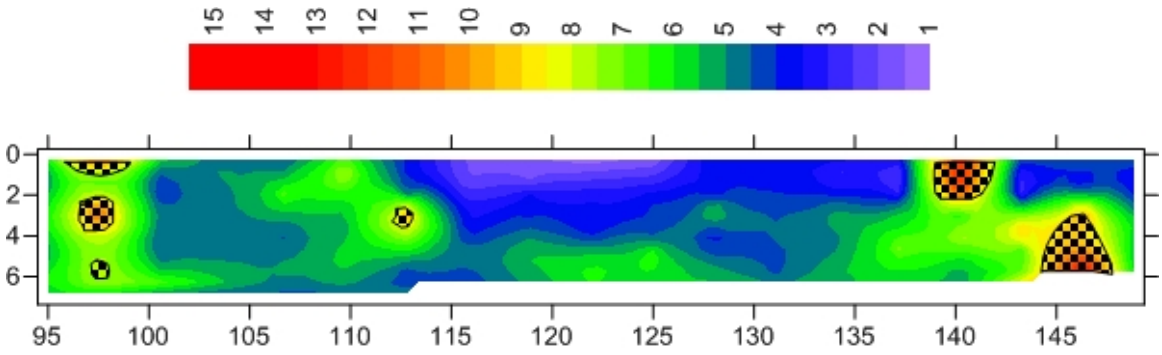

Reach 3

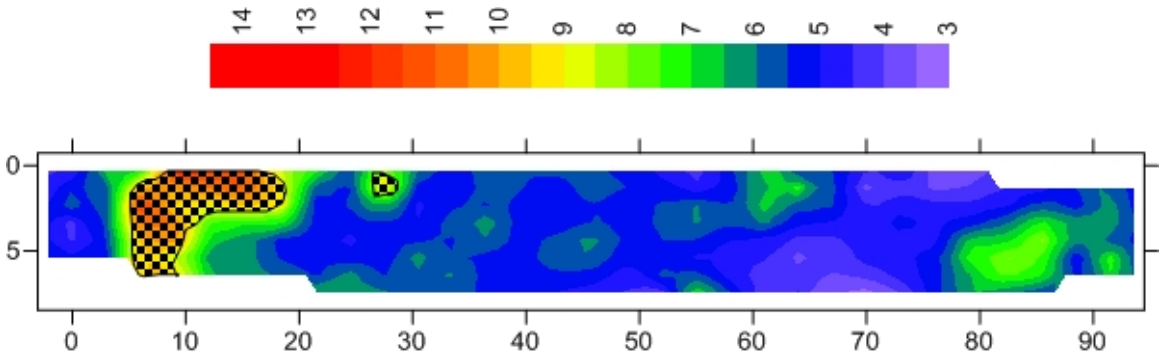

Focused discharge area: August 2011

Reach 1

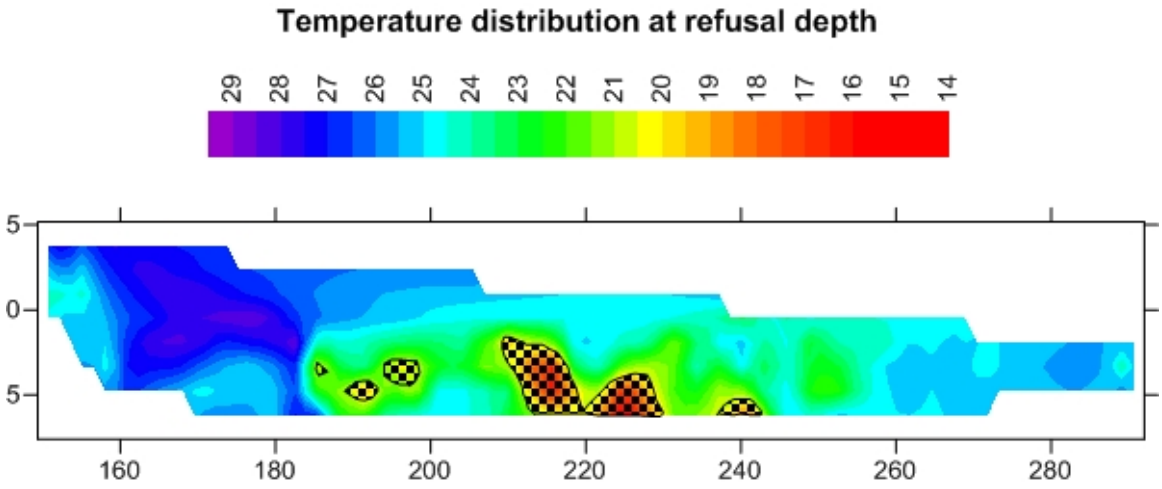

Reach 2

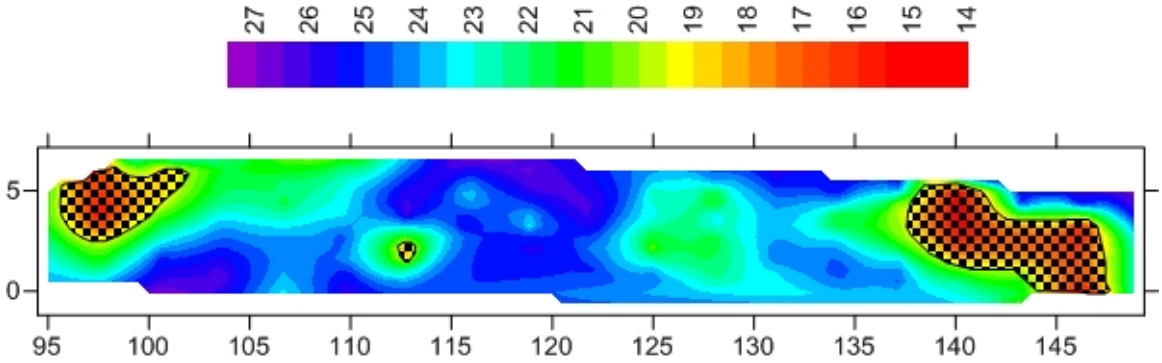

Reach 3

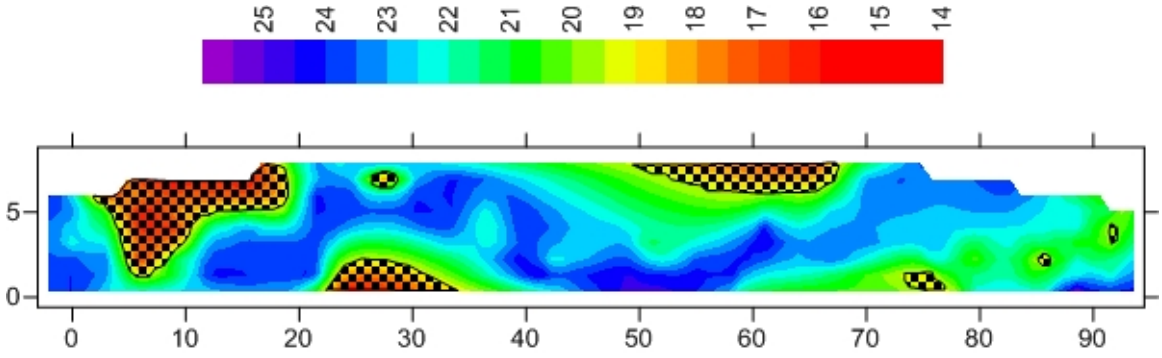

References

ATSDR (Agency for Toxic Substances and Disease Registry), 2009. Public health assessments and health consultations, *Paducah Gaseous Diffusion Plant (USDOE)*. http://www.atsdr.cdc.gov/HAC/pha/pha.asp?docid=791&pg=1.

Carter, R. W., and Davidian, J., 1968. General Procedure for gaging streams. *U. S. Geological Survey Techniques of Water Resources Investigations,* **Book 3** (Chapter A6): 13 p.

Cey, E. E., Rudolph, D. L., Parkin, G. W., and Aravena, R., 1998. Quantifying groundwater discharge to a small perennial stream in southern Ontario, Canada. *Journal of Hydrology* **210** (1–4), 21-37.

Clausen, J. L., Douthitt, J. W., Davis, K. R., and Phillips, B. E., 1992. Report of the Paducah Gaseous Diffusion Plant ground water investigation phase III. Document KY/E-150, prepared by Martin Marietta Energy Systems, Inc., for the *U. S. Department of Energy*: 147 p.

Clausen, J. L., Zutman, J., and Farrow, N., 1993. Characterization of the northwest plume utilizing a driven discrete-depth sampling system. Environmental Restoration Program, Martin Marietta KY/ER-22: 66 p.

Clausen, J. L., Sturchio, N. C., Heraty, L. J., Huang, L., and Abrajano, T., 1997. Evaluation of natural attenuation processes for trichloroethylene and technetium-99 in the northeast and northwest plumes at the Paducah Gaseous Diffusion Plant, Paducah, Kentucky. Report KY/EM-113, prepared by Martin Marietta Energy Systems, Inc. for the U. S. Department of Energy: 65p.

Clow, D. W., and Fleming, A. C., 2008. Tracer gauge: An automated dye dilution gauging system for ice-affected streams. *Water Resources Research* **44** (12), W12441, doi:1029/2008WR007090.

Conant Jr., B., 2004. Delineating and quantifying ground water discharge zones using streambed temperatures. *Ground Water* **42** (2): 243-257.

Conant Jr., B., Cherry, J. A., and Gillham, R. W. 2004. A PCE groundwater plume discharging to a river: influence of the streambed and near-river zone on contaminant distributions. *Journal of Contaminant Hydrology* **73**: 249-279.

Fryar, A. E., Wallin, E. J., and Brown, D. L., 2000. Spatial and temporal variability in seepage between a contaminated aquifer and tributaries to the Ohio River. *Ground Water Monitoring & Remediation* **20** (3): 129-146, doi:110.1111/j.1745-6592.2000.tb00279.x.

Hagerty, D. J., 1991. Piping/sapping erosion. I: Basic considerations. *Journal of Hydraulic Engineering* **117** (8): 991-1008.

Harvey, J. W., and Wagner, B. J., 2000. Quantifying hydrologic interactions between streams and their subsurface hyporheic zones. In: Jones, J. B., Mulholland, P. J. (Eds.), *Streams and Ground Waters*, Academic Press, San Diego, CA.

Hatch, C. E., Fisher, A. T., Revenaugh, J. S., Constantz, J., and Ruehl, C., 2006. Quantifying surface water-groundwater interactions using time series analysis of streambed thermal records: Method development. *Water Resources Research* **42,** W10410, doi:10.1029/2005WR004787.

Hill, A. R., 2000. Stream chemistry and riparian zones. In: Jones, J. B., and Mulholland, P. J. (Eds.), *Streams and Ground Waters*, Academic Press, San Diego**,** CA: 83 - 110.

Ho, S. V., Athmer, C., Sheridan, P. W., Hughes, B. M., Orth, R., Mckenzie, D., Brodsky, P. H., Shapiro, A. M., Sivavec, T. M., Salvo, J., Schultz, D., Landis, R., Griffith, R., and
Shoemaker, S., 1999. The Lasagna technology for in situ soil remediation. 2. Large field test. *Environmental Science & Technology* **33** (7): 1092-1099.

Howard, A. D., 1988. Groundwater sapping on Mars and Earth. Sapping features of Colorado Plateau: a comparative planetary geology field guide, Scientific and Technical Information Division, National Aeronautics and Space Administration **Chapter 1**: 108 p.

Hvorslev, M.J., 1951. Time lag and soil permeability in groundwater observations. In: US Army Corps Engineers Waterways Experiment Station Bulletin 36, Vicksburg, MS, 50 p.

Joly, D.R., 1996. First annual report for the northwest plume interim remedial action pilot plant at the Paducah Gaseous Diffusion Plant, Paducah, Kentucky. U. S. Department of Energy report DOE/OR/07-1531&D1: 18 p.

Kalbus, E., Reinstorf, F., and Schirmer M., 2006. Measuring methods for groundwater - surface water interactions: a review. *Hydrology and Earth System Sciences* **10**: 873 - 887.

Keery, J., Binley, A., Crook, N., and Smith, J. W. N., 2007. Temporal and spatial variability of groundwater–surface water fluxes: Development and application of analytical methods using temperature time series. *Journal of Hydrology* **336**, 1-16.

Kennedy, C. D., Genereux, D. P., Corbett, R., and Mitasova, H., 2007. Design of a light-oil piezomanometer for measurement of hydraulic head differences and collection

of groundwater samples. *Water Resources Research* **43**, W09501, doi:10.1029/2007WR005904.

Kennedy, C. D., Genereux, D. P., Corbett, D. R., and Mitasova, H. 2009. Spatial and temporal dynamics of coupled groundwater and nitrogen fluxes through a streambed in an agricultural watershed. *Water Resources Research* **45**, W09401, doi:10.1029/2008WR007397: 18 p.

Kennedy, C. D., Murdoch, L. C., Genereux, D. P., Corbett, D. R., Stone, K., Pham, P., and Mitasova, H., 2010. Comparison of Darcian flux calculations and seepage meter measurements in a sandy streambed in North Carolina, United States. *Water Resources Research* **46,** W09501, doi:10.1029/2009WR008342, 2010.

Kikuchi, C. P., Ferré, T. P. A., and Welker, J. M., 2012. Spatially telescoping measurements of improved characterization of ground water-surface water interactions. *Journal of Hydrology* **446 – 447**, 1-12.

Kilpatrick, E. F., and Wilson, J. F., Jr., 1989. Measurement of time of travel in streams by dye tracing. *U. S. Geological Survey Techniques of Water-Resources Investigations* **Book 3** (Chapter A-9): 27.

Kilpatrick, F. A., and Cobb, E. D., 1985. Measurement of discharge using tracers. *U. S. Geological Survey Techniques of Water-Resources Investigations* **Book 3** (Chapter A-16).

Lowry, C. S., Walker, J. F., Hunt, R. J., and Anderson, M. P., 2007. Identifying spatial variability of groundwater discharge in a wetland stream using a distributed temperature sensor. *Water Resources Research* **43**: 9.

Lamb, M. P., 2008. Formation of amphitheater-headed Canyons. University of California, Berkeley, Ph. D. dissertation, 297 p.

Kochel, R. C., and Piper, J. F., 1986. Morphology of large valleys on Hawaii: Evidence for groundwater sapping and comparisons with martian valleys. *Journal of Geophysical Research* **91**(B13): E175-E192.

Laity, J. E., and Malin, M. C., 1985. Sapping processes and development of theater-headed valley networks on the Colorado Plateau. *Geological Society of America Bulletin* **96**: 203-217.

Langston, C., McIntyre, J., and Street, R., 1998. Investigation of the shallow subsurface near the Paducah Gaseous Diffusion Plant using SH-wave seismic methods. *Society of Exploration Geophysicists, 1998 Technical Program, Expanded Abstracts* **1**: 878-880.

LaSage, D. M., Sexton, J. L., Mukherjee, A., Fryar, A. E., and Greb, S. F., 2008a. Groundwater discharge along a channelized Coastal Plain stream. *Journal of Hydrology* **360** (1-4): 252-264.

LaSage, D. M., Fryar, A. E., Mukherjee, A., Sturchio, N. C., and Heraty, L. J., 2008b. Groundwater-derived contaminant fluxes along a channelized Coastal Plain stream. *Journal of Hydrology* **360** (1-4): 265-280.

Lee, D. R., 1977. A device for measuring seepage flux in lakes and estuaries. *Limnology and Oceanography* **22** (1): 140-147.

Libelo, E. L., and MacIntyre, W. G., 1994. Effects of surface-water movement on seepage-meter measurements of flow through the sediment-water interface. *Hydrogeology Journal* **2** (4): 49-54, doi:10.1007/s100400050047.

Lowry, C. S., Walker, J. F., Hunt, R. J., and Anderson, M. P., 2007. Identifying spatial variability of groundwater discharge in a wetland stream using a distributed temperature sensor. *Water Resources Research* **43**, W10408, doi:10.1029/2007WR006145: 9.

Luo, W., Arvidson, R. E., Sultan, M., Becker, R., Crombie, M. K., Sturchio, N., and Alfy, Z. El., 1997. Ground-water sapping processes, Western Desert, Egypt. *Geological Society of America Bulletin* **109** (1): 43–62.

McCallum, J. L., Cook, P. G., Berhane, D., Rumpf, C., and McMahon, G. A., 2012. Quantifying groundwater flows to streams using differential flow gaugings and water chemistry. *Journal of Hydrology* (**416 -417**): 118-132.

Mukherjee, A., 2003. Identification of natural attenuation of trichloroethene and technetium-99 along Little Bayou Creek, McCracken County, Kentucky. University of Kentucky, M. S. Thesis, 163 p.

Mukherjee, A., Fryar, A. E., and LaSage, D. M., 2005. Using tracer tests to assess natural attenuation of contaminants along a channelized Coastal Plain stream. *Environmental & Engineering Geoscience* **11** (4): 371-382.

Murdoch, L. C., and Kelly, S. E., 2003. Factors affecting the performance of conventional seepage meters. *Water Resources Research* **39** (6): 1163, doi:1110.1029/2002WR001347.

Olive, W. W., 1980. Geological maps of Jackson Purchase Region, Kentucky. *U. S. Geological Survey.*

Oryx, 2007. Oryx DTS user manual. Sensornet Ltd, 340 Centennial Park, Elstree, London, WD6 3TJ, United Kingdom, 88 p.

Rantz, S. E., 1982. Measurement and computation of streamflow, volume 1, Measurement of stage and discharge. *U. S. Geological Survey Water-Supply Paper 2175*: 284 p.

Rao, Y. J., Webb, D. J., Jackson, D. A., Zhang, L., and Bennion, I., 1997. In-fiber Bragg-grating temperature sensor system for medical applications. *Journal of Lightwave Technology* **15** (5): 779-785.

Ruehl, C., Fisher, A. T., Hatch, C., Los Huertos, M. L., Stemler, G., and Shennan, C., 2006. Differential gauging and tracer tests resolve seepage fluxes in a strongly-losing stream. *Journal of Hydrology*, **330** (1-2), 235-248.

Runkel, R. L.,1998. One-dimensional transport with inflow and storage (OTIS): A solute transport model for streams and rivers: *U. S. Geological Survey Water-Resources Investigations Report 98-4018*, 73 p.

Schuetz, T., and Weiler, M., 2011. Quantification of localized groundwater inflow into streams using ground-based infrared thermography. *Geophysical Research Letters* **38**, L03401, doi:10.1029/2010GL046198.

Schwartz, F. W., Zhang, H., 2003. Fundamentals of Ground Water. John Wiley & Sons, New York, 583 p.

Selker, J. S., Thevenaz, L., Huwald, H., Mallet, A., Luxemburg, W., Giesen, N. van de, Stejskal, M., Zeman, J., Westhoff, M., and Parlange, M. B., 2006. Distributed fiber-optic temperature sensing for hydrologic systems. *Water Resources Research* **42**, W12202, doi:10.1029/2006WR005326.

Shanafield, M., Hatch, C., and Pohll, G., 2011. Uncertainty in thermal time series analysis estimates of streambed water flux. *Water Resources Research* **47**, W03504, doi:10.1029/2010WR009574, 2011.

Shaw, R. D., and Prepas, E. E., 1989. Anomalous, short-term influx of water into seepage meters. *Limnology and Oceanography* **34** (7): 1343-1351.

Silliman, S. E., and David, F. B., 1993. Analysis of time-series measurements of sediment temparature for identification of gaining vs. losing portions of Juday Creek, Indiana. *Journal of Hydrology* **146**: 131-148.

Smart, J. L., 2005. Application of six-phase soil heating technology for groundwater remediation. *Environmental Progress* **24** (1): 34 - 43.

Smart, P. L., and Laidlaw, I. M. S., 1977. An evaluation of some fluorescent dyes for water tracing. *Water Resources Research* **13** (1): 19.

Smith, R. F., 1984. Historical impact of reactor tails on the Paducah cascade. Paducah Gaseous Diffusion Plant, Paducah, Kentucky for *the U. S. Department of Energy* under contract No. W-7405-Eng-26.

Smolen, J. J., and Spek, A. v. d., 2003. Distributed temperature sensing. A DTS primer for oil and gas production.

Tyler, S. W., Selker, J. S., Hausner, M. B., Hatch, C. E., Torgersen, T., Thodal, C. E., and Schladow, G., 2009. Environmental temperature sensing using Raman spectra DTS fiber-optic methods. *Water Resources Research* **45**, W00D23, doi:10.1029/2008WR007052.

USEPA (U. S. Environmental Protection Agency), 2000. Trichloroethylene hazard summary: http://www.epa.gov/ttn/atw/hlthef/tri-ethy.html.

Wilson, J. F., Cobb, E. D, and Kilpatrick, F. A., 1986. Fluorometric procedures for dye tracing. *Techniques of Water-Resources Investigations of the U. S. Geological Survey* **Book 3 (**Chapter A12): 34 p.

Winter, T. C., Harvey, J. W., Franke, O. L., and Alley, W. M., 1998. Ground water and surface water: a single resource. *U. S. Geological Survey Circular 1139*: 79 p.

Wood, W. W., 1981. Guidelines for collection and field analysis of ground-water samples for selected unstable constituents. *U. S. Geological Survey Techniques of Water-Resources Investigations,* **Book 1** (Chapter D2): 24 p.

Zellweger, G. W., Avanzino, R. J., and Bencala, K. E., 1989. Comparison of tracer-dilution and current-meter discharge measurements in a small gravel-bed stream, Little Lost Man Creek, California. *U. S. Geological Survey Water-Resources Investigations Report 89 - 4150*: 20 p.

VITA

Ganesh Nath Tripathi is a permanent resident of Nepal. After completing a Master of Science in Geology from Tribhuvan University in 2001, he joined the Nepal Electricity Authority, Kathmandu, Nepal, as a geologist for two years. He has been appointed as a geologist at the Department of Mines and Geology since 2003. He served as a teaching and research assistant at the Department of Earth and Environmental Sciences, University of Kentucky, from 2007 to 2013, where he earned second Master of Science in Geology in 2009.

Publications:

- Tripathi, G. N., and Fryar, A. E., 2012. Integrating hydraulic and thermal techniques to examine focused groundwater discharge at multiple scales. Geological Society of America Abstracts with Programs, v. 44, no. 7, p. 50.

- Tripathi, G. N., and Fryar, A. E., 2011. Spatial and seasonal variability in groundwater discharge and contaminant fluxes along a channelized stream in western Kentucky. The 56th Annual Midwest Groundwater Conference Proceedings, Lexington, Lexington, Kentucky.

- Tripathi, G. N., and Fryar, A. E., Mukherjee, A., and LaSage, D. M., 2011. Thermal profiling of focused groundwater discharge along a channelized stream in western Kentucky. Geological Society of America Abstracts with Programs, v. 43, no. 5, p. 390.

- Phillips, J. D., McCormack, S., Duan, J., Russo, J. P., Schumacher, A. M., Tripathi, G. N., Brockman, R. B., Mays, A. B., Pulugurtha, S., 2010. Origin and interpretation of knickpoints in the Big South Fork River basin, Kentucky-Tennessee. Geomorphology, v. 114, Issue 3, p. 188 – 198.

- Tripathi, G.N., Fryar, A.E., Paylor, R.L., Dinger, J.S., Currens, J.C., and Strohmeyer, J.S., 2009, Use of integrated geophysical techniques to locate a karst conduit in the Inner Bluegrass region, Kentucky: Geological Society of America Abstracts with Programs, v. 41, no. 4, p. 15.

- Tripathi, G.N., Fryar, A.E., Paylor, R.L., Dinger, J.S., Currens, J.C., and Strohmeyer, J.S., 2009, Use of surface geophysical techniques to locate a karst conduit in the Cane Run – Royal Spring basin, Kentucky, *in* Kentucky Water Resources Annual Symposium Proceedings: Lexington, University of Kentucky, Kentucky Water Resources Research Institute, p. 73.